

Year        2020        Doctor Thesis

Research on wearable measurement system  
for physical performance and biomedical  
information

Supervisor    Prof. Koichi Sagawa

2019 December

Graduate School of Science and Technology,  
Hirosaki University

Amir Mukhriz bin Azman

# Contents

<b>1</b>	<b>Preface</b>	<b>1</b>
<b>2</b>	<b>Development of Wireless Inertial Measurement Unit (WIMU)</b>	<b>8</b>
2.1	Introduction . . . . .	8
2.2	Overview of WIMU . . . . .	9
2.3	Hardware and software structure . . . . .	11
2.4	WIMU for surface mounting . . . . .	16
2.5	Interpolation of value exceeding measurement ranges . . . . .	23
<b>3</b>	<b>Principle of gait analysis</b>	<b>25</b>
3.1	Construction of integration section . . . . .	25
3.1.1	Distinction between stance phase and swing phase . . . . .	25
3.1.2	Integration section determination . . . . .	26
3.2	Theory of measuring bipedal walking motion of human . . . . .	33
3.2.1	Acceleration derivation on fixed coordinate system . . . . .	33
3.2.2	Calculation of OM during stance phase . . . . .	34
3.2.3	Foot movement estimation . . . . .	36
3.2.4	Gait parameters . . . . .	38
3.2.5	Detection of running . . . . .	39
<b>4</b>	<b>Inertial gait analysis measurement system for large-scale health check- ups</b>	<b>43</b>
4.1	Introduction . . . . .	43
4.2	Mini-Mental State Examination (MMSE) . . . . .	45
4.3	10 m fastest gait experiment . . . . .	48

4.4	Results . . . . .	53
4.4.1	Compensation of gait distance with actual value . . . . .	53
4.4.2	Classification of subjects by running incidence . . . . .	54
4.4.3	Correlation between MMSE with gait parameter . . . . .	54
4.5	Discussion . . . . .	61
4.6	Conclusion . . . . .	62
<b>5</b>	<b>Simultaneous measurement of 3D foot trajectory and center of gravity</b>	<b>63</b>
5.1	Introduction . . . . .	63
5.2	Principle . . . . .	64
5.2.1	Type of force sensors . . . . .	64
5.2.2	Gait measurement system . . . . .	65
5.2.3	Gait trajectory . . . . .	66
5.3	Experiment . . . . .	71
5.3.1	Equipment . . . . .	71
5.3.2	Method . . . . .	71
5.4	Results . . . . .	71
5.5	Discussion . . . . .	84
5.6	Conclusion . . . . .	84
<b>6</b>	<b>Continuous blood pressure estimation during exercise using pulse photoplethysmographic signal</b>	<b>85</b>
6.1	Introduction . . . . .	85
6.2	Principle . . . . .	86
6.3	Method . . . . .	90
6.3.1	Subjects . . . . .	90
6.3.2	Equipments . . . . .	90
6.3.3	Exercise protocols . . . . .	91
6.3.4	Determination of pulse width . . . . .	91
6.3.5	Statistics . . . . .	92
6.3.6	Model for the PPG-BP relation . . . . .	92
6.4	Results . . . . .	104

6.5	Discussion . . . . .	108
6.6	Conclusions . . . . .	110
<b>7</b>	<b>Conclusion</b>	<b>111</b>
	<b>References</b>	<b>113</b>
	<b>Acknowledgments</b>	<b>122</b>



# Chapter 1

## Preface

Research on wearable measurement system for physical performance and biomedical information has been conducted for the purposes of understanding the basic and advance characteristics of human body. For the past decade, there has been a remarkable development of wearable systems, enabling sensors and mobile devices with unprecedented characteristics utilized in wide area. Their high computational power, small size, low cost, and robustness allow people to interact with the devices as part of their daily living. Particularly, the measurement of human activities has become a task of high interest within the field, especially for medical purpose. For instance, patients with diabetes, obesity, or heart disease are often required to follow a well defined exercise routine as part of their treatments<sup>[1]</sup>. Therefore, measuring activities such as walking, running, or cycling become useful for exercise level assessment and provide feedback to the exerciser or caregiver. Likewise, patients with dementia and other mental pathologies could be monitored to detect abnormal activities and thereby prevent undesirable consequences<sup>[2]</sup>.

However, there are still many issues that motivate the development of new techniques to improve the accuracy under more realistic conditions. Some of these challenges are the selection of the attributes to be measured, the development of a portable, unobtrusive, and inexpensive data acquisition system, the design of feature extraction and estimation methods, the collection of data under realistic conditions, and the flexibility to support new users without the need of re-training the system.

Quantitative evaluation of human activities has been approached in two different ways, using external and wearable sensors. In the former, the devices are fixed in predetermined points of interest, where interaction of the users with the devices takes place in predetermined space. In the latter, the devices are attached to the user and there is no limit in

area of activity.

Cameras have been employed for motion measurement and human activity recognition (HAR). In fact, the recognition of activities and gestures from video sequences has been the focus of extensive research<sup>[3–6]</sup>. However, video sequences certainly have some problems in motion monitoring. The monitored individuals need to stay within an area defined by the position and the capabilities of the cameras. Another problem is video processing is complex and needs professional techniques.

The aforementioned limitations motivate the use of wearable sensors in HAR. Most of the measured attributes are related to the user’s movement (e.g. using accelerometer or gyroscope), environmental variables (e.g. temperature), or physiological signals (e.g. heart rate or blood pressure). These data are naturally indexed over the time dimension, allowing researches to define the human healthiness and fitness. Researches have been conducted on body-worn measurement devices using sensors such as accelerometer, gyroscope, geomagnetic sensor, force sensor, and pulse sensor.

When acceleration acts on the mass held by elastic element and viscous damping element, an IC type accelerometer can measure the acceleration acting on an object by capturing the displacement due to the inertial force of the mass as a change in the amount of material strain or capacitance. Gyroscope can measure Coriolis force when reciprocating vibrating element rotates. Motion measurement using these sensors has the advantages of simplicity, low cost, and low restraint compared to the optical devices described above. So, it is expected to play roles not only in the sports field but also in the welfare and physical therapy fields. To date, methods for estimating joint angles during human movement<sup>[7]</sup>, methods for discriminating behavior and activity<sup>[8]</sup>, and methods for measuring gait velocity during gait<sup>[9]</sup> have been reported. In addition, due to recent developments in MEMS technology, miniaturization, light weight, and high precision measuring are progressing that sensors can be incorporated into smartphones and wristwatches. There is a report of portable activity monitoring system with objective for better management of rehabilitation<sup>[10]</sup>. The monitoring system was based on three-axis accelerometer used for detection walking step-peak and calculating temporal gait parameters. However, the system functions like a pedometer and could not actually numerically measures gait parameter such as stride length and toe’s angle. To solve this problem, accelerometer and gyroscope are used together as a sensor unit to measure acceleration

and angular velocity. Algorithm is also developed for measuring temporal gait parameter at each cycle.

Spatial and temporal plantar pressure distributions are important and useful measures in footwear evaluation, athletic training, clinical gait analysis, and pathology foot diagnosis. However, present plantar pressure measurement and analysis systems are bulky, uncomfortable to wear and expensive. Study has been conducted on in-shoe plantar pressure measurement and analysis system based on a textile fabric sensor array<sup>[11]</sup>. The sensors are connected with a soft polymeric board through conductive yarns and integrated into an insole. A real-time display and analysis software are presented to calculate parameters such as mean force, peak force, center of foot force (COF), and shift speed of COF. However, acquiring force reading and COF has become common and commercialized. Therefore, by using force sensor as extension to the current inertial sensor unit, the information acquired during gait is broaden because other than motion capture system (MCS), there is almost no device that offer force plate information and 3D motion information at the same time has been developed.

Methods for continuously monitoring blood pressure from other physiological parameters have been widely studied. Most of these studies correlate blood pressure (BP) with pulse transit time (PTT), based on the relationship between BP and pulse wave velocity (PWV)<sup>[12]</sup>. BP is often estimated by means of linear models in which the variables are the extracted parameters from ECG and pulse photoplethysmography signal (PPG), representing the response of the cardiovascular system. Awad et al.<sup>[13]</sup> have suggested that pulse width is more sensitive to changes in Systemic Vascular Resistance (SVR) than other indices of pulse wave. The SVR is determined by changes in artery diameter or changes in blood viscosity. Changes in pulse width provide valuable evidence with respect to changes in PWV too. However, for the purpose of recreation and daily use, using sophisticated devices to measure multiple parameters is not practicable. Utilization of a pulse sensor is proposed to capture PPG for BP estimation.

Therefore, it is expected that sensors can be incorporated into various devices for various purposes in the future. In this way, body-mounted sensors are expected to be used more and more widely in the future, but there are following problems with high-speed sports 3D motion measurement.

### **The conventional measurement system is wired and has an adverse effect on motion measurement**

In order to measure human movements using inertial sensors, it is necessary to wear a several number of sensors on multiple parts of the body and record the measurement data. To record this in one data logger, multiple signal cables are required which may hinder operation.

### **Real-time data transmission using wireless communication technology is difficult**

In order to solve the problem that wired measurement adversely affects operation, wireless transmission of measurement data can be considered. However, at high sampling frequencies, the amount of data measured per unit time is large, and when the number of measurement points increases, it is difficult to transmit data in real time even using current wireless communication technology.

### **Ingenuity is required for high-precision measurement of high-speed sports movements**

Fastest gait measuring results in acceleration and angular velocity occur in a wide range. Therefore, it is necessary to measure at a high sampling frequency using an inertial sensor with a wide measurement range. On the other hand, an inertial sensor with a wide measuring range has a small SN ratio and is easily affected by electrical noise.

### **Highly accurate path estimation is difficult due to integration error**

In order to estimate the posture and movement path during exercise using an inertial sensor, numerical integration of acceleration and angular velocity is required. However, even with the use of accelerometer and gyroscope that are becoming more accurate, it is impossible to completely eliminate integration errors due to circuit noise and sensor drift, and it is difficult to estimate the path with high accuracy. Therefore, in this thesis, wireless inertial measurement unit (WIMU) that supports high-speed movements is developed in order to realize 3D high-precision unconstrained maximum speed gait measurement. Then, 3D motion analysis system that measures and analyzes inertial data acquired is developed to estimate gait parameter at maximum possible precision.

First, WIMU that has high sampling rate, wide measuring range, and large data recording capacity is developed in order to support high-speed operation. With the increase in capacity and decrease in price of storage devices such as microSD cards, a method of storing data in a wearable sensor system without transmitting large-capacity measurement data in real time is considered practical. Control such as measurement start and end of the sensors attached to the body is performed wirelessly. In addition, by using a protocol that allows one-to-many wireless communication, high communication speed is not required and the number of usable sensors become unlimited. By using this wireless sensor system, high-speed, and unconstrained motion measurement becomes possible. After evaluating the hardware and software using a prototype, a sensor system is developed using a surface-mount substrate and the applicability of gait motion measurement is investigated.

There are also some tasks on measuring parameter of the foot plantar.

### **Platform system is lack in accessibility**

Platform system such as force plate are usually embedded in a walkway. However, this kind of system is restricted to use in a laboratory or hospital, and used for barefoot measurements.

### **Force sensors were rigid and have limited flexibility**

Most developed sensors have a common problem which is the inadaptability towards human body curvature during application of sensors. Due to rigid sensor, users are unable to walk as natural as they can because the sensor rigidity affects the comfort of the user.

With the purpose of collecting valid long-period data in all kinds of terrains, the plantar pressure measurement system should have the following features. First, it should be wearable to realize outdoor measurements without limiting activity area of the user. In this case, in-shoe systems are preferred than platform ones. Second, the equipment should not bring inconvenience and discomfort to the wearer in order to make sure the wearer is in a natural status as usual. It is the most important feature for getting real plantar pressure data without interferences.

Multiple use of force sensor for gait mapping is considered better than using mat type sensor. The sensors is embedded in an insole. WIMU is used together with the force sensors to measure gait during swing phase and stance phase. The gait trajectory and COF is calculated and expressed in 3D figure.

The usage of sensor also makes the estimation of blood pressure possible without using cuff. However, to replace measurement using cuff-based methods which provides adequate data in medical field, there are problems with cuffless estimation method.

### **Technique involves measuring the transit time of the pulse pressure wave through the arterial tree**

Measurement of PTT involves detecting the pulse arrival at two separate arterial sites. This can be achieved by using infrared PPG, and differential PTT. The ECG R-wave is often used as a proximal timing point because it is simple to detect and tolerant of motion artifact. However, using ECG itself is expensive, cumbersome, and not wearable to be used during exercise.

Many technical innovations have been developed for cuffless-based BP monitoring such as smart phone applications and wearable device. However, no system has been developed to enable BP estimation and continuous monitoring by a single sensor during exercise that has comparable fidelity to the cuff-based method. In this thesis, system for recording BP without cuff for measurement during exercise or hard work is developed. A novel system for estimation of systolic BP that requires only one sensor for capturing PPG signal is proposed.

The chapters in this thesis are as follows.

## **Chapter 2 Development of Wireless Inertial Measurement Unit (WIMU)**

This chapter describes the development of a body-mounted wireless inertial measurement device. Hardware and software for wireless inertial measurement equipment is developed and its performance is confirmed. The miniaturization is realized for the purpose of surface mounting.

### **Chapter 3 Principle of gait analysis**

This chapter describes the method of calculating gait parameter from inertial data taken from WIMU. Integration section is constructed to derive 3D trajectory of the toe at minimal error. Calculation of gait parameters is described and detection of running is made possible by using two sensors.

### **Chapter 4 Inertial gait analysis measurement system for large-scale health checkups**

This chapter describes utilization of the developed WIMU in gait analysis for large-scale health checkups. The inertial measurement system is used to estimate gait parameter to find an indicator to evaluate cognitive impairment.

### **Chapter 5 Simultaneous measurement of 3D foot trajectory and center of gravity**

This chapter describes the development of sensor system which can measure gait parameters during swing phase and stance phase. Force sensor is used as an extension to the WIMU and embedded into shoe. WIMU measures gait parameter during swing phase and pressure sensor measures gait parameter during stance phase.

### **Chapter 6 Continuous blood pressure estimation during exercise using pulse photoplethysmographic signal**

This chapter describes a cuff-less method to estimate BP during exercise. Pulse sensor is used to obtain PPG which has high relationship with changes in BP. Linear function is created to estimate systolic BP that matches best for each subject. The WIMU is used as a data logger as well as the measurement unit.

### **Chapter 7 Conclusion**

The results of this thesis are summarized. This thesis describes the possibility of applying wearable sensor to clinical practice by measuring physical performance and biomedical information of human body.

## Chapter 2

# Development of Wireless Inertial Measurement Unit (WIMU)

### 2.1 Introduction

MCS is used widely for measuring motion such as sports movement and filmmaking. Motion capture is the process of recording movement of objects mostly when reflective markers are attached. In order to record movement using MCS, firstly, several infrared cameras are required around the measuring area. Next, reflective markers need to be attached on the targeted object or on specific positions using adhesive tape. Each camera will then record the movement of reflective marker in 2 dimensional coordinate, combining record data from all cameras gives coordinate of the marker in 3 dimensional space. Motion capture offers several advantages such as low latency, recorded marker's position is less than 1 [mm] in error, and results obtained is close to real time.

However, MCS are very costly and some fundamental knowledge is needed to operate one. Since the system uses infrared light to capture the reflective marker, it is almost impossible to record motion outdoors especially during the day. Moreover, the marker must always be visible to the cameras for tracking. This limited the measurable movement and also limited the activity area of the user. Furthermore, it takes time to make preparation from setting the camera to attaching the markers before shooting can start.

On the other hand, there are many researches who use inertial sensor such as acceleration sensor, gyro sensor, and geomagnetic sensor which are equippable on objects or body for motion measuring since plenty of time can be saved on preparation and it has no limitation on space of measuring compared to MCS<sup>[14]</sup>. However, the downsides of using inertial measurement system instead of MCS are the low precision in measuring mainly



caused by integration errors due to circuit noise and sensor drift, and it is difficult to estimate the path with high accuracy.

This chapter propose improvement on the older version of the WIMU developed to measure normal gait for better experience in motion measuring. The author determined its specification and evaluated the functionality of the system in both hardware and software to measure fast motion. After the function of the sensor system is tested, the author designed and made it to be compact and sturdy to implement body surface mounting of the sensor.

## 2.2 Overview of WIMU

During fast motion, large acceleration and angular velocity occur, and to measure these, sensor with wide measuring range is necessary. In addition to sensor which has small measuring range, the author introduced sensor which has wide measuring range. Two types of inertial sensors with different measuring ranges are used for acceleration sensor and gyro sensor. Sensor with small measuring range is called ‘high sensitivity sensor’ and sensor with large measuring range is called ‘low sensitivity sensor’. The outline of the whole sensor unit is as shown in Fig. 2.1. These sensors are programmed to measure at sampling rate of 100 [Hz]. WIMU is made of two circuit boards superimposing each other. One of the circuit board consists of high sensitivity acceleration sensor, high sensitivity gyro sensor, geomagnetic sensor, microprocessor unit (MPU, dsPIC33FJ128GP802, Microchip Technology Inc.), wireless communication module (XBee, MaxStream, Digi International Inc.), and microSD card slot. Another one consists of low sensitivity acceleration sensor and low sensitivity gyro sensor. Both circuit boards are connected vertical to a board which consists of controller switches, LEDs for information display, USB slot with charging function, and connected to lithium ion battery. Depending on the contents of experiment, the sampling rate of the sensor can be raised to 1 [kHz] to cope with extremely fast movement and also to record vibration precisely. Simple commands such as ‘start’ and ‘end’ can be send wirelessly with remote controller.

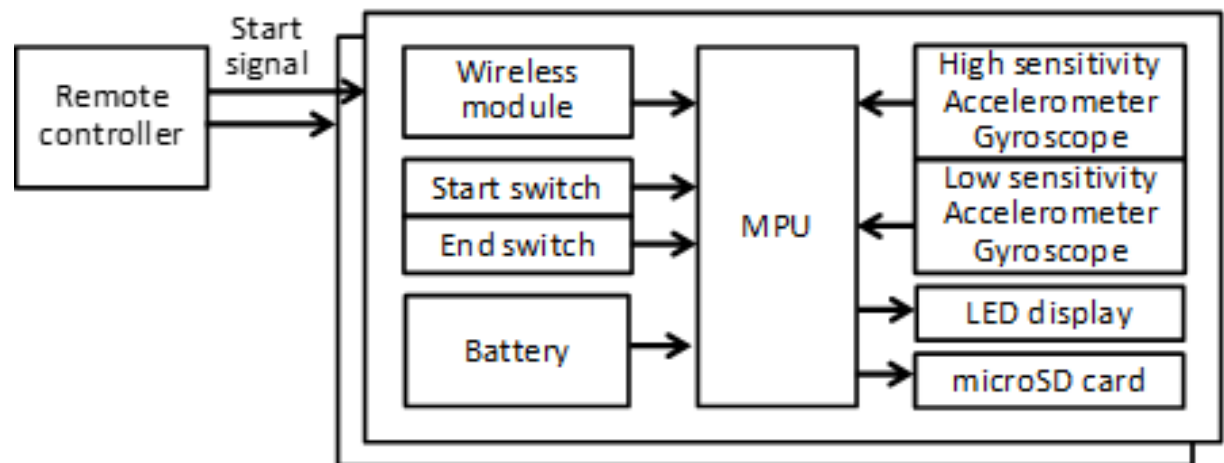


Fig. 2.1: Block diagram of inertial measurement system.

## 2.3 Hardware and software structure

The MPU used on this sensor system has 10 pins which can be used as AD converter. Power-supply voltage of the MPU is 3.3 [V]. To cope with various and changing speed of movement, the author uses two types of sensors with different ranges of measurement. The high sensitivity sensor is necessary to record minute motion precisely and low sensitivity sensor is used for recording extremely fast motion which cannot be measured by high sensitivity sensor. Fig.2.2 and Fig.2.3 shows the structure of circuit board with high sensitivity sensors, Fig.2.4 and Fig.2.5 shows the structure of circuit board with low sensitivity sensors, Fig.2.6 and Fig.2.7 shows the switch board, and Table 2.1 shows the list of components. The author uses 3 axes high sensitivity acceleration sensor and 3 axes gyro sensor (MPU-6050, InvenSense Inc.) in which the measuring range of the acceleration sensor is  $\pm 16$  [G] and measuring range of the gyro sensor is  $\pm 2000$  [deg/s]. The author uses 3 axes low sensitivity acceleration sensor (ADXL375, Analog Devices Inc.) with measuring range of  $\pm 200$  [G] and two 2 axes low sensitivity gyro sensors (LPY4150AL, STMicroelectronics) with measuring range of  $\pm 6000$  [deg/s]. The two low sensitivity gyro sensors were arranged to make 3 axes which make right angle to each other. Apart of these sensors, a 3 axes geomagnetic sensor (HMC5883L, Honeywell) is also used in the sensor system. All of the sensors work on 3.3 [V] power supply. Eventually there are 15 channels for data recording with 2 byte precision and each one is recorded at sampling rate of 100 [Hz] which means the volume of data recorded per second is 3000 bytes. These data are sent and saved directly into microSD card. The author uses MaxStream's XBee S1/S2 for radio frequency RF module. Wireless communication is used when controlling the sensor unit from a remote controller and when checking connection and functionality of the sensor from computer. Lithium ion polymer battery (110 [mAh], 3.7 [V]) is used to power up the sensor unit.

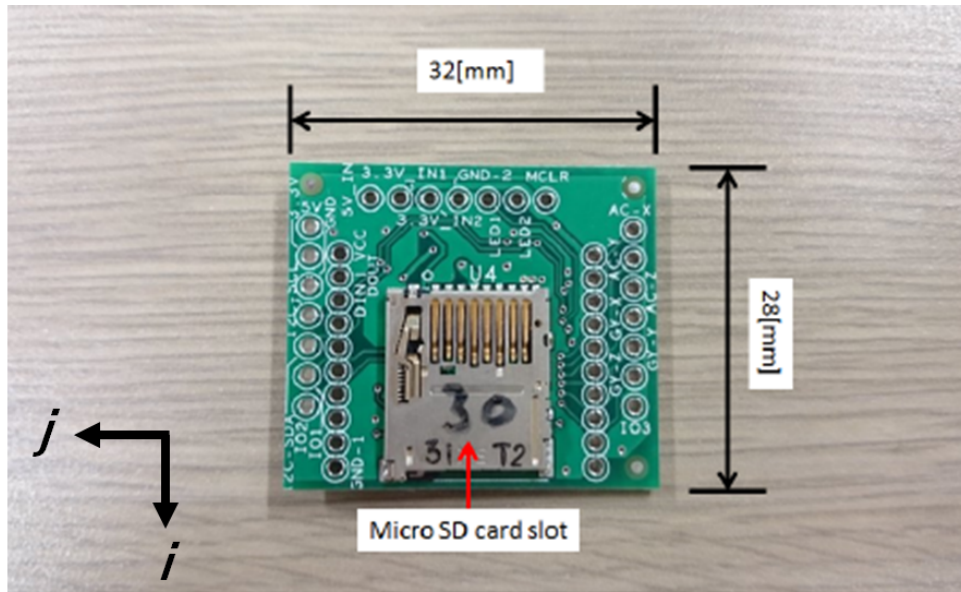


Fig. 2.2: Front of the high sensitivity sensor board

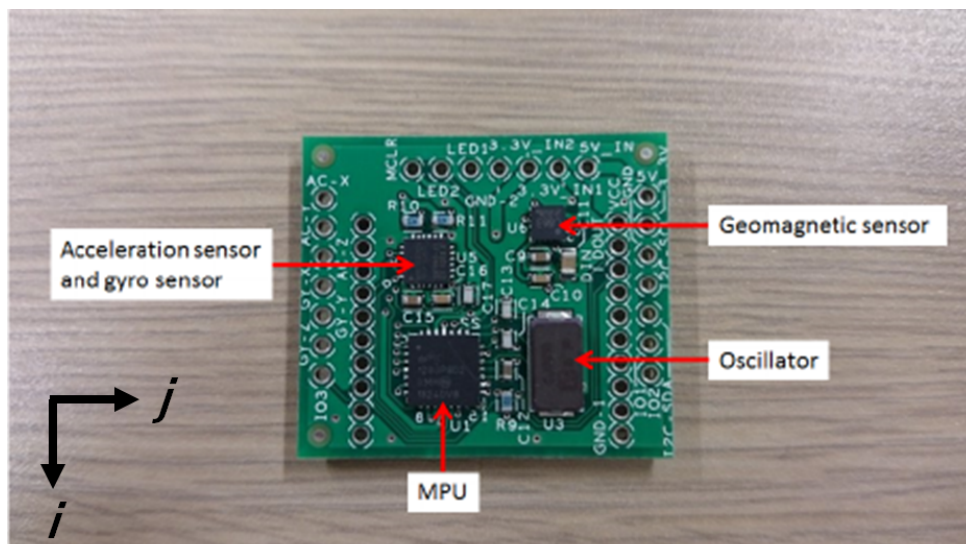


Fig. 2.3: Back of the high sensitivity sensor board

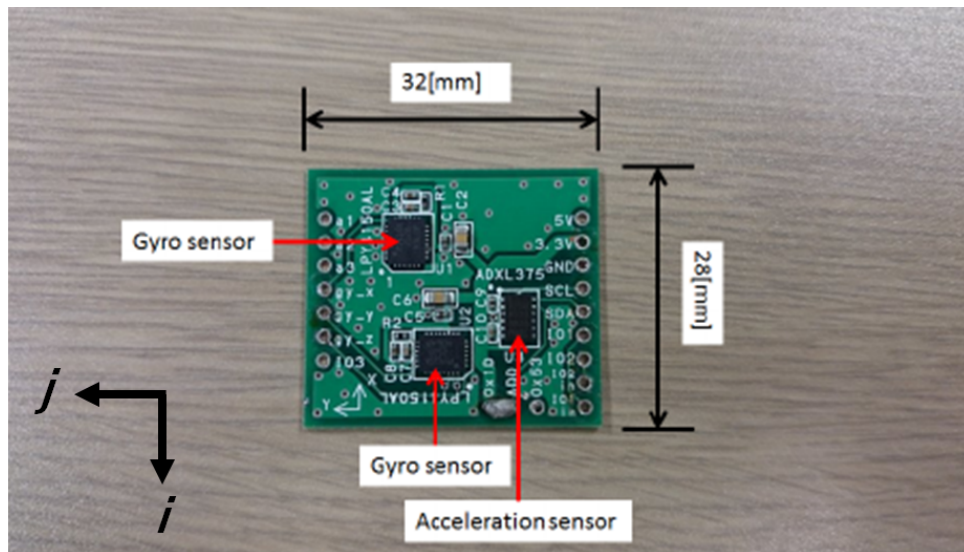


Fig. 2.4: Front of the low sensitivity sensor board

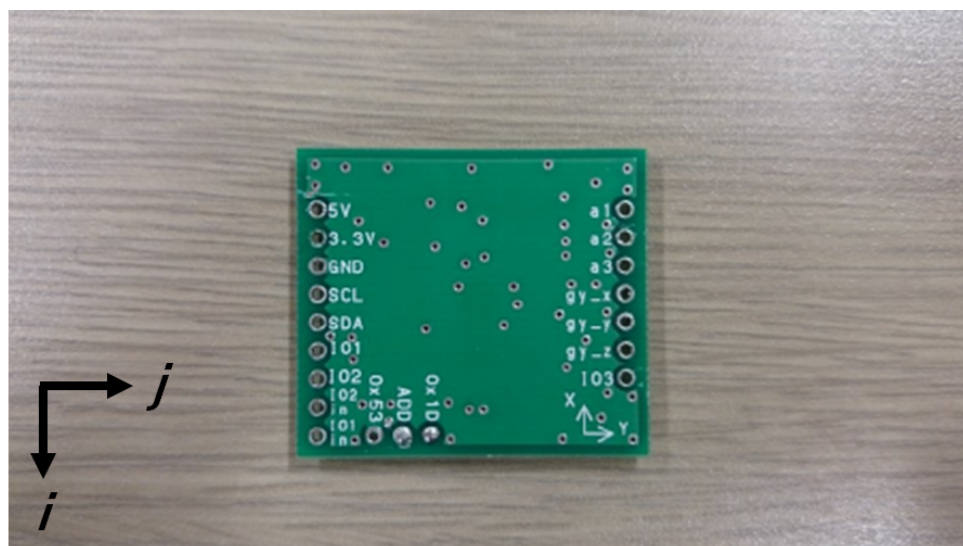


Fig. 2.5: Back of the low sensitivity sensor board

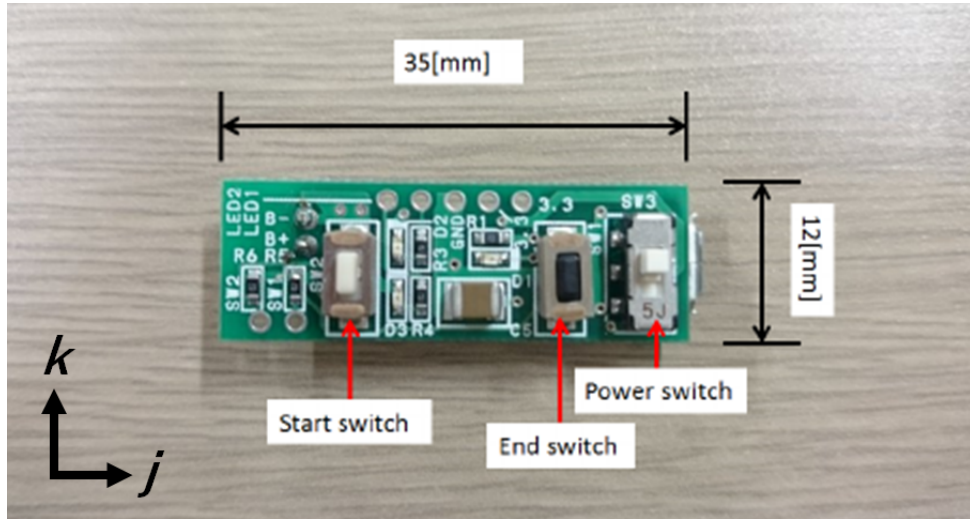


Fig. 2.6: Front of the switch board

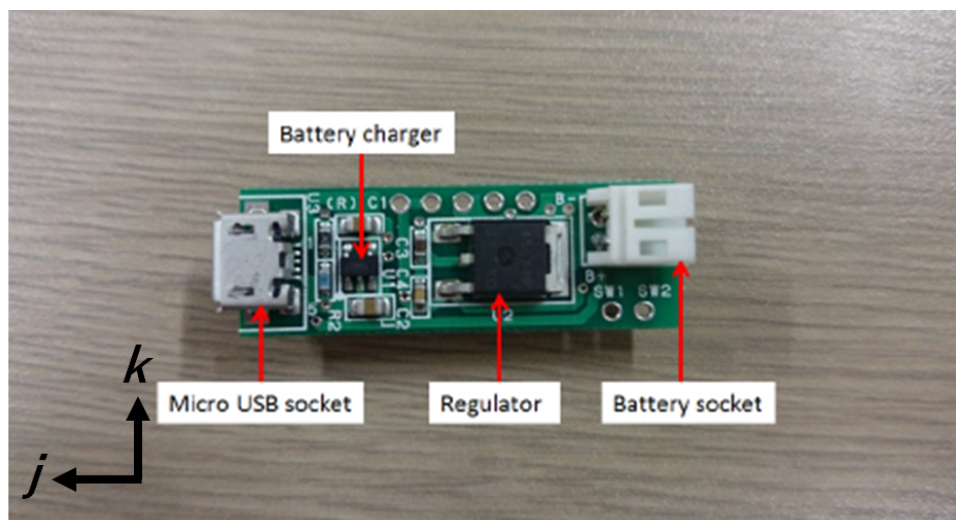


Fig. 2.7: Back of the switch board

Table 2.1: List of components

Component name	Pattern number	Manufacturer	Specification
MPU	dsPIC33FJ128GP802	Microchip Technology	28 pin
RF module	XBee	MaxStream	S1, S2
Acceleration sensor	MPU-6050	InvenSense Inc.	/ 16 [g]
Gyro sensor			/ 2000 [dps]
Acceleration sensor	ADXL375	Analog Devices Inc.	/ 200 [g]
Gyro sensor	LPY4150AL	STMicroelectronics	/ 6000 [dps]
Geomagnetic sensor	HMC5883L	Honeywell	/ 8 [Gauss]



## 2.4 WIMU for surface mounting

After the operation of WIMU in term of hardware and software is checked using discrete electronic components on the breadboard, the author confirmed that the WIMU works just as specified. Circuit boards for surface mounting are made to achieve small and light sensor unit. The sensor components are arranged compactly to fit into two small circuit boards. Circuit diagrams of high sensitivity sensor and low sensitivity sensor are shown in Fig. 2.8 and Fig. 2.9. Circuit diagram of the switch board is shown in Fig. 2.10. These circuit boards, together with a switch board, RF module and a battery are fitted into a case to mount the WIMU on human body. Previous sensor model (Fig. 2.11) only consists of high sensitivity sensor and was powered up by lithium ion polymer battery (GSP652535, 400 [mAh], 3.7 [V], 1.48 [Wh],  $36\pm23\pm5$  [mm]) which can last for about 2 hours when used continuously. However, to make space for the low sensitivity sensor and the sensor unit as small as possible, the author used smaller lithium ion polymer battery (GSP061225, 110 [mAh], 3.7 [V], 0.407 [Wh],  $29\pm11\pm5$  [mm]) which is smaller in size and battery capacity than the previous model. Even though this battery can only last around 30 minutes when used continuously with the new sensor unit, the author decided that 30 minutes would be enough at the large scale health checkups and never used a sensor more than 15 minutes for one subject. This battery can be charged using micro USB power cable when connected to switch board.

The case of the sensor unit is designed using AutoCAD and printed out with 3D printer using ABS resin as material. The whole case is made of 2 parts, the casing and the cover. The dimension of the casing is  $42\pm39.7\pm19$  [mm] and the dimension of the cover is  $42\pm39.7\pm5.5$  [mm]. When the casing is closed with the cover, the overall dimension of the case is  $42\pm39.7\pm21$  [mm]. Figure. 2.12 shows the sensor components, dimension, and weight. Wall is made around the switch board when designing the case. This is crucial to prevent the switch from being pushed accidentally during measurement. Figure 2.13 shows a photo of mounting two WIMUs on toptoe for gait analysis experiment.



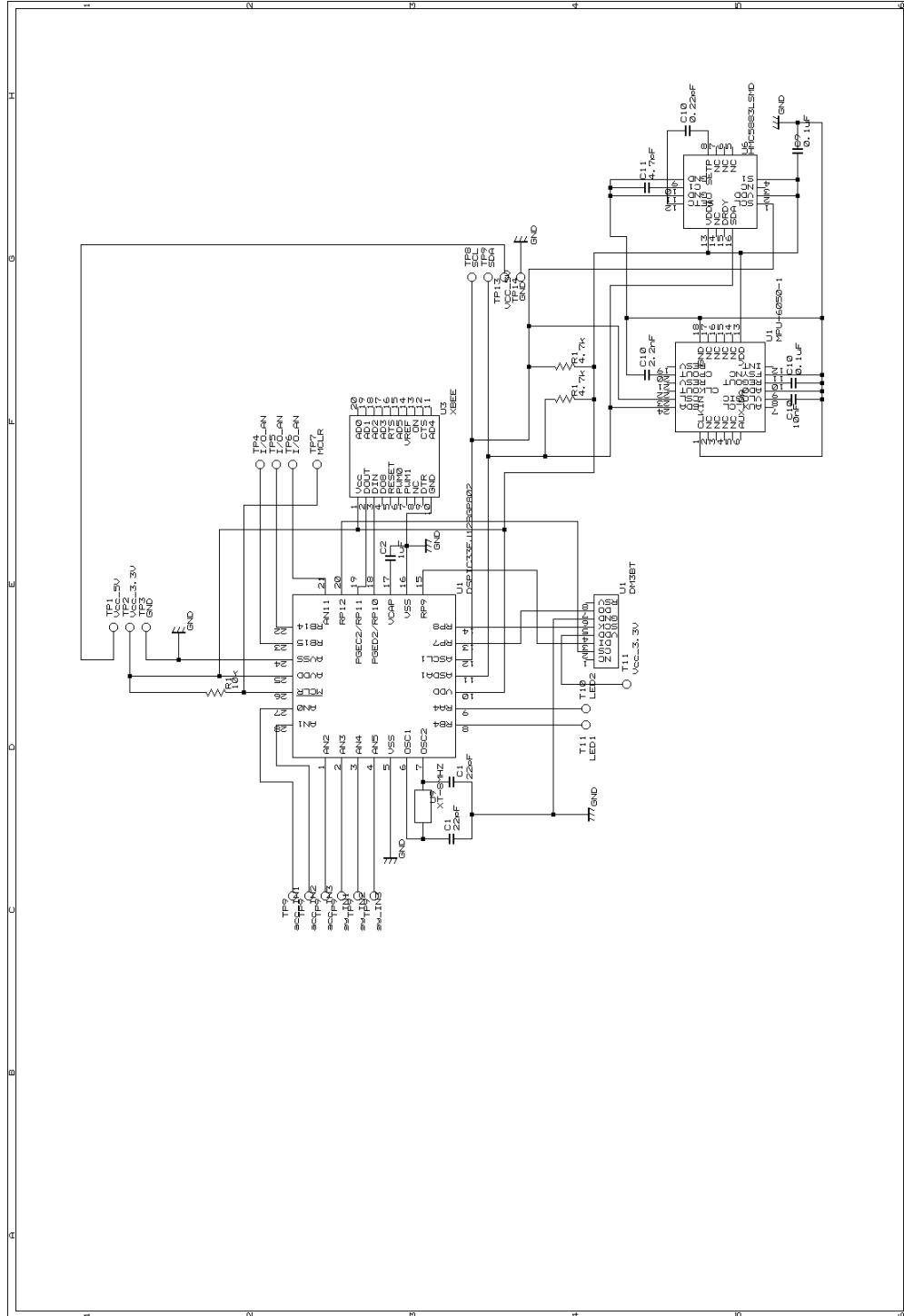


Fig. 2.8: Circuit connection of high sensitivity sensor



18

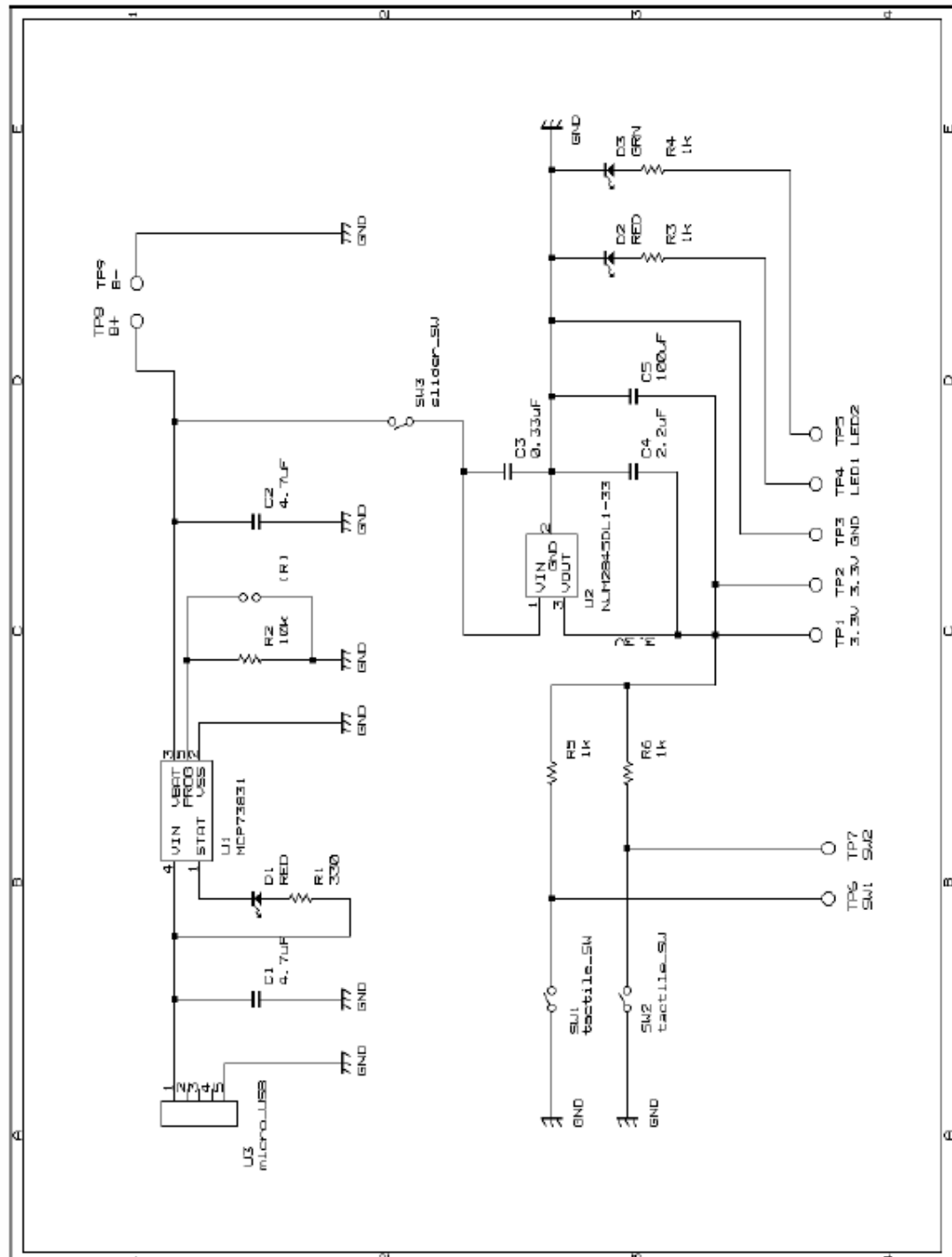


Fig. 2.10: Circuit connection of switch board

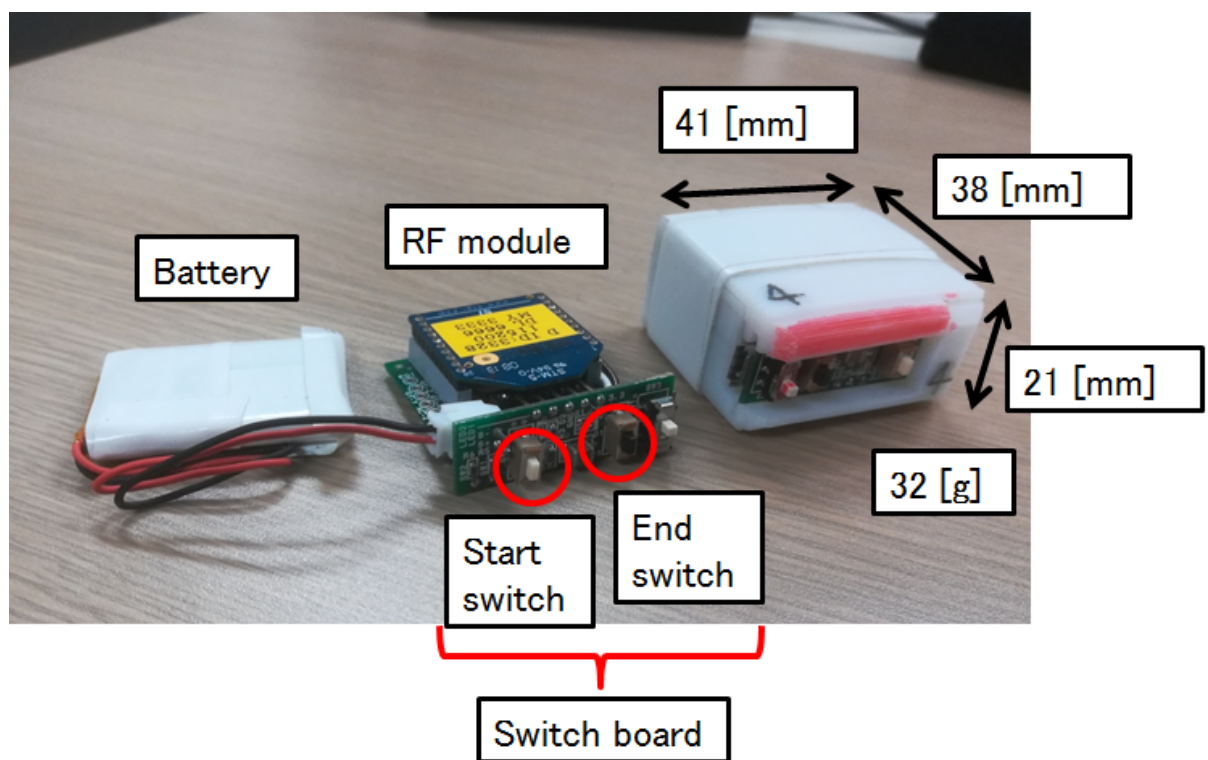


Fig. 2.11: Previous sensor model has battery life that can last up to 2 hours but only consists of high sensitivity sensor.

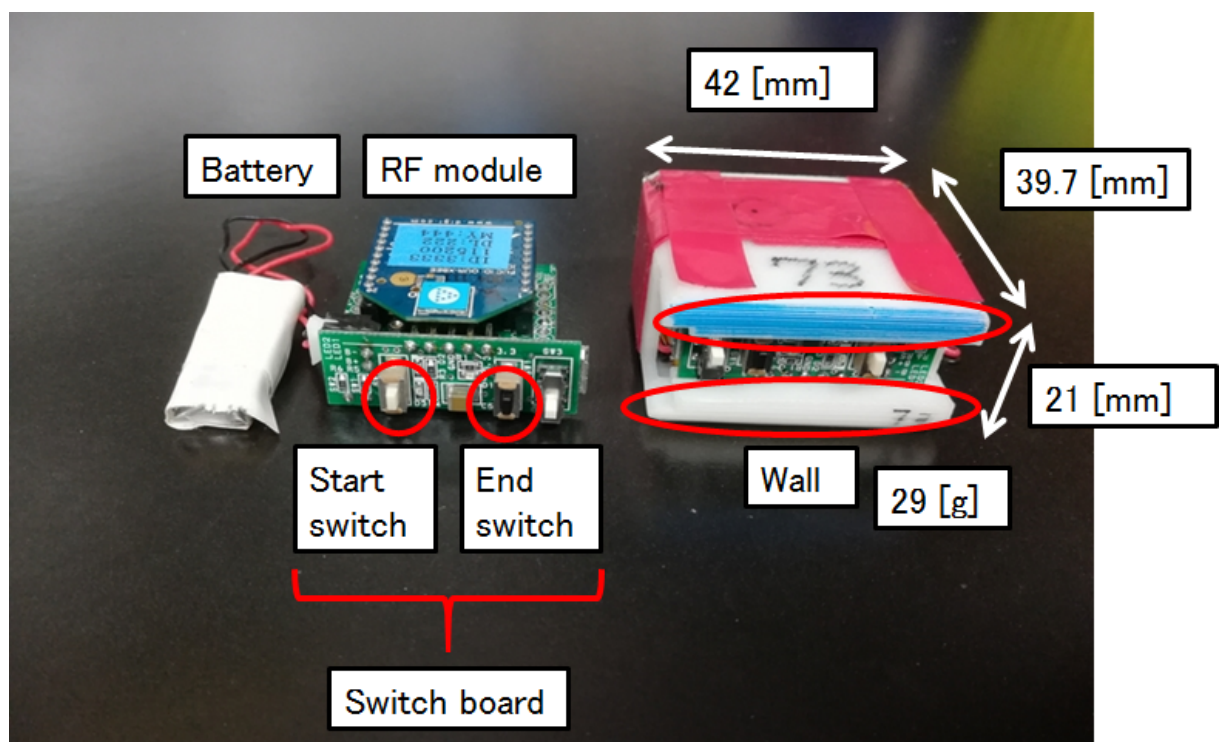


Fig. 2.12: New sensor model has short battery life about 30 minutes but consists of high and low sensitivity sensors. Wall is made around the switch board to prevent the switch from being pushed accidentally during measurement.

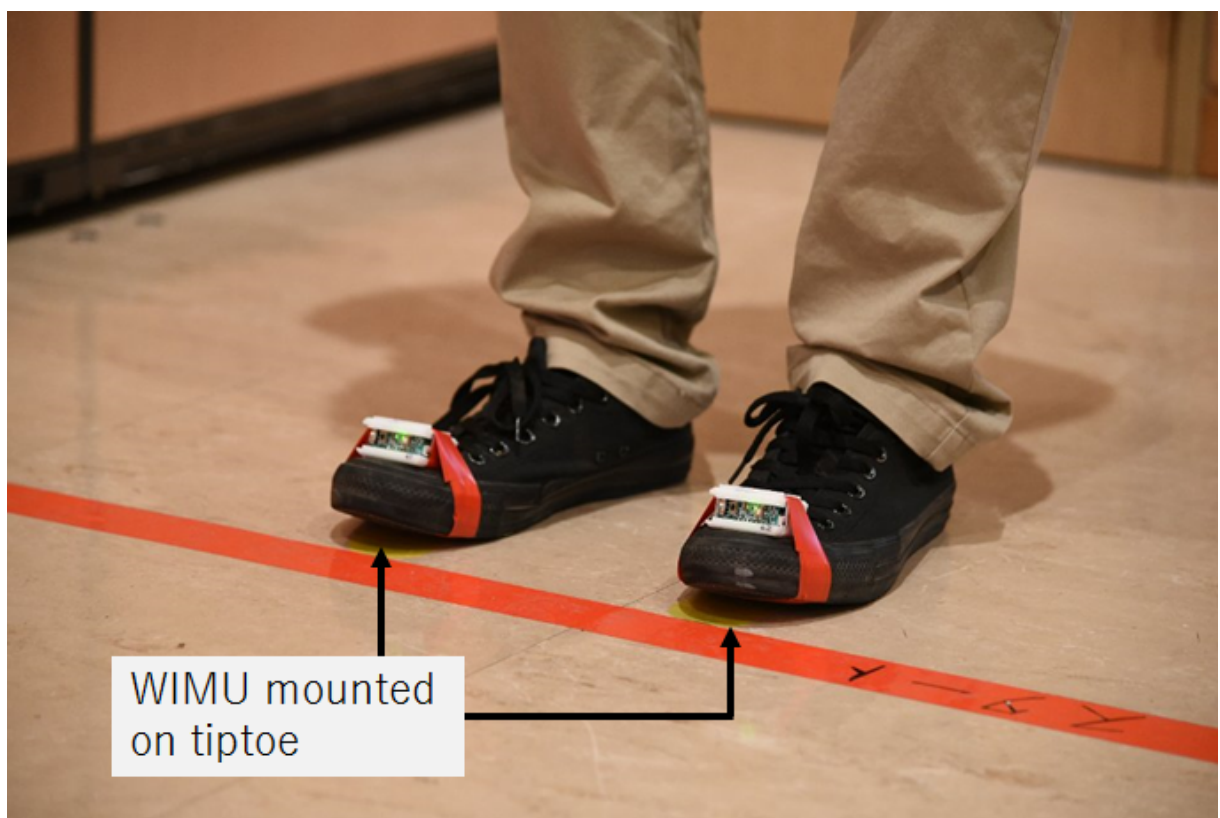


Fig. 2.13: WIMU are mounted on tiptoes for gait analysis experiment.

## 2.5 Interpolation of value exceeding measurement ranges

Gait analysis is performed using measured values of acceleration and angular velocity obtained from sensor attached to the toe. However, when measuring fastest gait of athletes and young persons especially, the acceleration and the angular velocity may exceed the measurement range of the high-sensitivity sensor used<sup>[15]</sup>. In this case, measurement values outside the measurement range cannot be obtained and the accuracy of gait analysis becomes low. Therefore in this thesis, in addition to the high sensitivity sensor, the author introduced low sensitivity sensor with wider measurement range although the resolution is lower than that of the high sensitivity sensor.

When the measured value of the high sensitivity sensor exceeds the predetermined threshold value, value over the threshold value is interpolated using the measured value of the low sensitivity sensor at the same time. The acceleration threshold is set at  $/100$  [m/s<sup>2</sup>] and the angular velocity threshold is set at  $/1000$  [deg/s]. Figure 2.14 shows the procedure of interpolation of value exceeding measurement ranges.

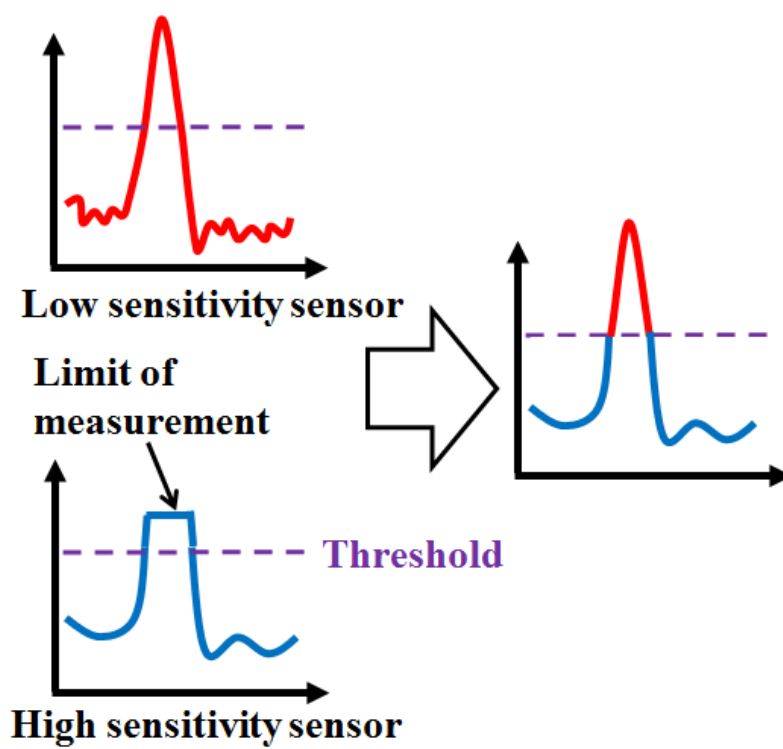


Fig. 2.14: When the measured value of the high sensitivity sensor exceeds the threshold, the measurement value of the low sensitivity sensor is used.



# Chapter 3

## Principle of gait analysis

### 3.1 Construction of integration section

#### 3.1.1 Distinction between stance phase and swing phase

Figure 3.1 shows the state of foot during gait. The gait direction is defined as x-axis, the direction to the left during gait is defined as y-axis, and the upward direction is defined as z-axis. The elapsed time from a heel contact (HC) to the next HC of the ipsilateral leg is called the gait cycle and is divided into the stance phase and the swing phase. The stance phase refers to the section from the HC to the toe off (TO) where the foot portion is in contact with the support surface. The time from the HC of one leg to the toe off of the other side of the leg is called double support phase, and the time from the TO of one leg to the HC of the same leg is called a single support phase. In addition, the swing phase refers to the section in which the foot portion is apart from the support surface. The swing phase is divided into three phases. The period in which the foot has the acceleration to the front is called the acceleration phase, the period in which the foot has almost constant speed is called the mid swing phase, and the period in which the foot has deceleration from the acceleration direction is called deceleration phase<sup>[16]</sup>.

Gait analysis is performed for each step. Integration section is taken from section of entire swing phase including part of section of the stance phase. Velocity is derived by integrating the acceleration obtained from the sensor attached to the toe and the movement path of the toe part is derived by further integration of the velocity. In this thesis, as shown in Fig. 3.2, the swing phase and the stance phase are distinguished based on the angular velocity of the plantar flexion and dorsiflexion. Fig. 3.3 shows the procedure for distinguishing the  $n$  step of swing phase and stance phase. When the foot is swing up,

minimum angular velocity  $c_n$  is detected. From this, it can be inferred that the positive peak value of angular velocity immediately before  $c_n$  is the toe-off action, and the positive peak value  $b_n$  immediately after  $c_n$  is the ground contact action. Therefore, it can be judged that the section from  $a_n$  to  $b_n$  including  $c_n$  is the swing phase, and the section between  $b_{n-1}$  to  $a_n$  and  $b_n$  to  $a_{n+1}$  which comes before and after the swing phase section is the stance phase.

### 3.1.2 Integration section determination

#### Conventional method

The method of determining the integral section for normal walk is explained using Fig. 3.4. The minimal value  $c_n$  indicating swing phase is found, and the TO time  $a_n$  and the HC time  $b_n$  are detected from the peak values of the angular velocities occurred during plantar flexion and dorsiflexion before and after the minimal value. This is repeated as many times as the minimum values are found. The integration section is derived by determining the integration section start time  $S$  and the end time  $E$  which are derived by multiplying  $T_a$  with  $A$  and  $T_b$  with  $B$  where  $T_a$  is the time duration between a current TO time and the previous TO time,  $T_b$  is the time duration between a current TO time and the next TO time,  $A$  is the percentage of time duration until the starting time of the swing phase, and  $B$  is the percentage of time duration until the ending time of the swing phase. Note that  $A$  and  $B$  are determined in trial and error by various experiment so that the error between the estimated distance and the actual distance of a gait becomes the smallest.  $A$  and  $B$  are calculated as follows.

$$A = 117.71 \pm \left( \frac{T_a}{2} \int^2 192.75 \pm \right) \frac{T_a}{2} \left( + 88.76 \quad [\%] \right) \quad (3.1)$$

$$B = 115.47 \pm \left( \frac{T_b}{2} \int^2 168.66 \pm \right) \frac{T_b}{2} \left( + 117.25 \quad [\%] \right) \quad (3.2)$$

For walking cycle of 0.8 [s/step],

$$A = 30 \quad [\%] \quad (3.3)$$

$$B = 64 \quad [\%] \quad (3.4)$$

were set as constant values. However, this method was initially developed for the use during experiment of forward walking, side stepping, and backward walking at normal

speed. With this method, the error of walking distance estimation may become large and is not compatible to short walking cycle at high speed walking. Therefore, the trend and characteristics need to be identified and based on the trend, a new integration section determination method is constructed so that the error of walking distance estimation becomes small.

### **Proposed method**

From past research, it was found that the accuracy of maximum speed walking in the large-scale health checkups is improved by setting the integration section based on the minimum value of the synthetic angular velocity within a specific range<sup>[15]</sup>. The reason why the accuracy was improved is that when the synthesized angular velocity is small, the motion is relatively calm, and the estimation error is small when the posture is estimated and results in the improved accuracy. The procedure for determining the integration section is shown as follows (Fig. 3.5). First, let the time of the TO of the target gait cycle be the origin, and let the section of the swing phase be 100 [%]. Subsequently, the time at which the synthesized angular velocity is minimum within the range of  $-45 / 10$  [%] is taken as the integration start time. Next, the time when the combined angular velocity is minimum within the range of  $140 \pm 10$  [%] is taken as the integration end time, and gait analysis is performed step by step based on the defined integration section.

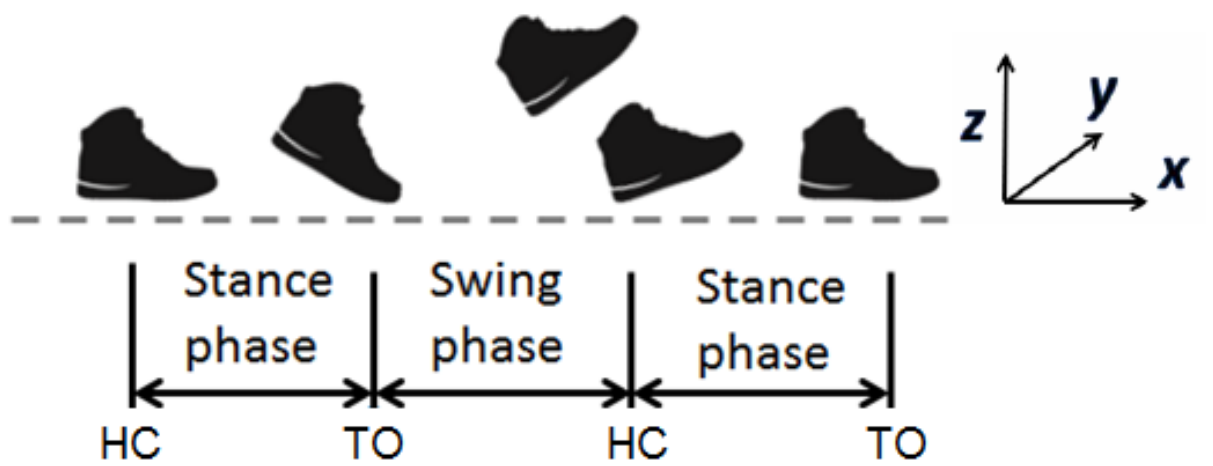


Fig. 3.1: The state of foot during gait is determined by TO time and HC time.

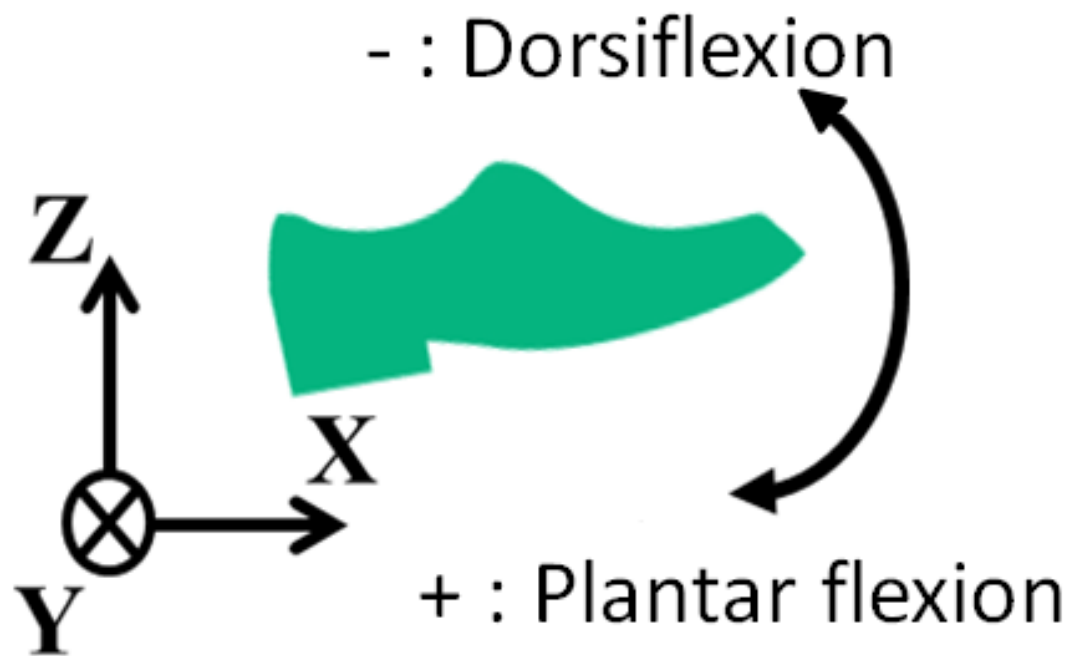


Fig. 3.2: Dorsiflexion is when the toe goes upward and the heel goes downward. Plantar flexion is when the toe goes downward and the heel goes upward.

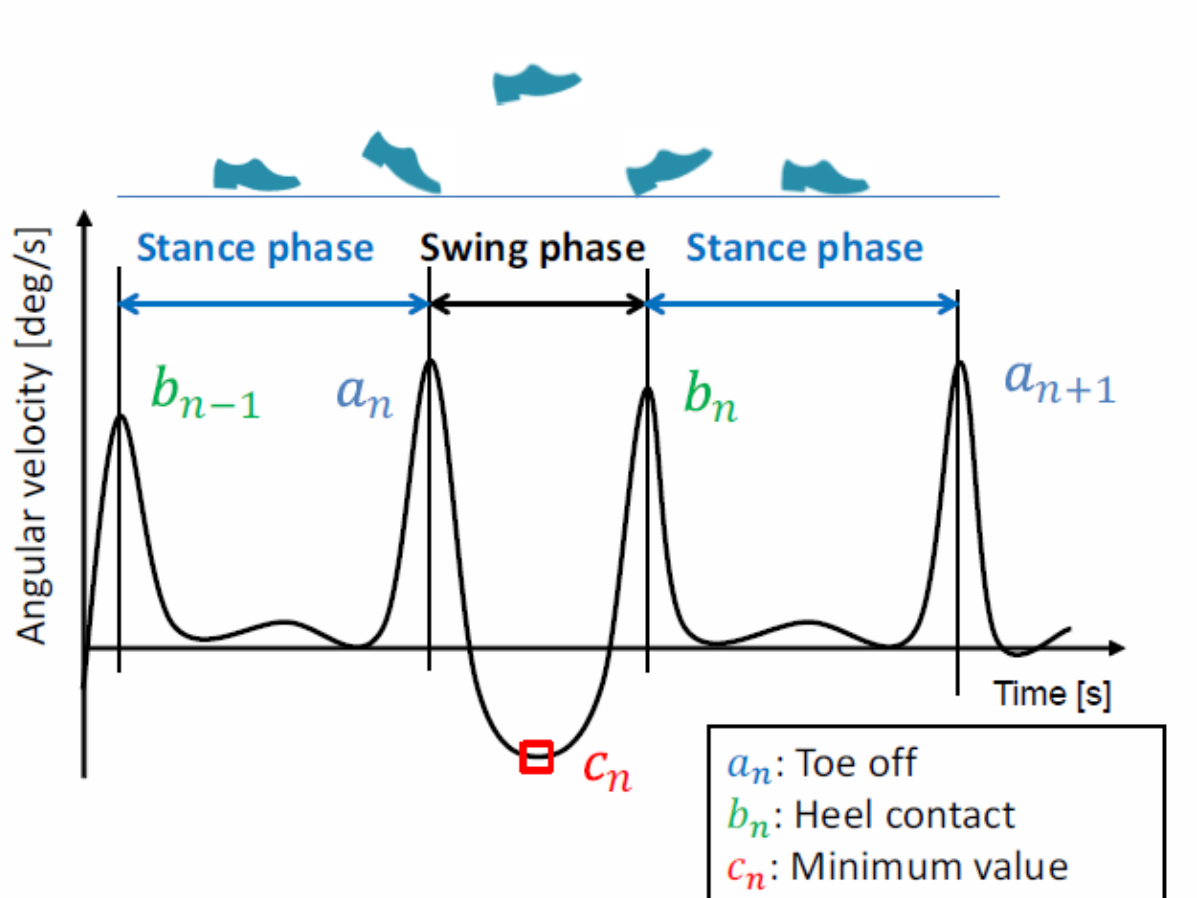
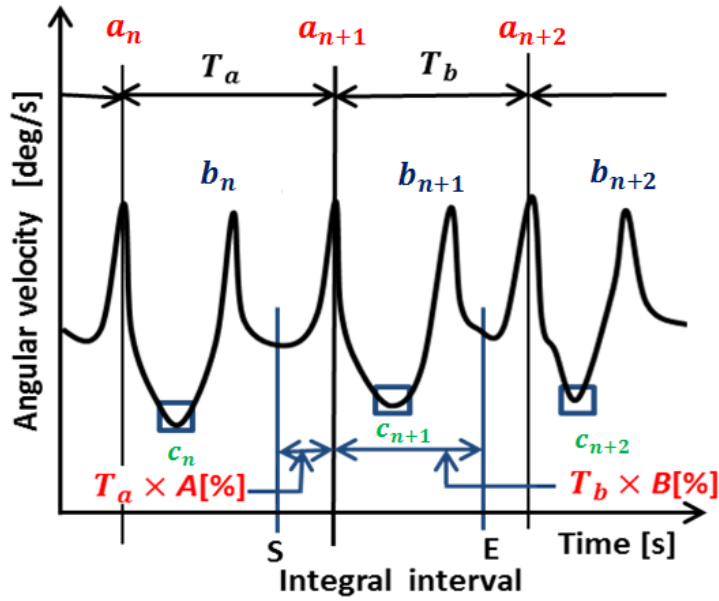


Fig. 3.3: Method of deciding stance phase and swing phase.

### Conventional integration section derivation method

$T_a$  : Time back to the previous TO time  
 $T_b$  : Time elapsed after the last TO time  
 $A$  : Percentage of time until the starting time of swing phase  
 $B$  : Percentage of time until the ending time of swing phase



$a$  : Time of TO  
 $b$  : Time of HC  
 $c$  : Minimal value

$S$  : Starting time of  
integral section  
 $E$  : Ending time of  
integral section

Fig. 3.4: Conventional method of deriving integration section from synthetic angular velocity waveform. This method was initially developed without considering experiment with fast gait.

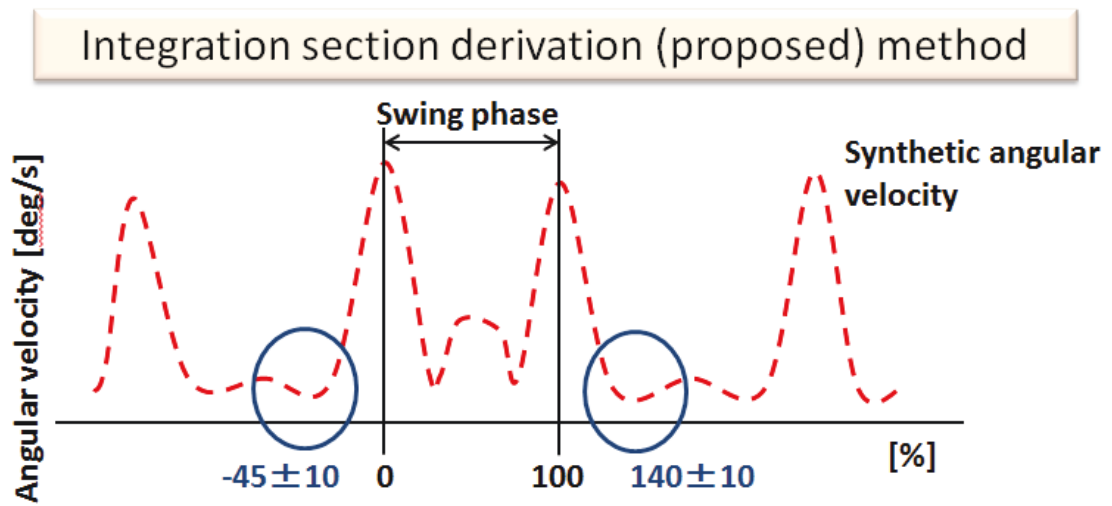


Fig. 3.5: The error in estimation of stride length is small when the integration section is set at  $-45/10$  [%] and  $140/10$  [%] of the swing phase



## 3.2 Theory of measuring bipedal walking motion of human

### 3.2.1 Acceleration derivation on fixed coordinate system

The walking velocity is derived by integrating three-dimensional (3D) acceleration data of the toe of the foot. Further integration derives the 3D trajectory of the toe. The trajectory during gait is calculated step-by-step to minimize effects of drift from the inertial sensor. This calculation is achieved by integrating the translational acceleration of the toe during each swing phase. During integration, 3D acceleration based on the sensor-fixed coordinate system is transformed into acceleration based on the earth coordinate system by defining the sensor coordinate system orientation. Let a three-by-three orientation matrix (OM) representing the sensor orientation with respect to the earth coordinate system be  $[\mathbf{i} \ \mathbf{j} \ \mathbf{k}] = E(t)$ , where  $\mathbf{i}$ ,  $\mathbf{j}$  and  $\mathbf{k}$  are three-by-one orthogonal unit vectors. The acceleration and angular velocity based on the earth coordinate system  ${}^E a(t)$  and  ${}^E \omega(t)$  are calculated from the acceleration and angular velocity based on the sensor-fixed coordinate system  ${}^S a(t)$  and  ${}^S \omega(t)$  using the following equations.

$${}^E a(t) = E(t) {}^S a(t) \quad (3.5)$$

$${}^E \omega(t) = E(t) {}^S \omega(t) \quad (3.6)$$

At this time,  $E(t)$  is a OM having the basic unit vector  $\mathbf{i}$ ,  $\mathbf{j}$ ,  $\mathbf{k}$  of the  $\Sigma$  coordinate system as its component.

$$E(t) = \begin{bmatrix} \mathbf{i} & \mathbf{j} & \mathbf{k} \end{bmatrix} \quad (3.7)$$

$$= \begin{bmatrix} i_x & j_x & k_x \\ i_y & j_y & k_y \\ i_z & j_z & k_z \end{bmatrix} \quad (3.8)$$

Furthermore,

$$a(t) = \begin{bmatrix} a_x & a_y & a_z \end{bmatrix}^T \quad (3.9)$$

$$\omega(t) = \begin{bmatrix} \omega_x & \omega_y & \omega_z \end{bmatrix}^T. \quad (3.10)$$

Symbols  $a_x, a_y, a_z$  and  $\omega_x, \omega_y, \omega_z$  are component of acceleration  $a$  and angular velocity  $\omega$  at  $\mathbf{i}$ ,  $\mathbf{j}$ ,  $\mathbf{k}$  direction. In this thesis, the temporal change in the sensor orientation with respect to the earth coordinate system during walking is estimated by time-integrating the

angular velocity of the sensor from the foot-flat time. The sensor orientation is updated at every sampling period  $\Delta t$  in the integration section as shown below.

$$E(t + \Delta t) = R(t)E(t) \quad (3.11)$$

where  $R(t)$  stands for a rotation matrix, which rotates the OM  $E(t)$  around  ${}^E\omega(t)$  by an angle  $\Delta t \cdot {}^E\omega(t)$ . Rotation matrix  $R(t)$  is defined as follows.

$$R(t) = \begin{bmatrix} \cos \theta + \lambda^2(1 - \cos \theta) & \lambda\mu(1 - \cos \theta) & \nu \sin \theta & \nu\lambda(1 - \cos \theta) + \mu \sin \theta \\ \lambda\mu(1 - \cos \theta) + \nu \sin \theta & \cos \theta + \mu^2(1 - \cos \theta) & \mu\nu(1 - \cos \theta) & \lambda \sin \theta \\ \nu\lambda(1 - \cos \theta) & \mu \sin \theta & \mu\nu(1 - \cos \theta) + \lambda \sin \theta & \cos \theta + \nu^2(1 - \cos \theta) \end{bmatrix} \begin{pmatrix} \lambda \\ \mu \\ \nu \end{pmatrix} \left[ \frac{{}^E\omega(t)}{\|{}^E\omega(t)\|} \right] \quad (3.12)$$

The OM during walking is updated by performing the above rotation conversion for every sampling period in the integration section. With this, the acceleration in the fixed coordinate system can be obtained using equation (3.5).

### 3.2.2 Calculation of OM during stance phase

The three-dimensional translational movement is derived by integrating the acceleration of section during swing phase and a part of stance phase. During this time, it is necessary to know the posture of OM just before the start of integration. The posture of OM is the component in each  $\mathbf{i}$ ,  $\mathbf{j}$ ,  $\mathbf{k}$  as expressed as follows. Fig. 3.7 shows the derivation method of OM in stance phase immediately before the start of integration. Let gravitational acceleration be  $g$  and the angle between  $\mathbf{i}$ ,  $\mathbf{j}$ ,  $\mathbf{k}$  and horizontal plane be  $\theta_x, \theta_y$ , and  $\theta_z$ . During this time, gravitational acceleration  $g$  is facing upward because it is equivalent to perform constant acceleration motion in the upward direction under the influence of gravity on the earth. Moreover, the angle between  $x$  axis and the vector obtained by projecting the  $\mathbf{i}$  axis on the  $xy$  plane is defined as  $\gamma$ .

$$\theta_x = \sin^{-1} \frac{a_x}{g}, \quad \theta_y = \sin^{-1} \frac{a_y}{g}, \quad \theta_z = \sin^{-1} \frac{a_z}{g} \quad (3.14)$$

Suppose that  $\mathbf{i}$  is on the  $x$  axis of the fixed coordinate system ( $\gamma=0$ ). At this time, the initial component of  $\mathbf{i}$ ,  $\mathbf{j}$ ,  $\mathbf{k}$  defined as  $\mathbf{i}_0, \mathbf{j}_0, \mathbf{k}_0$  is searched. The  $x$  component  $j_x$  of  $j_0$  is

expressed as follows.

$$\tan \theta_x = \frac{j_x}{\sin \theta_y} \quad (3.15)$$

when viewed from the positive y-axis direction and

$$j_x = \tan \theta_x \sin \theta_y \quad (3.16)$$

can be obtained. Similarly for  $k_x$ ,

$$\tan \theta_x = \frac{k_x}{\sin \theta_z} \quad (3.17)$$

and

$$k_x = \tan \theta_x \sin \theta_z \quad (3.18)$$

can be obtained. For  $j_y$ , using the cross product formula,

$$k_z = i_x \times j_y - i_y \times j_x \quad (3.19)$$

$$\sin \theta_z = \cos \theta_x \times j_y \quad (3.20)$$

$$j_y = \frac{\sin \theta_z}{\cos \theta_x} \quad (3.21)$$

can be obtained. Similarly component  $k_y$  can also be calculated and becomes the following equation.

$$k_y = i_z \times j_x - i_x \times j_z \quad (3.22)$$

$$= \sin \theta_x \tan \theta_x \sin \theta_y - \cos \theta_x \sin \theta_y \quad (3.23)$$

$$= \sin \theta_y \times \frac{\sin^2 \theta_x + \cos^2 \theta_x}{\cos \theta_x} \quad (3.24)$$

$$= \frac{\sin \theta_y}{\cos \theta_x} \quad (3.25)$$

Eventually, initial OM can be obtained as follows.

$$i_0 = (\cos \theta_x \ 0 \ \sin \theta_x)^T \quad (3.26)$$

$$j_0 = \begin{pmatrix} \tan \theta_x \sin \theta_y & \frac{\sin \theta_z}{\cos \theta_x} & \sin \theta_y \end{pmatrix}^T \quad (3.27)$$

$$k_0 = \begin{pmatrix} \tan \theta_x \sin \theta_z & \frac{\sin \theta_y}{\cos \theta_x} & \sin \theta_z \end{pmatrix}^T \quad (3.28)$$

Also, when  $\gamma \neq 0$ , the OM in the stance phase becomes as follows.

$$\mathbf{i} \ \mathbf{j} \ \mathbf{k} \begin{bmatrix} = R^{z\gamma}(i_0 \ j_0 \ k_0) \end{bmatrix} \quad (3.29)$$

However,  $R^{z\gamma}$  is a rotation matrix that rotates  $\gamma$  around the z-axis of the fixed coordinate system and can be expressed by the following equation.

$$R^{z\gamma} = \begin{bmatrix} \cos \gamma & \sin \gamma & 0 \\ \sin \gamma & \cos \gamma & 0 \\ 0 & 0 & 1 \end{bmatrix} \quad (3.30)$$

Thus,

$$\mathbf{i} = \begin{pmatrix} \cos \gamma \cos \theta_x \\ \sin \gamma \cos \theta_x \\ \sin \theta_x \end{pmatrix} \quad (3.31)$$

$$\mathbf{j} = \begin{pmatrix} \frac{\cos \gamma \sin \theta_x \sin \theta_y}{\cos \theta_x} & \frac{\sin \gamma \sin \theta_z}{\cos \theta_x} \\ \frac{\sin \gamma \sin \theta_x \sin \theta_y}{\sin \theta_y} & \cos \gamma \sin \theta_z \\ \cos \theta_x & \sin \theta_y \end{pmatrix} \quad (3.32)$$

$$\mathbf{k} = \mathbf{i} \pm \mathbf{j}. \quad (3.33)$$

Here, immediately before the start of integration of the first step,

$$\gamma = 0 \quad (3.34)$$

From the second step onwards, from the  $\mathbf{i}$  which is the component of OM just before the end of integration,

$$\gamma = \tan^{-1} \frac{\dot{i}_y}{\dot{i}_x} \quad (3.35)$$

As stated above, the OM during stance phase is updated by calculating  $\gamma$  every time it shifts to the stance phase and substitutes it into the equations (3.31), (3.32), and (3.33). Then, assuming that the calculated OM of stance phase is equal to OM at the integration start time, OM of the subsequent integration section is calculated as OM  $E_n(t)$  immediately after integration start as stated in the next section.

### 3.2.3 Foot movement estimation

In this thesis, toe acceleration  $^E a(t)$  is time-integrated from the time that the foot starts moving ( $t_0$ ) to the time that the foot movement stops ( $t_{\text{end}}$ ) during one stride. At this time, because the integral error accumulates as a result of drifting, sensor noise, sensor system misalignment and wrong estimation of OM caused by sensor vibration, the estimated velocity of the sensor at  $t_{\text{end}}$  rarely becomes zero. However, it is difficult to

measure and remove these errors. On the other hand, the velocity of foot at  $t_{\text{end}}$  becomes zero. Therefore, assuming that the integral error accumulates linearly with time between  $t_0$  and  $t_{\text{end}}$  and setting that the estimated velocity at  $t_{\text{end}}$  is  $v_e$ , the toe velocity  $v(t)$  during one step is modified by subtracting error which increases linearly between zero and  $v_e$  from the time-integrated acceleration. The toe velocity  $v(t)$  is calculated as shown below.

$$v(t) = \int_{t_0}^t {}^E a(\tau) d\tau - \frac{t - t_0}{t_{\text{end}} - t_0} v_e \quad (3.36)$$

Applying this modification method, the toe velocity reaches zero at  $t_{\text{end}}$  in every step. The 3D trajectory of the toe  $P(t) = [P_x(t) \ P_y(t) \ P_z(t)]$  is obtained by further integration of velocity  $v(t)$ . Because no slope exists on the walking surface, the vertical displacement of the sensor at  $t_{\text{end}}$  must be zero. However, integration result of the vertical velocity rarely becomes zero because the assumption that integration error of the acceleration accumulates linearly is applied and the effect of sensor error remains still. Therefore, similar to the modification of the toe velocity, the vertical toe displacement  $P_z(t)$  between  $t_0$  and  $t_{\text{end}}$  is modified by subtracting integration error of vertical velocity from the time-integrated vertical velocity. When the result of integrating vertical toe velocity is  $p_{ez}$  at  $t_{\text{end}}$ ,  $P_z(t)$  is calculated as shown below.

$$P_z(t) = \int_{t_0}^t v(\tau) d\tau - \frac{t - t_0}{t_{\text{end}} - t_0} p_{ez} \quad (3.37)$$

The time trajectory of horizontal displacement of the toe  $D_e(t)$  from the start location of gait ( $t = 0$ ) to the stop location is calculated as shown below.

$$D_e(t) = \sqrt{(P_x(t))^2 + (P_y(t))^2} \quad (3.38)$$

However,  $D_e(t)$  fundamentally includes integration error and differs from the actual displacement with which the subject walked. Therefore,  $D_e(t)$  is modified linearly so that the estimated displacement with which the subject stopped agrees with the actual displacement. When the total walking time estimated by the waveform measured by the inertia sensor is  $t_w$  and the actual displacement obtained by reading the scale on the floor where the subject has stopped is  $D_a$ , the modified horizontal displacement  $D(t)$  can be recalculated as shown below.

$$D(t) = D_e(t) - \frac{t}{t_w} (D_e(t_w) - D_a) \quad (3.39)$$

### 3.2.4 Gait parameters

In the experiment, subjects are asked to walk on 16 [m] walking course and gait parameters are obtained from 10 [m] section between 3 [m] point and 13 [m] point. Gait parameters derived in this thesis are the 10 [m] gait time (GT), stride length (SL), gait cycle (GC), gait velocity (GV), maximum toe angle ( $\theta_{\max}$ ), minimum toe angle ( $\theta_{\min}$ ), maximum toe clearance (TC), and percentage of swing phase ( $S_p$ ). These are calculated off-line based on measured sensor data. Gait parameters obtained during one gait cycle are shown in Fig. 3.8. The GT is derived by first calculating  $D(t)$ . Of those variables,  $D(t)$  of the right and left toe are calculated separately. Then the time at which the horizontal displacement of both toes reached 3 [m] and 13 [m] earlier are defined as  $t_{3m}$  and  $t_{13m}$ . Eventually, GT can be calculated as presented below.

$$GT = t_{13m} - t_{3m} \quad (3.40)$$

The SL is the horizontal displacement of the toe between TO and heel contact HC of the same side of the foot. Assuming the times of TO and HC of the  $n$ th stride as  $t_{TO}(n)$  and  $t_{HC}(n)$ , respectively, then SL of the  $n$ th stride is obtained as shown below.

$$SL(n) = \sqrt{(P_x(t_{HC}(n)) - P_x(t_{TO}(n)))^2 + (P_y(t_{HC}(n)) - P_y(t_{TO}(n)))^2} \quad (3.41)$$

The GC is the elapsed time from one HC on  $t_{HC}(n)$  to the next HC of the ipsilateral leg on  $t_{HC}(n+1)$ . The gait cycle of the  $n$ th stride is calculated as

$$GC(n) = t_{HC}(n+1) - t_{HC}(n) \quad (3.42)$$

The GC is divisible into a stance phase and a swing phase. The stance phase refers to the period from the HC to the TO. The foot is in contact with the support surface in this period. The swing phase refers to the duration between the TO and the following HC. The foot is not in contact with the ground during this period. The TO time is ascertained from the synthesized angular velocity. The HC time is found from the synthesized angular acceleration, which is obtained by differentiating three axis of angular velocity and then synthesizing the results. The synthesized angular velocity reaches a peak at TO, which marks the end of the stance phase and the beginning of the swing phase. The synthesized angular acceleration reaches a peak at HC, which marks the end of the swing phase and

the beginning of the stance phase<sup>[17]</sup>. The GV of the  $n$ th stride is obtained as shown below.

$$GV(n) = \frac{SL(n)}{GC(n)} \quad (3.43)$$

During one gait cycle, which starts with a HC and ends with the successive HC, the maximum toe clearance TC can be found from the peak of the vertical foot displacement  $P_z(t)$ . The toe angle is the amplitude of the angle of the toe direction from the floor. The inertial sensor is attached on the toe tip. Therefore, the toe angle is derived using the elevation angle of the unit vector  $\mathbf{i}$  in OM. Assuming the vertical component of  $\mathbf{i}$  during the swing phase and that of the stance phase as  $i_{sw}$  and  $i_{st}$ , the toe angle  $\theta$  is calculated as presented below.

$$\theta = \sin^{-1} i_{sw} \quad \sin^{-1} i_{st} \quad (3.44)$$

Maximum and minimum toe angles  $\theta_{\max}$  and  $\theta_{\min}$  are obtained at every swing phase. Also,  $S_p$  is a ratio of the duration of the swing phase to the duration of one gait cycle. The time of TO within the  $n$ th gait cycle is  $t_{TO}(n)$ . Therefore,  $S_p$  of the  $n$ th step is defined as shown below.

$$S_p(n) = \frac{t_{HC}(n+1) - t_{TO}(n)}{GC(n)} \quad (3.45)$$

### 3.2.5 Detection of running

Subjects are asked to walk as fast as possible through 10 [m] gait time measurement. However, running accidentally or intentionally occurs, causing inappropriate evaluation of the health checkup. Therefore, the measured data evaluated as a running condition must be removed from the experimentally obtained results. Running technically requires both feet to be off the ground during a stride, although walking always has at least one foot touching the ground. The gait condition is ascertained by the HC and TO time of both feet. During walking, TO of one foot occurs after the HC of the other foot, meaning both feet touch the ground simultaneously. During running, TO of one foot occurs before the HC of the other foot, meaning that both feet are off from the ground at a time.

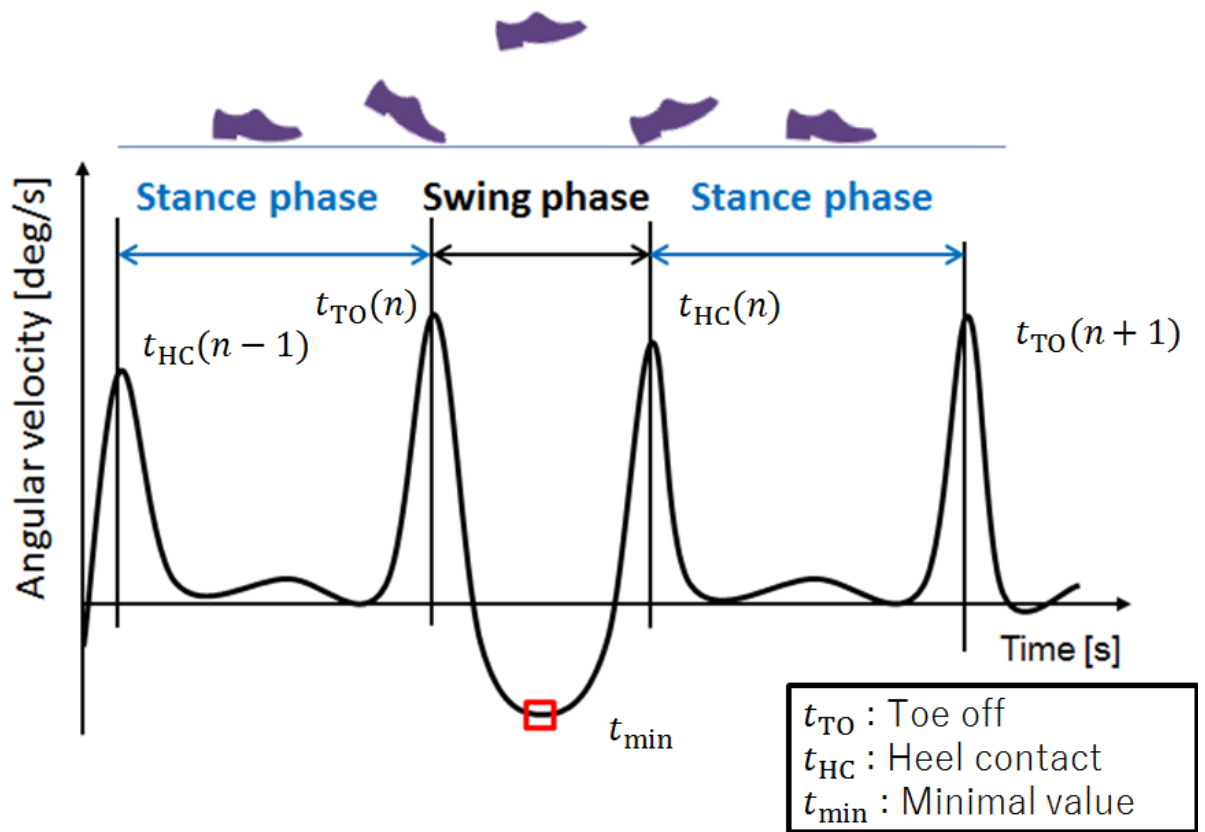


Fig. 3.6: Phases during a gait are roughly divided into two, the stance phase and the swing phase. The swing phase starts with a TO and ends with a HC. In synthetic angular velocity waveform, maximal value is observed during TO and HC.



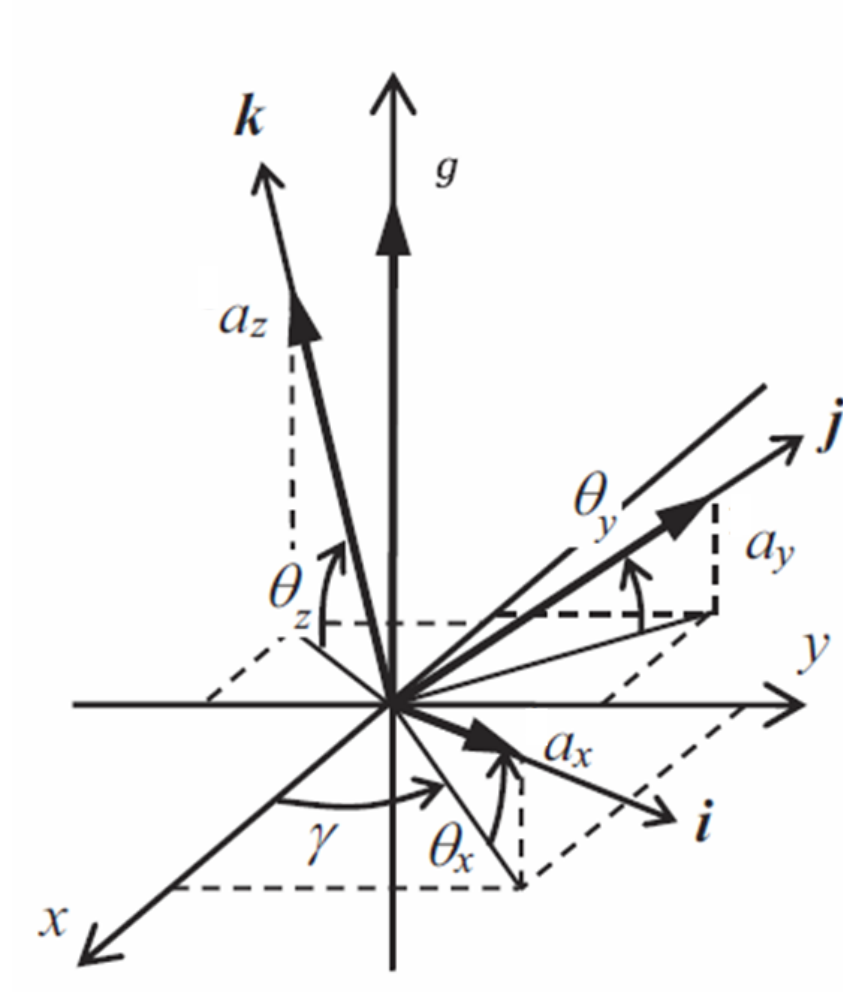


Fig. 3.7: Definition of coordinate system to the OM during the stance phase.  $g$  is the gravitational acceleration and the angles  $\theta_x, \theta_y, \theta_z$  are relative to horizontal plane  $i, j, k$ .

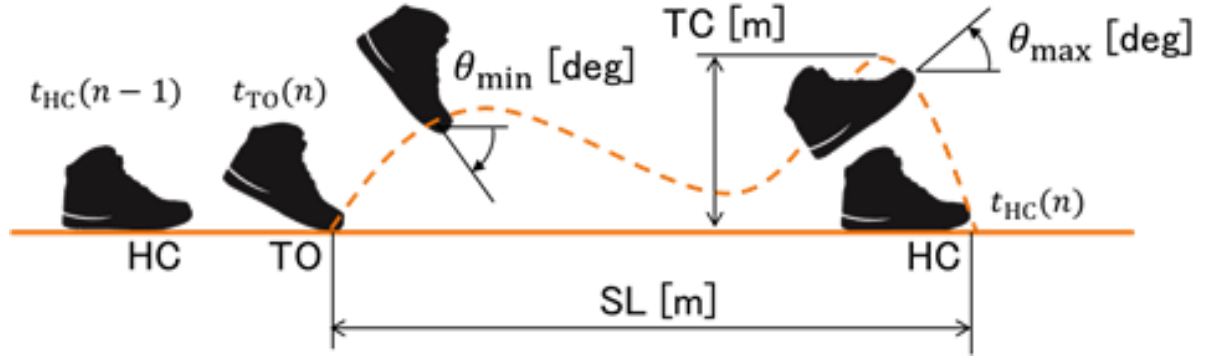


Fig. 3.8: Gait parameters estimated using the sensor unit during one gait cycle (GC). Stride length, maximum toe angle, minimum toe angle, and toe clearance are represented as  $SL$ ,  $\theta_{\max}$ ,  $\theta_{\min}$ , and  $TC$ , respectively.  $SL$  is the distance between toe off (TO) and heel contact (HC).  $t_{HC}$  and  $t_{TO}$  are time of HC and TO, and  $n$  is the number of steps. GC is the time difference between  $t_{HC}(n)$  and  $t_{HC}(n-1)$ . Gait velocity (GV) and percentage of swing phase ( $S_p$ ) are also obtained.

# Chapter 4

## Inertial gait analysis measurement system for large-scale health checkups

### 4.1 Introduction

Dementia is the loss of cognitive functioning such as thinking, memory, and reasoning as well as behavioral capabilities to such an extent that it interferes with daily life activities. Dementia is usually regarded as a predominantly cognitive disorder. However, aside from cognitive decline, discussion has been made on neurocognitive function as related with physical activity<sup>[18]</sup>. Recently reported evidence suggests that gait abnormalities can also be found in early stages of the disease<sup>[19]</sup>. Gait abnormalities include decreased walking speed, step length, step frequency, and increased gait variation<sup>[20–22]</sup>. People with risk of dementia also tend to walk shorter distances, which can be caused by declining physical function<sup>[23]</sup>. These gait disturbances are greater than the gait impairments that can be expected to result from normal aging process<sup>[24]</sup>. Current evidence suggests that walking is related closely to executive function<sup>[25–27]</sup>. Impaired executive function has been related to decreased walking speed, increased stride time variation, increased incidence of falls, and decreased performance of complex motor tasks<sup>[28,29]</sup>. Although fall risk and gait have often been the object of investigations in adults with dementia, few studies have yet investigated the relation between executive function and measures of gait variation and stability, which are associated with fall risk<sup>[30–34]</sup>. A clearer picture of the relation between gait parameter and executive function can be of great clinical relevance with respect to the diagnosis of dementia and the early detection of increased fall risk in this population.

The School of Medicine of Hirosaki University has conducted health examinations for approximately 1000 citizens of Hirosaki city in Japan per year since 2005 as part of a cohort study. This project has been conducted to raise the health level of residents in the city and to extend the average healthy lifespan. The 10 [m] fastest gait examination has been conducted to investigate signs of cognitive impairment by measuring the gait time, which is known as an indicator of predicting dementia<sup>[35]</sup>. However, the earlier method requires that numerous staff members measure the gait time with a stopwatch by following subjects back and forth throughout a walking course<sup>[36]</sup>. Moreover, some subjects may run during the examination for good results, which leads to incorrect diagnostic results. It is difficult to visually judge whether they are walking or running. Therefore, movement of both feet for every step must be investigated to predict the deterioration of neurocognitive functions, such as that related to dementia, and to detect other disease precursors.

Gait parameters are obtainable from analysis of foot kinematics. Although spatiotemporal gait analysis is conducted using MCS, such a system is unsuitable when measuring numerous subjects in a short time as with a large-scale health checkup because it requires a dedicated laboratory and appropriate clothing of subjects. Ambulatory measurement devices using body-worn inertial sensors can overcome some of these limitations and enables analyze gait kinematics. Use of inertial sensors in physical activity monitoring have gained popularity<sup>[37–40]</sup> because more accurate, more inexpensive, and smaller sensors are available with the advancement of MEMS technology. Many systems are proposed to classify various physical activities such as walking, running, sitting, standing, walking upstairs or downstairs, and cycling by placing sensors on human body<sup>[41–44]</sup>. Activity monitoring systems using accelerometer can also be applied to identify different gait parameters and walking pattern classification<sup>[45]</sup> and abnormal gait detection<sup>[46]</sup>. However, the inertial measurement system is hardly used for quantitative evaluation in medical field because measurement method using accelerometer and gyroscope are adversely affected by measurement errors and integration drifts. Furthermore, many researchers have worked on quantitative analysis of normal velocity movement utilizing inertial sensor to overcome shortcoming of the inertial sensor extensively<sup>[47–50]</sup>. However, few researches deal with quantitative measurement of high-speed movement like the 10 [m] fastest gait examination because amplitudes of acceleration and angular velocity measured are so large that they exceed the measurement range of the inertial sensors commonly used.

In this chapter, the inertial measurement system for 10 [m] fastest gait examination at large-scale health checkups is proposed, where numerous subjects take the examination simultaneously. The sensor system consists of an accelerometer and gyroscope with a wide measurement range to investigate the movement of one foot during fast walking precisely<sup>[51,52]</sup>. The sensor unit is useful to measure several kinds of spatiotemporal gait parameters. Measurement error from numerical integration of inertial data can be corrected periodically by assuming null velocity of the foot during the stance phase. Because the 10 [m] fastest gait examination must be performed while walk, not run, two sensor units are used to identify the gait condition by mounting them on both feet. Gait parameters derived from the inertial sensor are gait time, stride length, gait cycle, gait velocity, toe angle, maximum toe clearance, and the percentage of swing phase. The gait time of 10 [m] fastest gait examination is estimated using the displacement of both feet and is compared with that measured by a stopwatch. Then the practicality of the system in place of the stopwatch is confirmed. Moreover, correlation coefficient between gait parameters estimated and the MMSE is investigated to find an indicator to evaluate cognitive impairment. Characteristics of estimated gait parameters by age are investigated and utilization of inertial sensor to measure the gait parameters in large-scale health checkups is discussed.

## 4.2 Mini-Mental State Examination (MMSE)

To measure the level of cognitive impairment, MMSE has been used extensively in clinical and research settings. MMSE is a 30-point test that includes simple questions and problems from several areas such as the recognition of time and place, repeating lists of words, arithmetic, language use and comprehension, and basic motor skills. A score of 24 or more indicates a normal cognition. A score of 23 or less indicates a possibility of mild (18-23) and severe (0-17) cognitive impairment. The MMSE consists of two sections that, together, contain 11 tasks of cognition. The first section involves verbal responses and addresses orientation, memory, and attention. The second section involves the ability to respond to verbal and written commands, such as to write a sentence and copy a polygon figure. Figure 4.1 shows an example of question sheet of MMSE taken before the gait experiment. Time to administer the screening ranges from 5 to 10 minutes and to

complete the test successfully, subjects must have adequate hearing and vision and they must demonstrate sufficient musculoskeletal function to be able to write with a pencil or pen<sup>[53,54]</sup>. A salient benefit of MMSE is that it requires no special equipment or training and that it has both validity and reliability for the diagnosis of dementia. Because the administration period is short and easy to use, MMSE is useful for cognitive assessment in the clinician's office space or at the bedside<sup>[55]</sup>.

Mini-Mental State Examination (MMSE)

検査日: 200 年 月 日 曜日 施設名: 

得点: 30点満点

被験者: 男・女 生年月日: 明・大・昭 年 月 日 歳

プロフィールは事前または事後に記入します。 検査者: \_\_\_\_\_

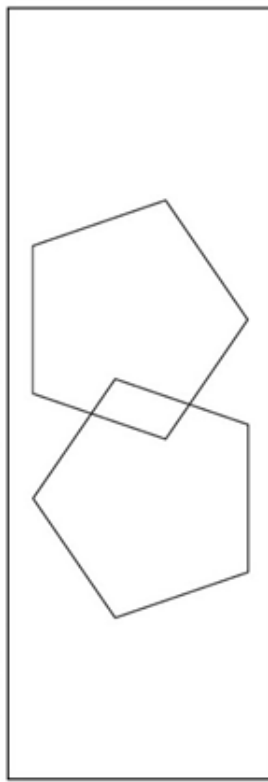
Mini-Mental State Examination (MMSE)

9. 「この文を読んで、この通りにしてください」

めと  
「目を閉じてください」

10. 「この部分に何か文章を書いてください。どんな文章でもかまいません」

11. 「この図形を正確にそのまま書き写してください」



質問と注意点		回 答	得 点
1 (5点) 時間の 見当識	「今日は何日ですか」 * 最初の質問で、被験者の回答に複数の項目が含まれていてもよい。その場合、該当する項目の質問は省く。	日	0 1
	「今年は何年ですか」	年	0 1
	「今の季節は何ですか」		0 1
	「今日は何曜日ですか」	曜日	0 1
	「今月は何月ですか」	月	0 1
2 (5点) 場所の 見当識	「ここは都道府県でいうと何ですか」		0 1
	「ここは何市 (*町・村・区など) ですか」		0 1
	「ここはどこですか」		0 1
	(※回答が地名の場合、この施設の名前は何か、と質問をかける。正答は建物名のみ)		0 1
	「ここは何階ですか」	階	0 1
3 (3点) 即時想起	「これから私がいう言葉を覚えてくり返し言ってください。 『さくら、ねこ、電車』はい、どうぞ」 * テキスターは3つの言葉を1秒に1つずつ言う。その後、被験者にくり返させ、この時点でいくつ言えたかで得点を与える。 * 正答1つにつき1点。合計3点満点。		0 1 2 3
	「今の言葉は、後で聞くので覚えておいてください」 * この3つの言葉は、質問5で再び復唱させるので3つ全部覚えられなかった被験者について、は、全部答えられるようになるまでくり返す (ただし1回まで)。		
	「100から順番に7をくり返しひいてください」 * 5回くり返して7を引かせ、正答1つにつき1点。合計5点満点。 正答例: 93 86 79 72 65 * 答えが止まってしまう場合は「それから」と促す。		0 1 2 3 4 5
	「さっき私が言った3つの言葉は何でしたか」 * 質問3で提示した言葉を再度復唱させる。		0 1 2 3
	時計 (又は図) を見せながら「これは何ですか?」 * 正答1つにつき1点。合計2点満点。		0 1 2
7 (1点) 文の復唱	「今から私がいう文を覚えてくり返し言ってください。 『みんなて力を合わせて綱を引きます』」 * 口頭でゆっくり、はっきりと書いてくり返させる。1回で正確に答えられた場合1点を与える。 * 紙を利に置いた状態で復唱を始める。		0 1
	「今から私がいう通りにしてください。 右手にこの紙を持ってください。それを半分に折りたたんでください。 そして私にください」 * 各段階毎に正しく作業した場合に1点ずつ与える。合計3点満点。		0 1 2 3
	「この文を読んで、この通りにしてください」 * 被験者は普段でも視覚でもかまわない。実際に目を閉じれば1点を与える。	画面に質問有	0 1
	「この部分に何か文章を書いてください。どんな文章でもかまいません」 * テキスターが明文を与えてはならない。意味のある文章ならば正答とする。(* 名前のみは別名、状態などを示す四字熟語は正答)	画面に質問有	0 1
	「この図形を正確にそのまま書き写してください」 * 複製は角が10個あり、2つの五角形が交差していることが正答の条件。手指のふるえなどはかまわない。	画面に質問有	0 1

Fig. 4.1: MMSE is conducted as indicator to the subject's level of cognitive impairment.

### 4.3 10 m fastest gait experiment

WIMU system is used as the measurement tool of gait parameters in health checkup. At the checkup site of the 10 [m] fastest gait measurement, several subjects wear sensor systems and wait in a row for the start of the measurement. The examiner turns on the power switch of two sensors attached on both feet before measurement starts. Then the examiner begins recording inertial data using a wireless controller to synchronize the start time of two sensors exactly (Fig. 4.2). However, sensors are turned off using the on-board switch because powering off wirelessly might cause other sensors used during measurements to stop. Data were sampled at 100 [Hz] and were stored into a microSD card.

Large-scale health checkups have been conducted by Hirosaki University, Japan, since 2005. About 1000 subjects receive health checkup every year. This study used measured data of 1406 people (604 men,  $52.3 \pm 15.4$  years old; 802 women,  $53.5 \pm 15.2$  years old) who had taken the 10 [m] fastest gait examination in 2016 and 2017. Figure 4.3 shows the number of subjects and their age distribution. The health checkup was approved by Hirosaki University Ethics Committee. Informed consent was obtained from all subjects.

Figure 4.4 portrays a schematic diagram of the experiment. If a subject wears shoes that are unsuitable for the measurement such as loose shoes, slippers and sandals, the prepared exercise shoes are used. Inertial sensors were fixed on the toe tips of both feet of the subject using adhesive tape so that the  $\mathbf{i}$  axis of the sensor unit coincides with the toe direction. The subjects were asked to move to the start line and then to walk on a 16 [m] walking course as fast as possible but were cautioned to avoid running. The 3 [m] and 13 [m] points on the walking course were marked with cones and adhesive tape pasted on the floor as a sign of 10 [m] distance. The examiner who walked along with the subject measured the 10 [m] gait time using a stopwatch and the actual walking distance by reading the scale at which the subjects stopped, as portrayed in Fig. 4.4. The subjects conducted the fastest gait three times, in which the first gait was for training. Data were recorded for the last two turns. Because the subjects were asked to walk with their fastest velocity, some were unable to stop on the 16 [m] line and passed the line. Measurements of the actual walking distance are necessary to compensate for the estimated gait time using the inertial sensors. After measurements, sensors are removed, and data recorded



on the microSD card are copied to the computer and are analyzed.

The feasibility of the inertial measurement system as a measurement tool of physical performance in health checkup is investigated. Gait parameters showing high correlation with MMSE are derived.

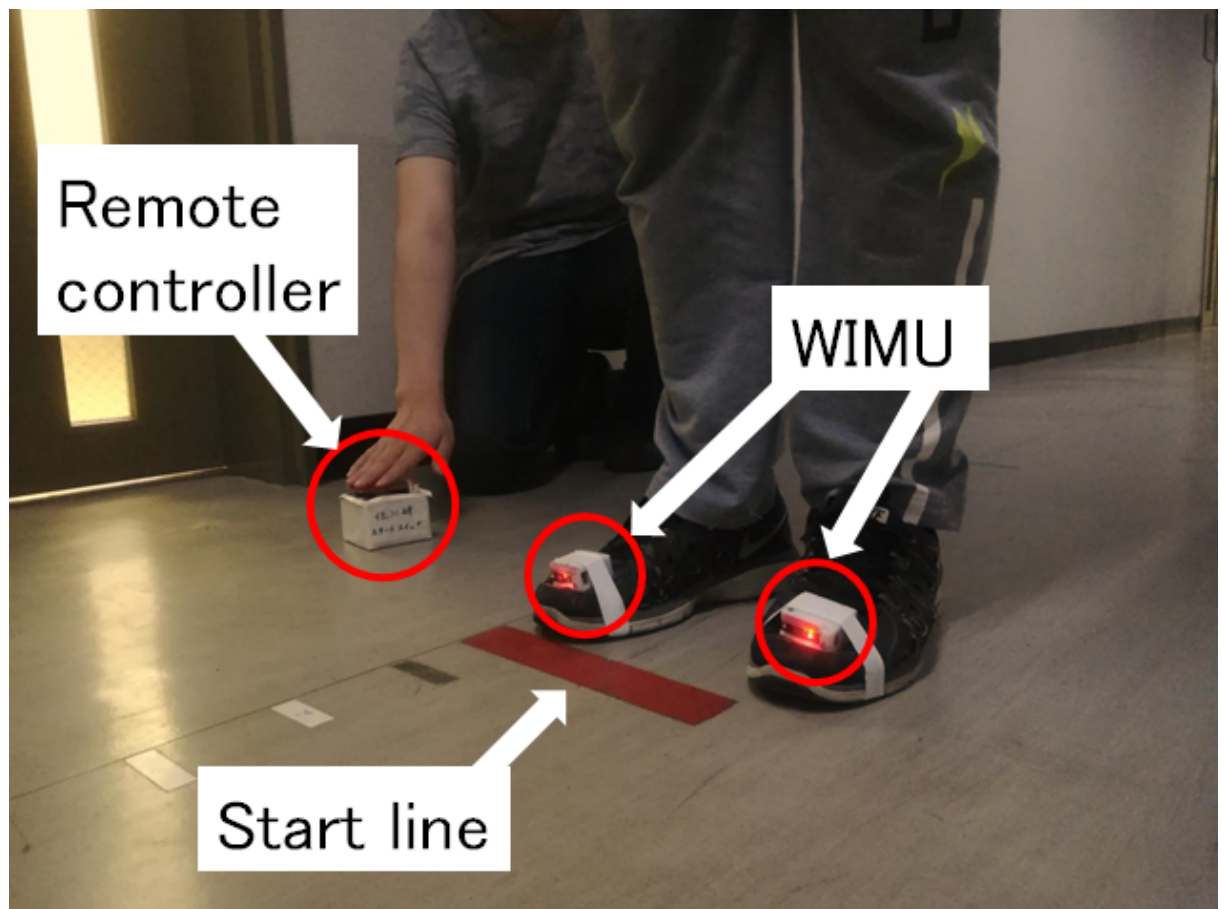


Fig. 4.2: A subject stands at the start line with inertial sensors equipped on both feet. A remote controller starts measurement.

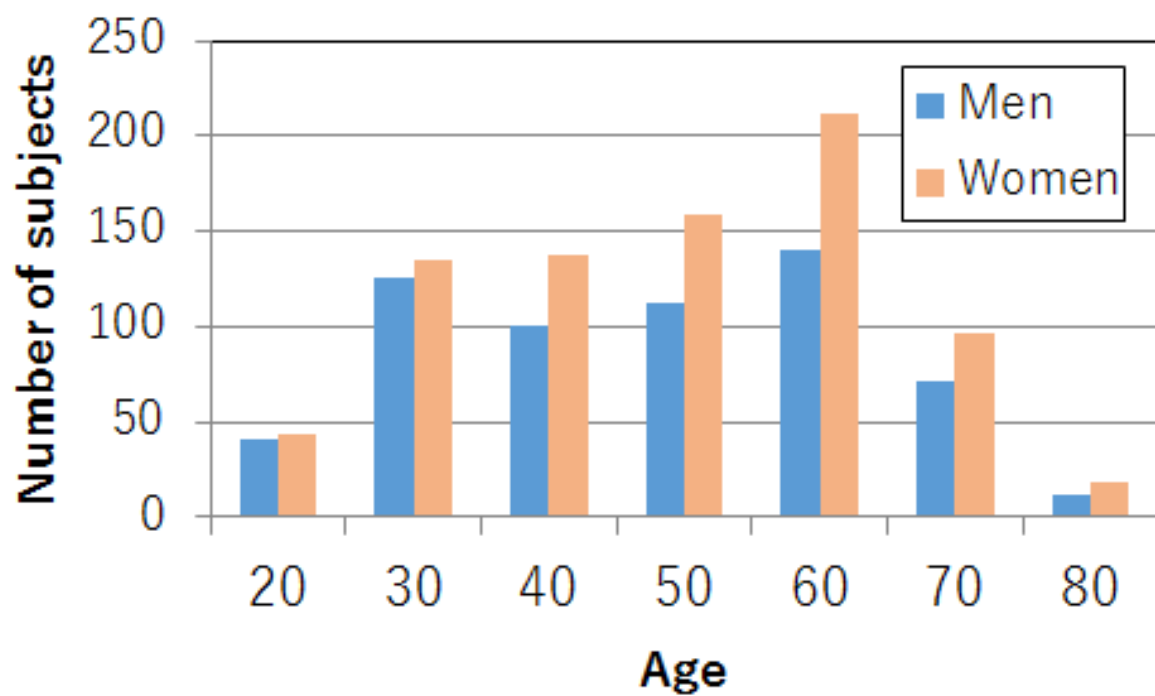


Fig. 4.3: Relation of the number of subjects by age.

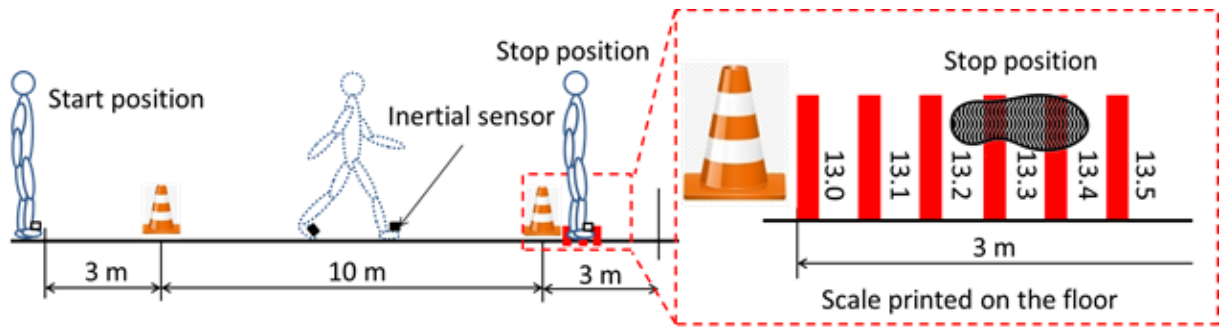


Fig. 4.4: Schematic diagram of the experiment. Distance walked is measured where the subject stopped from the scale on the floor. For example, when the front foot stopped as in the figure, the total length walked is recorded as 13.5 [m].

## 4.4 Results

### 4.4.1 Compensation of gait distance with actual value

The time taken for the whole measurement process was about two to three min. The time taken for analyzing raw inertial data to obtain gait parameters was about 9 [s] per subject using programming software (MATLAB; Mathworks Inc.). Figure 4.5 presents an example of experimental results of horizontal displacement for both toes and gait parameters estimated for a subject (woman, 44 years old; MMSE score 30) using the inertial measurement system. From top left to lower right, horizontal displacement of both feet, stride length (SL), gait cycle (GC), gait velocity (GV), maximum toe angle ( $\theta_{\max}$ ), minimum toe angle ( $\theta_{\min}$ ), maximum toe clearance (TC), and percentage of swing phase ( $S_p$ ) are depicted. The red lines indicate the 3 [m] and 13 [m] points and is obtained from the horizontal displacement of both feet. Circles are places where the stance phase occurred. In this example, the actual walking distance was 14.9 [m]; the estimated distance was 14.5 [m]. Applying equation (3.39) for modification of the horizontal displacement, the right foot passed the 3 [m] line and 13 [m] line at 13.93 [s] and 17.61 [s], and the left foot passed the 3 [m] line and the 13 [m] line at 13.69 [s] and 17.84 [s], respectively.

The horizontal displacement of each subject can be measured by reading the scale where the subject stopped on the walking course. It is regarded as the reference displacement. The displacement estimated using the inertial measurement system is modified linearly to match the reference displacement using equation (3.39). The 10 [m] gait time is recalculated and then compared with time recorded using a stopwatch, which is the reference time. The relation between the actual gait time  $GT_{SW}$  and the estimated gait time  $GT_{IS}$  using inertial measurement system of all subjects is shown in Fig. 4.6. The average and standard deviation of  $GT_{SW}$  and  $GT_{IS}$  are 3.58 / 0.85 [s] and 3.56 / 0.84 [s], respectively, and root mean square error is 0.24 [s]. The correlation coefficient is 0.96, which is sufficiently high. When no modification is applied to the estimated horizontal displacement, the correlation coefficient is reduced to 0.91 as shown by red circles and a red line in Fig. 4.6. This indicates the effectiveness of the compensation of the gait time using the actual displacement. The newly estimated gait time  $GT_{IS}$  is useful as a gait parameter for use instead of the stopwatch.

#### 4.4.2 Classification of subjects by running incidence

Figure 4.7 depicts the relation between running incidence rate (RIR) and the number of measurements of all subjects. The RIR is the ratio of the number of steps ran to the number of total steps during one measurement and is derived from the temporal relation of the TO and the HC of both feet. When a subject runs three steps and the total number of steps taken is ten during the measurement, RIR is 0.3, for example. The total number of measurements is 2814, and it is confirmed that 1944 measurements (69.1 [%]) resulted in almost no running with RIR of 0.2 or less and 97 measurements (3.5 [%]) were almost running with RIR of 0.8 or more across the entire 10 [m] section. In this study, RIR of 0.2 or less is treated as walking, otherwise it is treated as running.

#### 4.4.3 Correlation between MMSE with gait parameter

The relation between ages of all subjects with gait parameters and MMSE score is presented in Fig. 4.8. It is readily apparent that the gait parameters deteriorate as the subjects become older. The changes in  $GT_{IS}$ , GC, and GV over the age of 60 are especially remarkable. Change ratios between the age of 20 and 80 of these gait parameters are 58.9 [%], -22.6 [%] and -22.55 [%], respectively. The average MMSE score also drops as age increased and the change ratio results in -5.5 [%]. From these results, it is suggested that the gait time is the most sensitive to the decline in physical performance with age. Next, the author leaves the calculation of gait parameters and moves to investigation of correlation between MMSE and gait parameters. Figure 4.9 represents the absolute values of correlation coefficient  $\|R\|$  between MMSE with gait parameters. The correlation coefficient with the gait time measured by a stopwatch  $GT_{SW}$  is also illustrated as the reference. Note that  $GT_{IS}$  is obtained using gait time without running data and  $GT_{SW}$  involves running data. The  $GT_{IS}$  shows the highest correlation with MMSE, with  $\|R\|$  value of 0.34, which indicates weak correlation. However, the  $GT_{SW}$  shows a slightly reduced correlation ( $\|R\| = 0.31$ ) with MMSE compared to  $GT_{IS}$ . Moreover,  $GT_{IS}$  including the running data shows  $\|R\|$  value of 0.31, which is the same value of  $GT_{SW}$ . The inclusion of running data in the 10 [m] fastest gait time measurement may lead to incorrect diagnostic results. Detection and rejection of running data are necessary for the precise evaluation of the relation between gait performance and cognitive impairment. The GC provides the

second highest correlation among the gait parameters obtained from the inertial measurement system. However, little relation is observed between SL and MMSE. Therefore, it is suggested that the prolonged gait time causing a decrease in MMSE score results from the extension of GC rather than the shortening of SL.

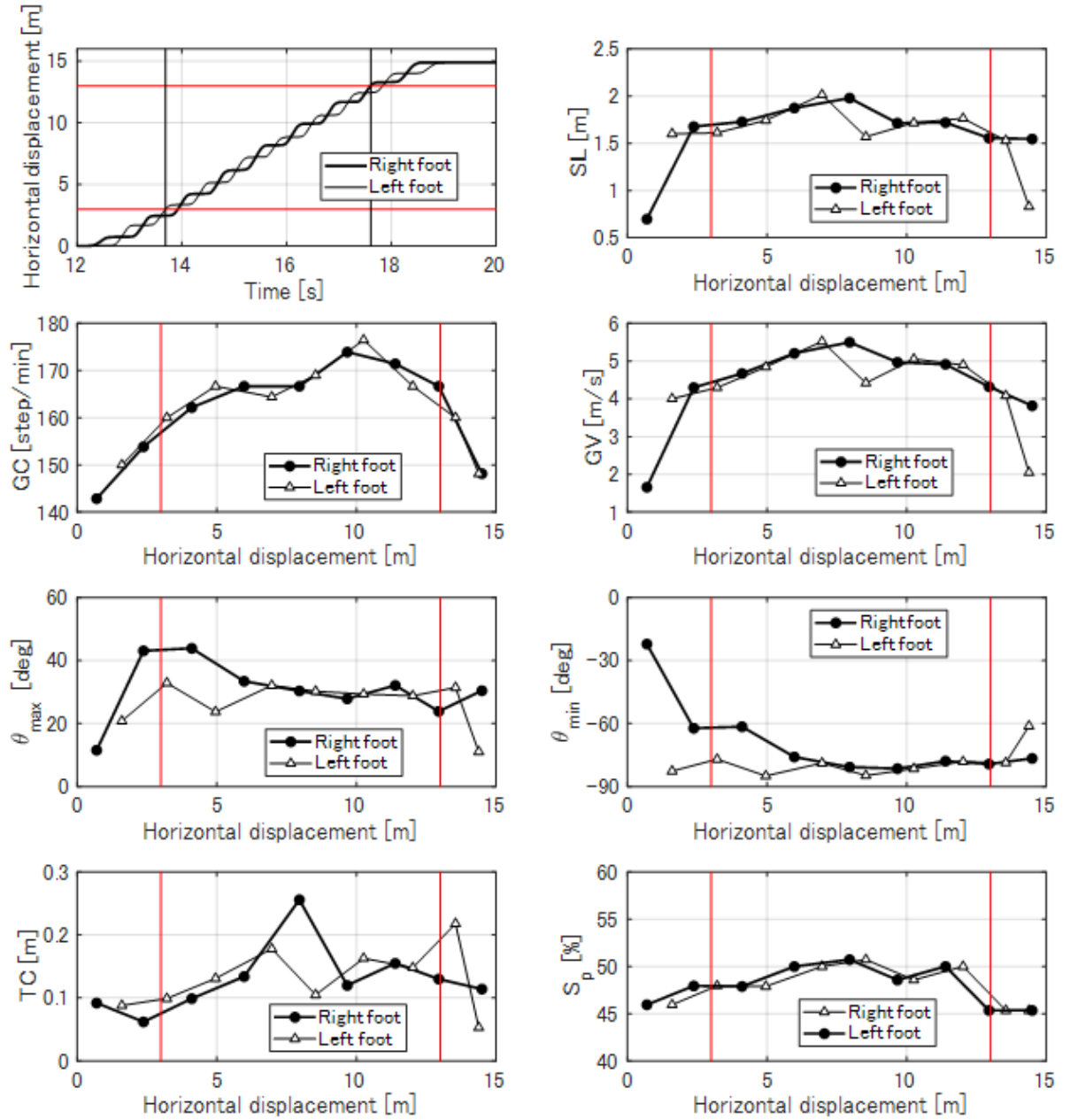


Fig. 4.5: Examples of gait parameters for a subject estimated with inertial sensor. Circles and triangles of the gait parameters are places where the stance phase occurred.



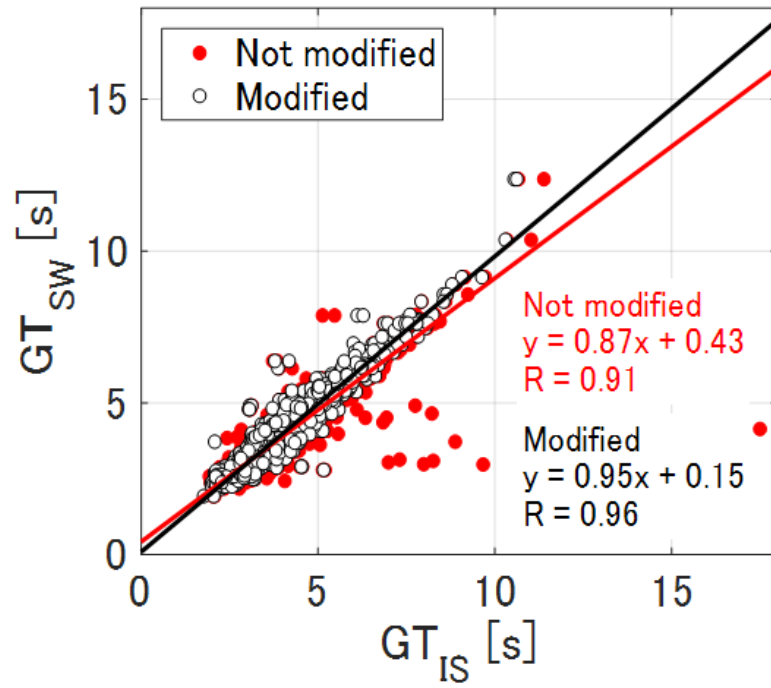


Fig. 4.6: Relation between estimated time  $GT_{IS}$  with reference time  $GT_{SW}$ . Correlation coefficient improved from 0.91 to 0.96 after modification of walking displacement.

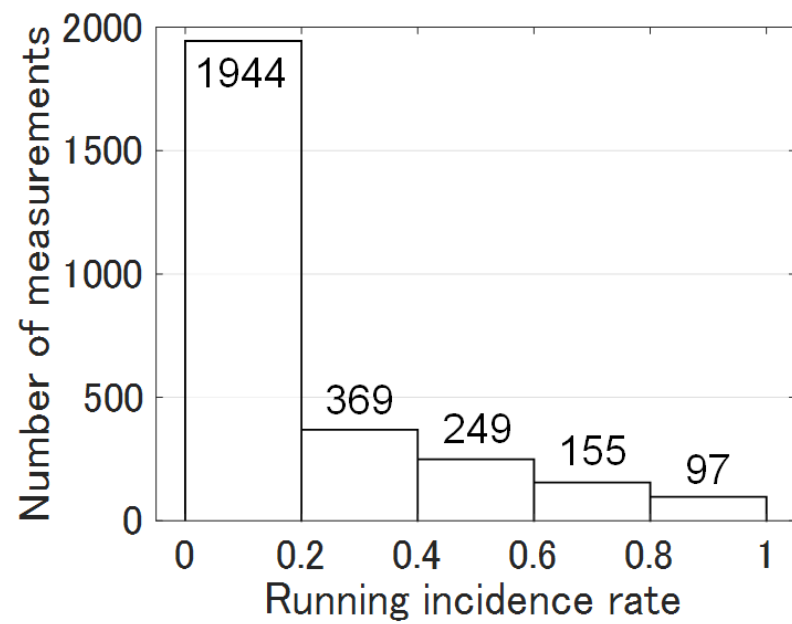


Fig. 4.7: Running incidence rate and the number of measurements. 1944 measurements (69.1 [%]) were rarely running and 97 (3.5 [%]) were almost running.

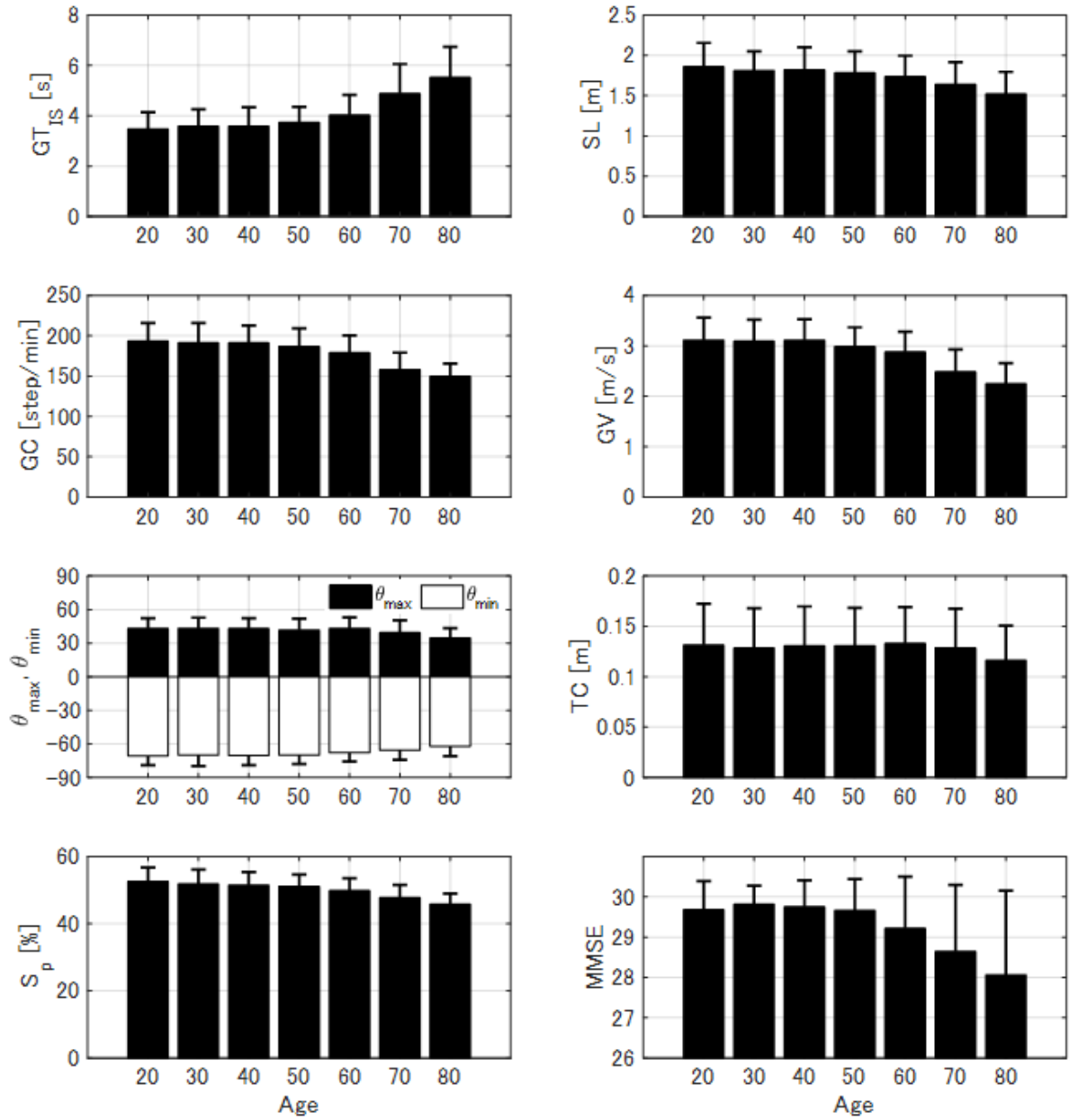


Fig. 4.8: Relation between age of subjects with gait parameters and MMSE score.

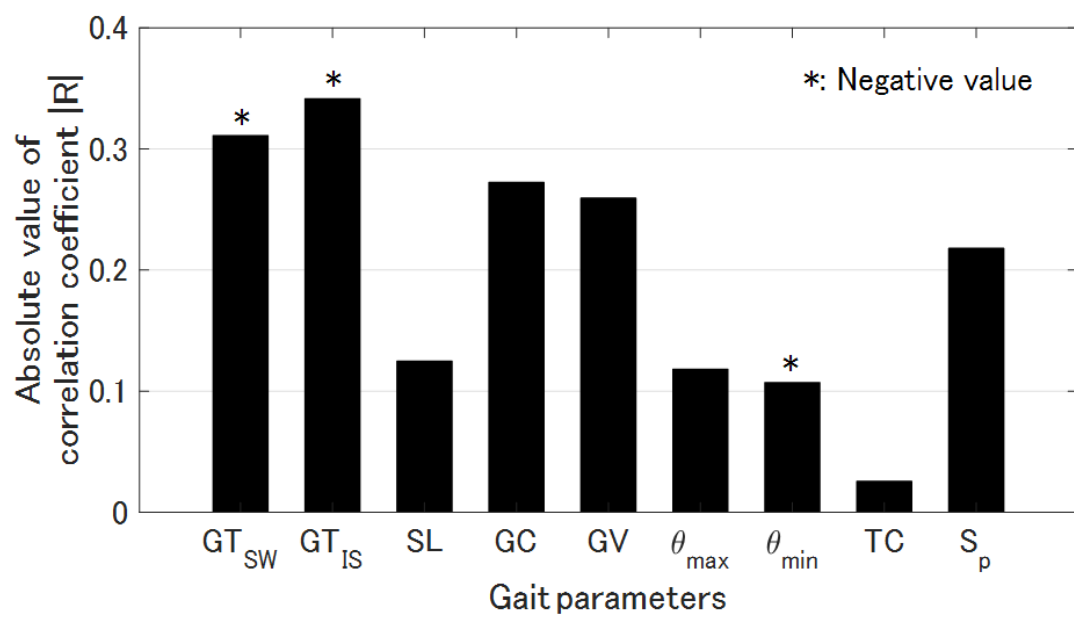


Fig. 4.9: Correlation coefficient between MMSE with gait parameters.

## 4.5 Discussion

This thesis presents a proposal for utilization of the inertial measurement system as a measurement tool of physical performance in the large-scale health checkup and the use of the fastest gait time as an indication to predict the possibility of mild cognitive impairment. The subject's gait was measured using two inertial sensors, which allowed the users to obtain diverse information related to gait parameters. Results show that the gait measurement is fast and easy and that it imparts a minimal burden on subjects in addition to the examiner. Calculating the gait parameters also takes short time. The results can be presented on the spot when requested.

MMSE results are used as an index of the subject's cognitive impairment level. From the 10 [m] fastest gait experiment, it is confirmed that  $GT_{IS}$  shows the highest correlation with the MMSE score. Moreover, removal of the running data improves the correlation coefficient. Reportedly, the increase in GT results from the extension of GC. Ijmker and Lamoth<sup>[19]</sup> conducted a gait experiment by classifying the study sample into three groups: dementia patients, healthy elderly people, and younger elderly people. The report described that dementia patients scored significantly lower on MMSE and gait speed than the other groups, which supports the author's result. The difference is that dementia patients were not joined to the measurement conducted in the study. The MMSE score was high in this study.

The inertial sensor estimation accuracy has been verified by comparing estimated data with data using MCS<sup>[51]</sup>. Error in estimation for the toe angle amplitude, toe height, and stride length are, respectively,  $6.9 / 3.7$  [deg],  $7.4 / 20.2$  [mm], and  $15.14 / 26.1$  [mm]. The system can estimate gait parameters with reasonable accuracy. An earlier report<sup>[56]</sup> described that the estimation precision of total gait distance has improved from  $5.23 / 5.64$  [%] to  $0.81 / 5.40$  [%] and that the estimation precision of 10 [m] gait time has improved from  $7.81 / 29.33$  [%] to  $1.27 / 8.60$  [%]. In this study, to eliminate error from gait displacement estimation, the estimated gait displacement was adjusted to match the measured displacement. The gait trajectory was recalculated. The modified estimated 10 m gait time shows preferable correlation with the reference time, as shown in Fig. 4.6. The result also demonstrates that by taking and analyzing data with no running during the fastest gait allowed the users to find better correlation between gait time with

MMSE.

A salient benefit of using two inertial sensors mounted on both feet instead of a stopwatch for the 10 [m] fastest gait experiment is that the inertial sensor can provide a gait condition whether the subject is walking or running. Information related to gait parameters can also be estimated at each step. The changes of spatiotemporal parameters are visible. A fully wearable inertial sensor is practical for use in supporting objective studies of gait casualties and that it is a good substitute for examiner operation.

An important limitation of this study is that weak correlation ( $|R| = 0.34$ ) has been found for the relation between MMSE and  $GT_{IS}$ ;  $GT_{IS}$  alone cannot be used for diagnosis. Machine learning technology using  $GT_{IS}$  and other gait parameters together with results of medical examination can provide a new method of diagnosing cognitive impairment.

## 4.6 Conclusion

The measurement system of gait parameters using two inertial sensors mounted on both feet was proposed for large-scale health checkups. Using two sensors, precise measurement of gait time and judgment of gait condition whether walk or run are achieved. The proposed method of predicting the mild cognitive impairment from gait parameters was evaluated by finding correlation with the MMSE score obtained from young to elderly subjects. By excluding the data evaluated as running, the correlation higher than the conventional gait time obtained using a stopwatch is confirmed. It showed good suitability for clinical gait evaluation. The current study has produced an important contribution to gait and posture research because the proposed system not only provides gait parameters from inertial data, but it also enables classification of the gait condition. The inertial measurement system is useful as an objective tool in many applications requiring gait evaluation and to investigate the importance of irregularity during gait for outcome evaluation of medical and rehabilitation interventions.

# Chapter 5

## Simultaneous measurement of 3D foot trajectory and center of gravity

### 5.1 Introduction

Development of healthcare sensor applications is an increasingly important research focus. Gait parameters are measured for evaluation of risk of fall, early diagnosis of dementia and so on. One method of acquiring gait parameters is the use of force sensor. Force sensor can be used to measure and monitor the physiological conditions of the wearer. Thus it can be used in healthcare systems. Measurement of plantar pressure is a valuable resource to healthcare professionals when assessing various foot pathologies<sup>[57]</sup>. In clinical settings, plantar pressure is usually monitored by clinicians during infrequent visits in a laboratory environment that can only provide a brief explanation on the condition of the foot over the day. This information is then used to prescribe shoes to address the issues relating to abnormal pressure which causes ulceration<sup>[58,59]</sup>. This raises the need for plantar pressure measuring devices that can continually monitor the pressure applied to the feet bottom.

In recent years, diverse types of force sensors to measure surface pressure have been introduced for biomedical engineering applications<sup>[60]</sup>. This is due to increasing interest in wearable technologies especially in the field of gait and biomechanics investigation. Multi array pressure mapping system is an important technology in biomedical devices. Pressure mapping system can be used to measure the internal carotid artery back pressure or stump pressure distribution of artificial limb user<sup>[61]</sup>. In gait and biomechanics, pressure mapping can be used in sport gait and performance investigations<sup>[11]</sup>. Apart from these, pressure mapping systems are now being considered in wearable devices such

as data gloves and heart rate breathing jackets<sup>[62,63]</sup>. The high demand on pressure mapping system triggers diverse investigations to further improve the system. Most developed sensors have a common problem which is the inadaptability towards human body curvature during application of sensors<sup>[64]</sup>. Most of surface force sensors were rigid and have limited flexibility. For example, due to rigid sensor, in lower limb prosthetic biomechanics investigations, users are unable to walk as natural as they can because the sensor rigidity affects the comfort of the user<sup>[65]</sup>.

Instead of using mat type force sensor, the author introduces the use of multiple of small force sensors for gait mapping. Force sensor is not only used for gait analysis, but is also recognized as the best sensor devices for measuring hand finger force because it has the characteristics such as repeatability for measuring the big force, small physical size, light weight, low cost and may function at high temperature<sup>[66]</sup>. In-shoe foot plantar sensors have paved the way to better efficiency, flexibility, and mobility. For the system to be mobile and wearable for monitoring activities, the system should be wireless with low power consumption. Wireless in-shoe foot plantar measurement systems have potential application to data transfer communication systems, miniaturized biomedical sensors and other uses.

In this chapter, in addition to the conventional method of gait analysis using WIMU, the author proposed the use of thin sheet force sensor for gait measurement system which measures gait performance of both stance phase and swing phase. These force sensors measure the force applied on the foot sole during gait. Center of foot force (COF) is calculated from the measured force during stance phase and information such as trunk control or body balance can be obtained. The merit of the proposed method is that the sensor system can measure characteristics of the entire gait regardless of location. Six force sensors are mounted under the inner sole of shoe and information of gait is taken from inertial sensor combined with force sensors.

## **5.2 Principle**

### **5.2.1 Type of force sensors**

There are a variety of plantar pressure measurement systems but in general they can be classified into two types which are platform systems and in-shoe systems. Platform



systems are constructed from a flat, rigid array of force sensing elements arranged in a matrix configuration and embedded in the floor to allow normal gait. Platform systems can be used for both static and dynamic studies but are generally restricted to research laboratories. One advantage is that a platform is easy to use because it is stationary and flat but disadvantage is that the subject needs to walk on limited spaces. Furthermore, it is important for the foot to contact the centre of the sensing area for an accurate reading. In the other hand, in-shoe sensors are flexible and embedded in the shoe so that measurements reflect the situation between the foot and the shoe directly. The system is flexible and portable, allowing a wider variety of studies with different gait tasks, footwear designs, and terrains<sup>[67]</sup>. They are therefore, highly recommended for studying orthotics and footwear design<sup>[68]</sup> but sensors should be suitably secured to prevent slippage and ensure reliable results. In this study, in-shoe force measurement system is used because of the merits mentioned above.

### **5.2.2 Gait measurement system**

There are several sensors for force measuring in the market. Such sensor technologies utilize capacitive sensors, resistive sensors, piezoelectric sensors, and piezo resistive sensors. These sensors provide electrical signal output that is proportional to the measured force. The required key specifications for a force sensor in terms of sensor performance include linearity, hysteresis, temperature sensitivity, sensing size, and measuring range. In this study, sensor used for force measuring is Force-Sensing Resistor (FSR) of resistive sensor. FSR is made of a conductive polymer that changes resistance with force. When force is applied, the resistance of conductive foam between two electrodes is reduced. The current through the resistive sensor increases because the conductive layer becomes thin under force. Application of force causes conductive particles to touch and increases the current through the sensors.

Six force sensors are used to measure the center of foot force during stance phase. Force sensors are placed where the body weight concentrates the most under the foot during walking as shown in Fig. 5.1<sup>[69]</sup>. Thin button-shaped rubber is attached to the force sensor to increase the sensitivity of the sensor. The sensors are placed under the shoe insole to minimize the rigid feeling of the rubber. The six force sensors are connected to analog channels of WIMU equipped on the tiptoe for data recording. Lateral and frontal position

of center of force  $x_{\text{COF}}$  and  $y_{\text{COF}}$  are calculated from the position and reading of the sensors during stance phase.

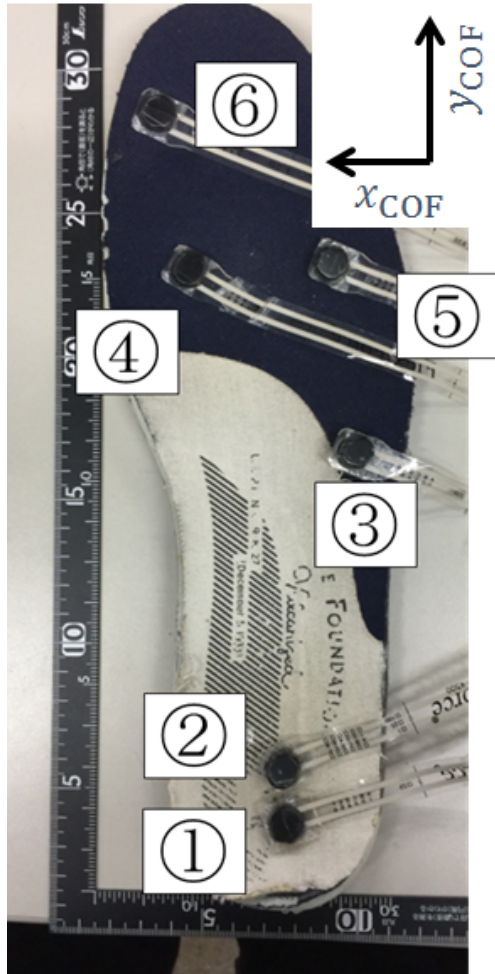
### 5.2.3 Gait trajectory

WIMU which consists of acceleration sensor and gyro sensor is equipped at the tiptoe and force sensors are connected to the analog input port of the WIMU. Figure 5.2 shows the block diagram of the measurement system. Gait parameters during swing phase such as gait time, stride length, gait cycle, gait velocity, toe angle, and toe height are calculated from data taken from the inertial sensors of WIMU and gait parameter during stance phase is calculated from data taken from force sensors. Figure 5.3 shows illustration of location of force sensors and WIMU on a shoe. Gait parameter obtained by force sensors during stance phase is the trajectory of center of foot force (COF). First, the 6 force sensors are fixed on the backside of a shoe insole as shown in Fig. 5.4. Coordinate of each sensor is measured by a ruler and recorded. COF  $x_{\text{COF}}, y_{\text{COF}}$  are calculated as follows:

$$x_{\text{COF}} = \frac{\sum x_n f_n}{\sum f_n} \quad (5.1)$$

$$y_{\text{COF}} = \frac{\sum y_n f_n}{\sum f_n} \quad (5.2)$$

where  $x_n$  and  $y_n$  are the position of the force sensors and  $f_n$  is the force reading.



### Sensor location

- ① Calcaneus ridge of sole
- ② Calcaneus ridge of sole
- ③ Cuboid bone
- ④ Caput ossis in the first
- ⑤ Caput ossis in the fifth
- ⑥ Ground plane thumb

### Coordinate of center of foot force (COF)

$$x_{\text{COF}} = \frac{\sum x_n f_n}{\sum f_n}$$

$$y_{\text{COF}} = \frac{\sum y_n f_n}{\sum f_n}$$

$x_n, y_n$  : Position of force sensor

$f_n$  : Force reading

Fig. 5.1: Placement of force sensors on the shoe insole.

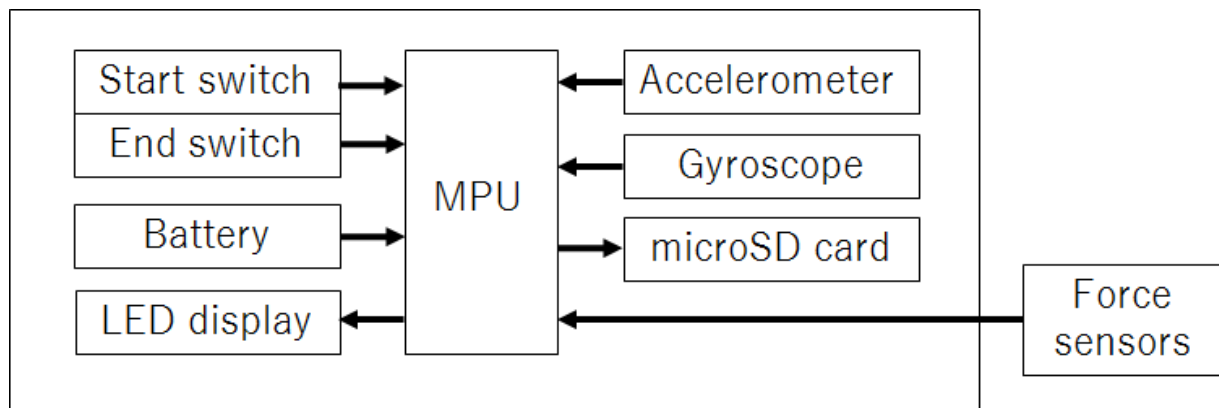


Fig. 5.2: Block diagram of measurement system. The system consists of inertial sensor and force sensor.

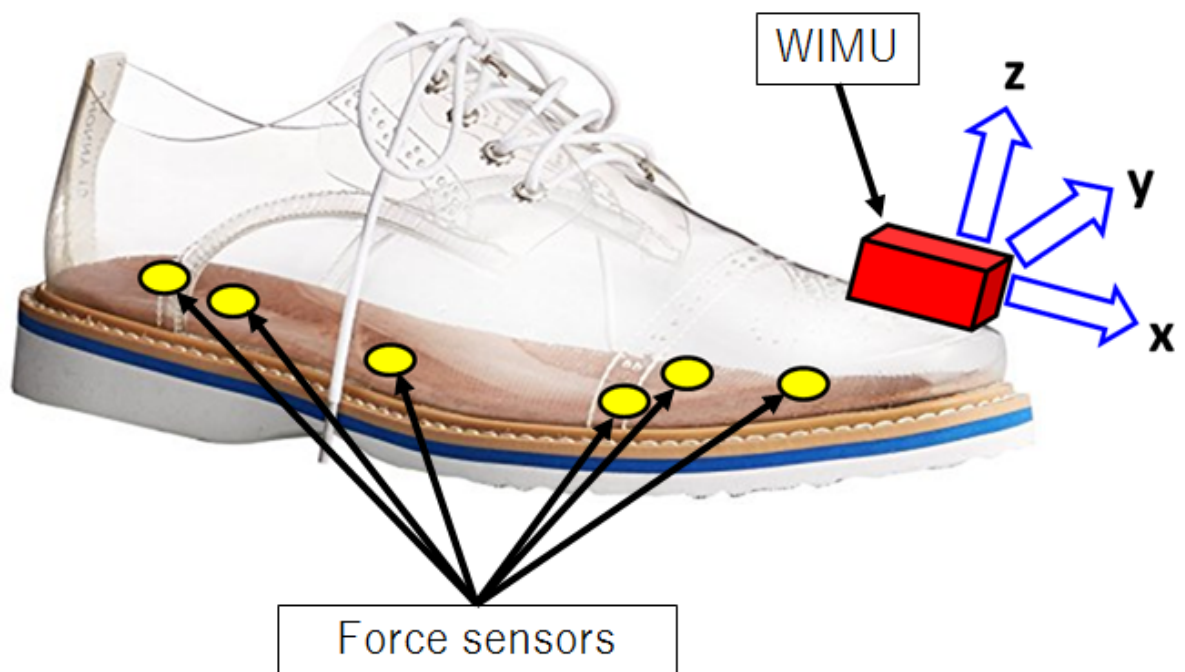


Fig. 5.3: Image of shoe with force sensor insole and 3D sensor on tiptoe.

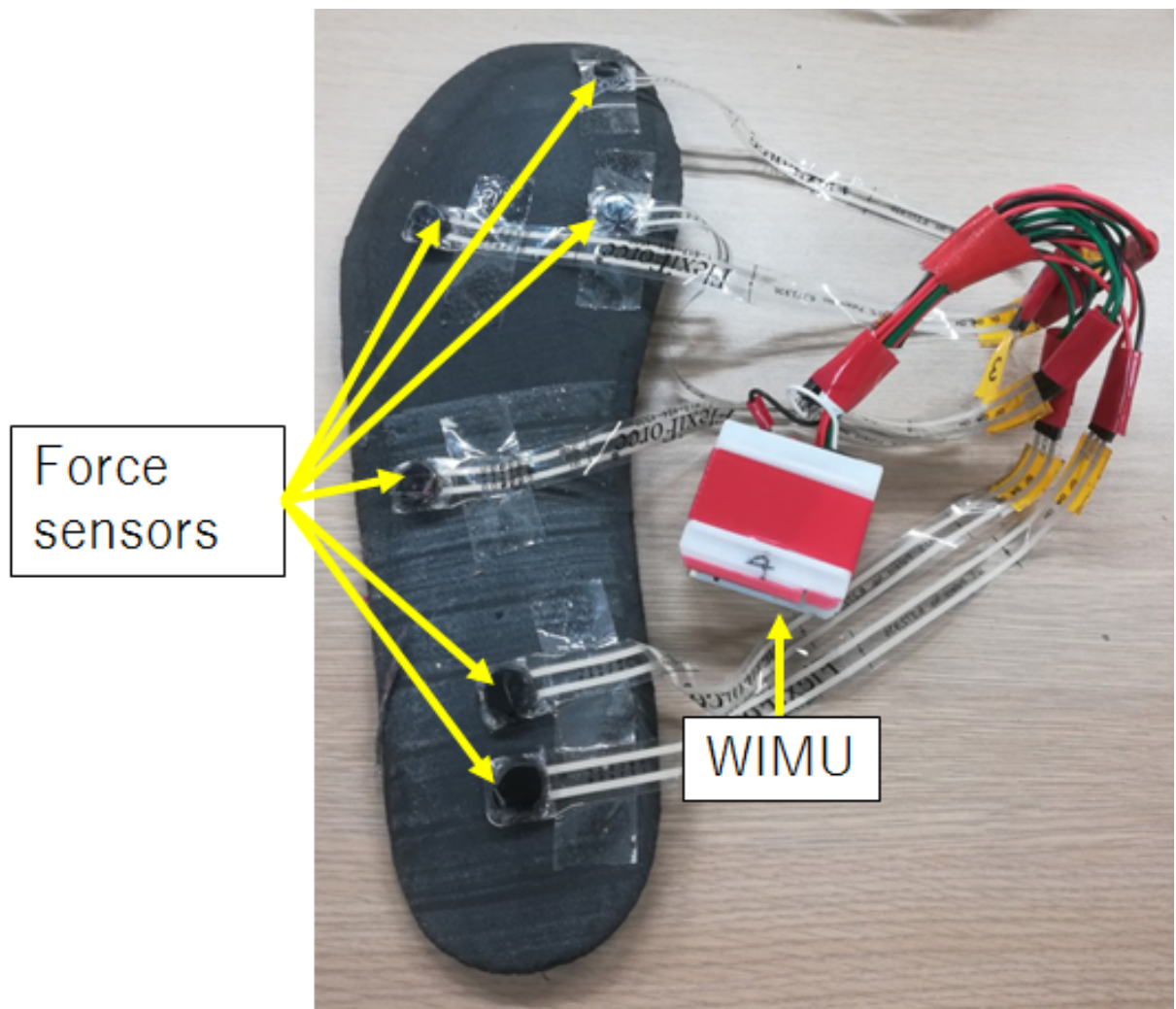


Fig. 5.4: Force sensors are placed under the shoe insole to prevent direct contact to the back of the foot. This is to reduce discomfort of the wearer. Force sensors are connected to the WIMU which is later mounted on the tiptoe.

## 5.3 Experiment

### 5.3.1 Equipment

The system estimates gait parameters during stance phase and swing phase. In addition to the WIMU system for estimating parameters during swing phase, force sensors (Flexi ForceA201-100, TekscanInc) with 0.13 [mm] thickness, sensing area diameter of 9.5 mm, and maximum load 440 [N] are used for estimating parameters during stance phase.

### 5.3.2 Method

The experiment is conducted on one healthy male (age 26, height 177 [cm], weight 85 [kg], foot size 27.5 [cm]). Only one subject is recruited because shoe size is limited and the experiment needs to be conducted with best fit shoes. Beforehand, weight test is conducted on each 6 force sensors and weight-voltage relationship is investigated. Result of the characteristics of each force sensors is shown in Figure 5.5 to Figure 5.10. Force sensors are calibrated using the weight test results.

Experiment protocol is as follows. Force sensors are placed at 6 points in insole of shoe. With WIMU and force sensor equipped on the right shoe, subject walked on a straight path at a self selected pace for a few stride. Gait trajectory is measured using WIMU mounted on tip-toe.

## 5.4 Results

Different gait parameters are obtained during swing phase and stance phase during a gait. Figure 5.11 shows toe's angle and Fig.5.12 shows toe clearance obtained during swing phase. In Fig.5.11, important parameters in toe's angle transition are maximum angle  $\theta_{\max}$  and minimum angle  $\theta_{\min}$ . In Fig.5.12, there are two maximum points ( $P_1$  and  $P_3$ ) and one minimum point ( $P_2$ ) in transition of toe clearance during swing phase. Usually  $P_3$  is referred as toe clearance. COF is calculated during stance phase when the foot is in contact with the ground. Figure 5.13 shows reading from each force sensor placed insole of shoe at one moment during stance phase (green). From these readings, trajectory of COF is calculated (red). Figure 5.14 shows trajectory of COF during stance phase at a series of time. Conclusion can be made that during normal gait, COF moves

from heel and curve out to foot thumb during stance phase. Figure 5.15 shows trajectory of COF and trajectory of foot during gait. The red lines on foot trajectory are the x-axis of the foot which are in the direction of the tiptoe. The green lines on foot trajectory are the y-axis of the foot which are in the left direction when walking forward. COF is highest when the heel lands on support surface and becomes smaller at the end of stance phase.



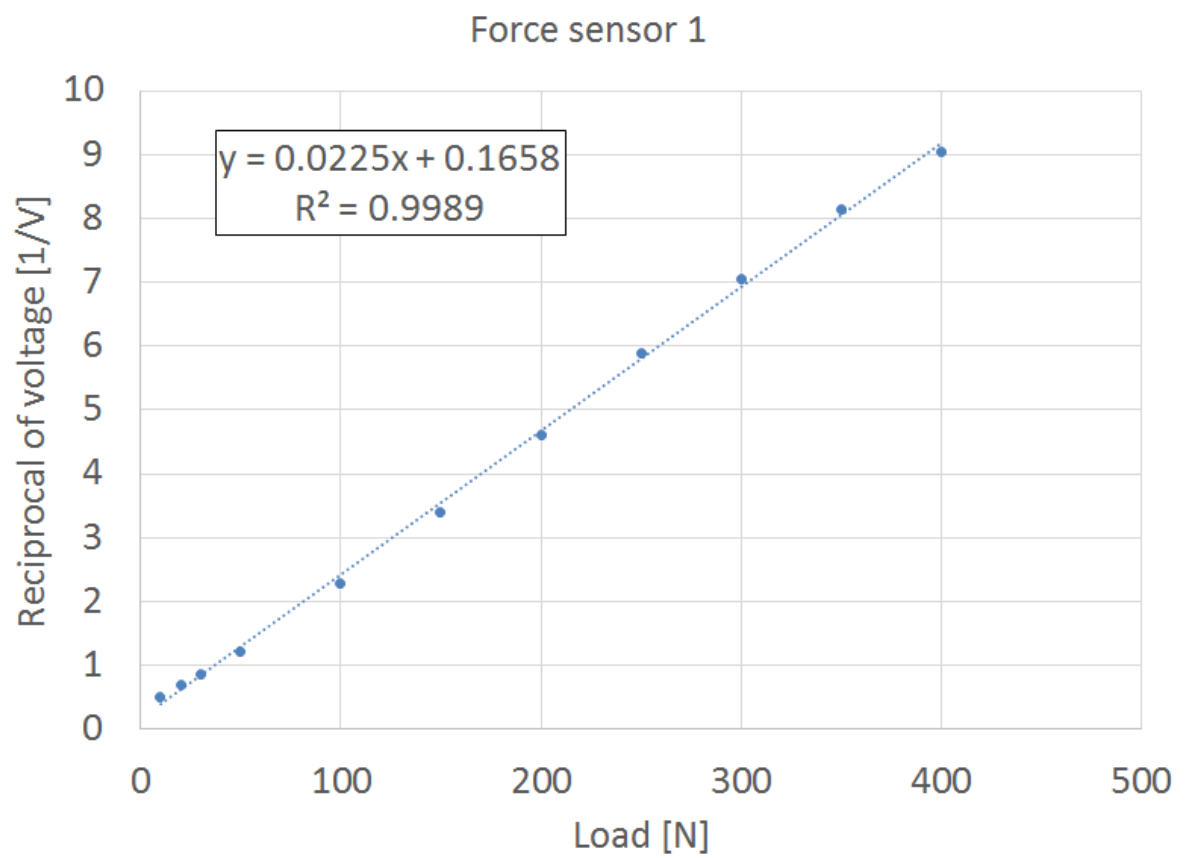


Fig. 5.5: Characteristic of force sensor 1. Sensor number is as allocated in Fig. 5.1.

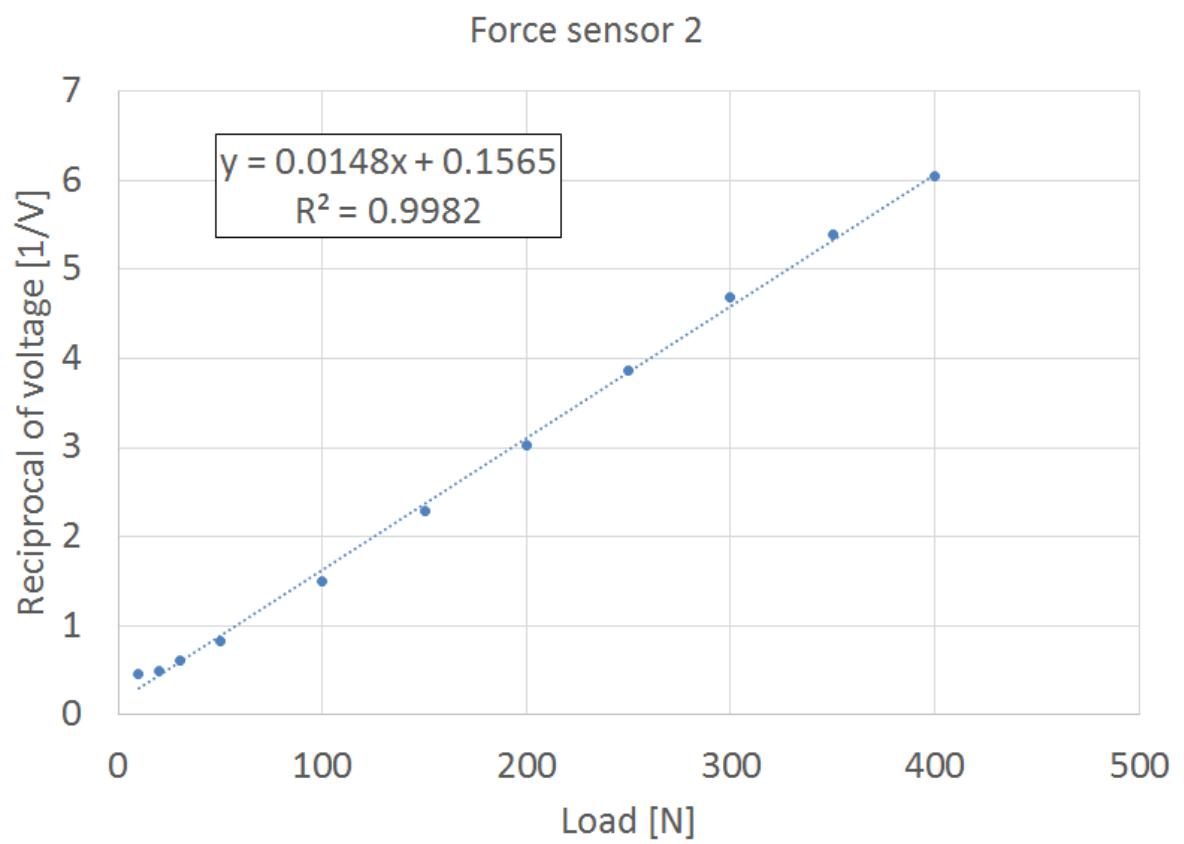


Fig. 5.6: Characteristic of force sensor 2. Sensor number is as allocated in Fig. 5.1.

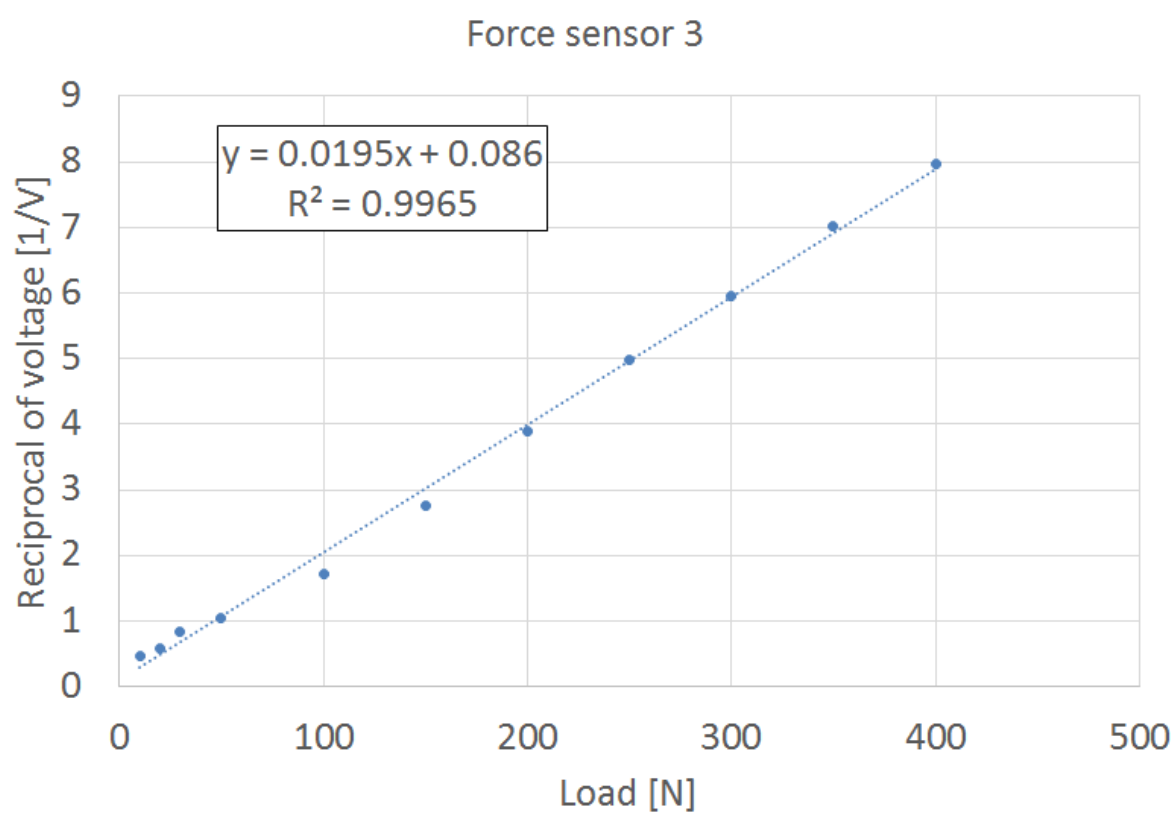


Fig. 5.7: Characteristic of force sensor 3. Sensor number is as allocated in Fig. 5.1.

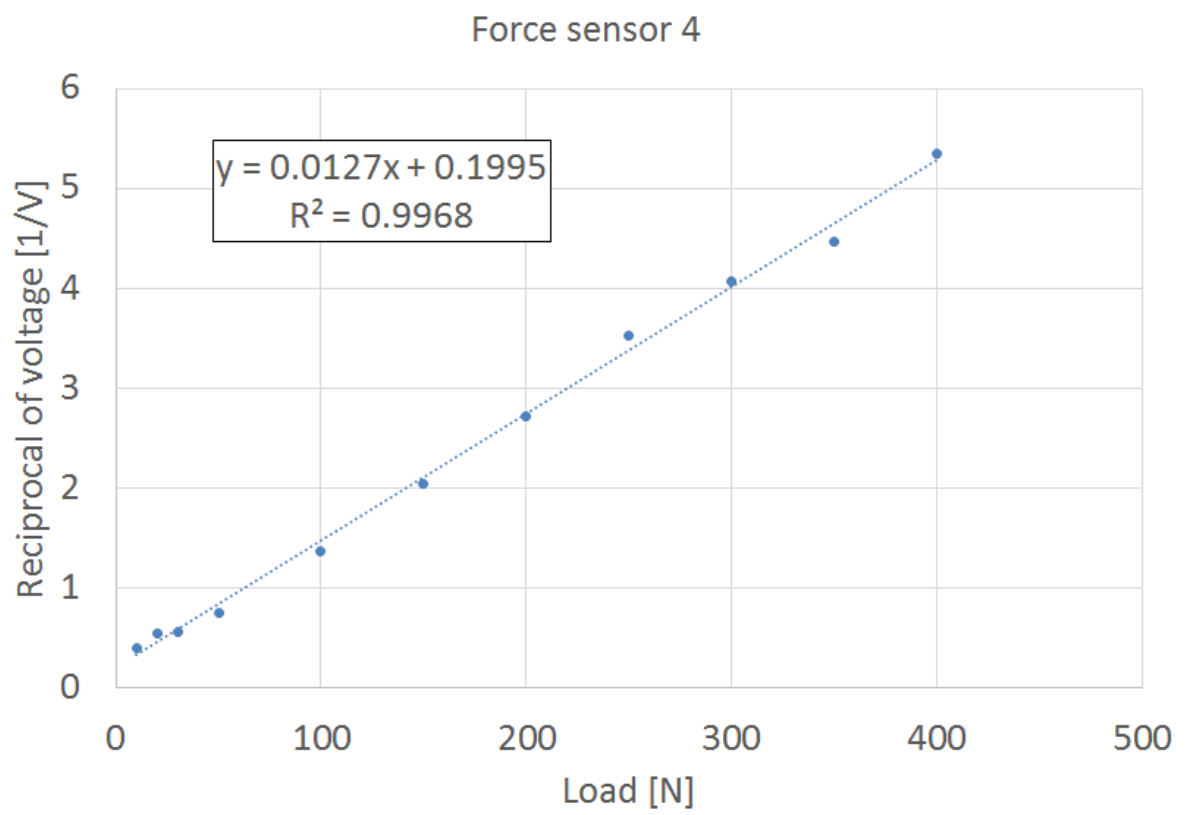


Fig. 5.8: Characteristic of force sensor 4. Sensor number is as allocated in Fig. 5.1.

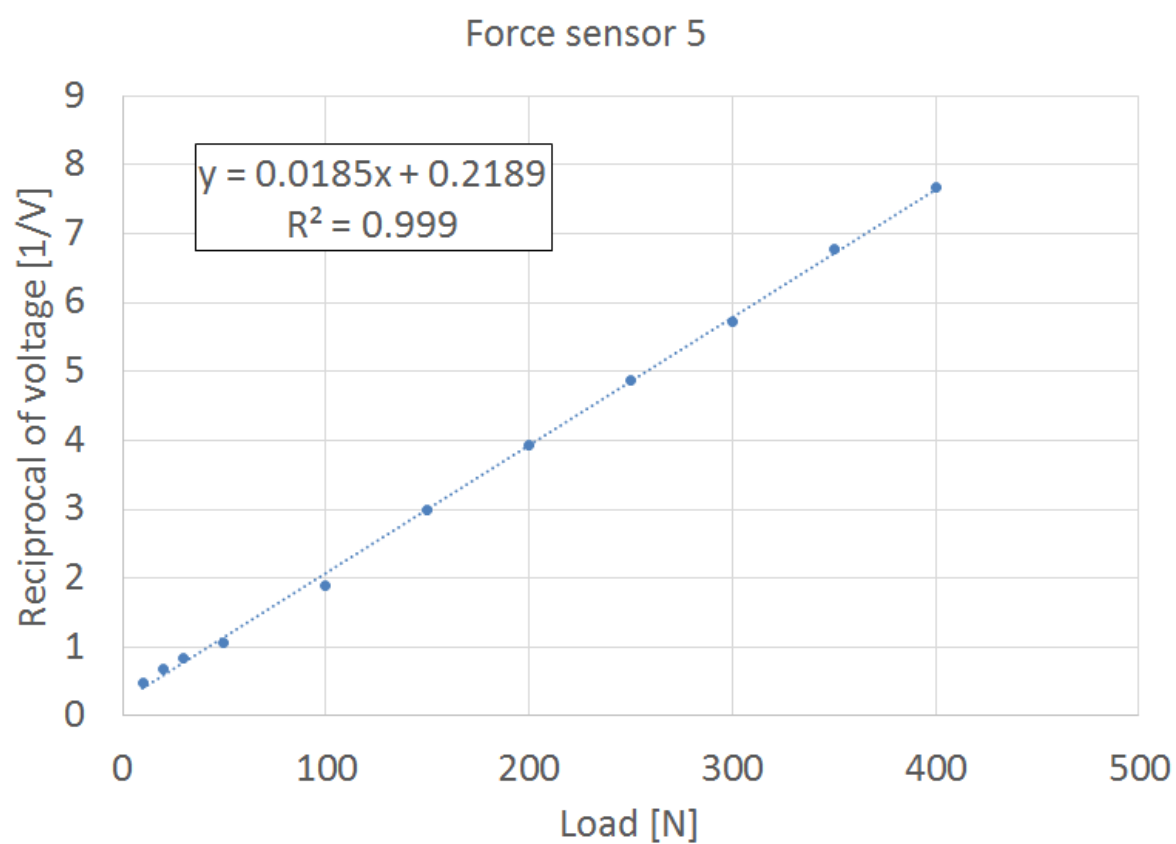


Fig. 5.9: Characteristic of force sensor 5. Sensor number is as allocated in Fig. 5.1.

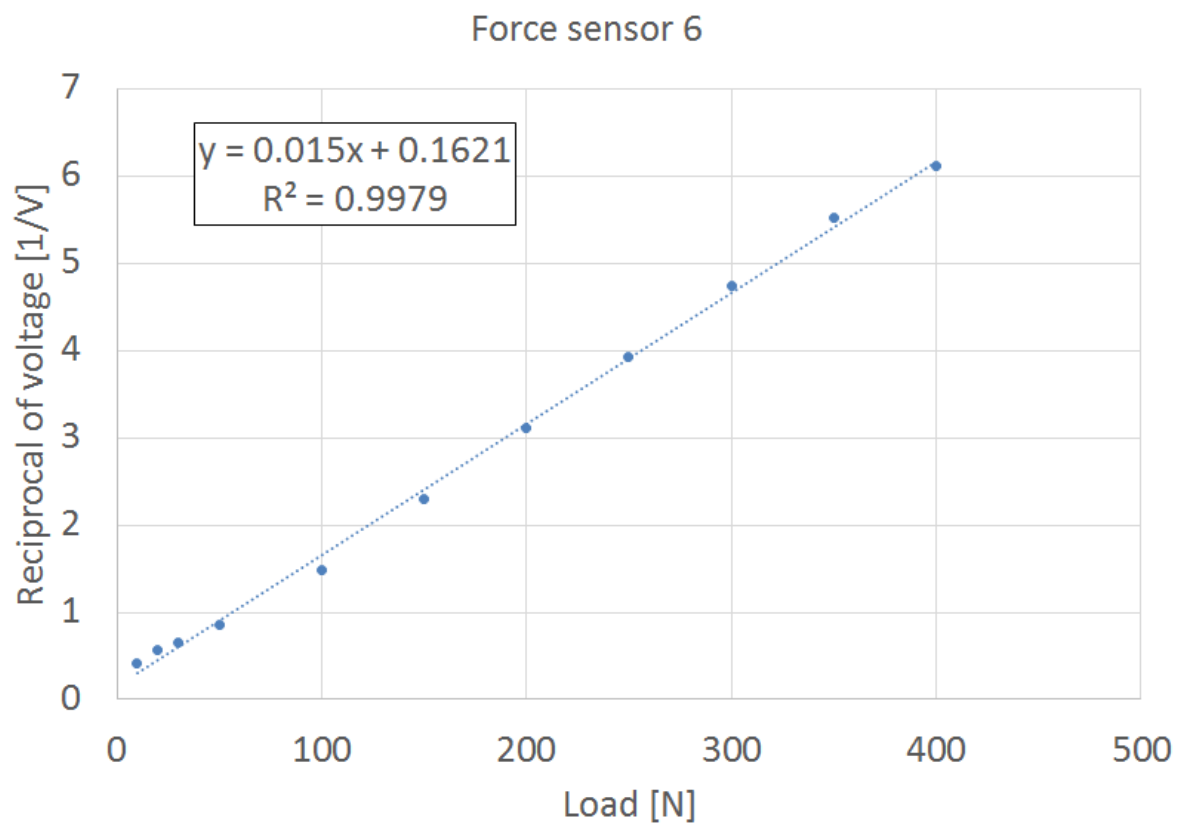


Fig. 5.10: Characteristic of force sensor 6. Sensor number is as allocated in Fig. 5.1.

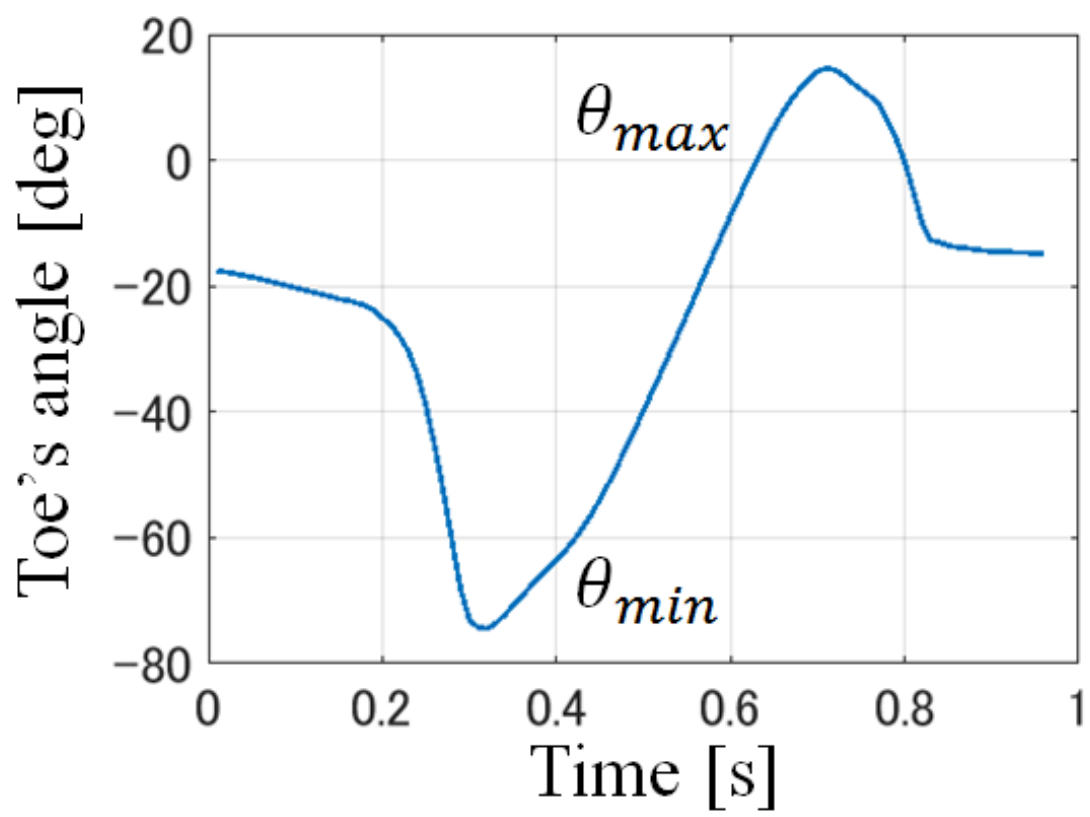


Fig. 5.11: Toe's angle recorded during swing phase.

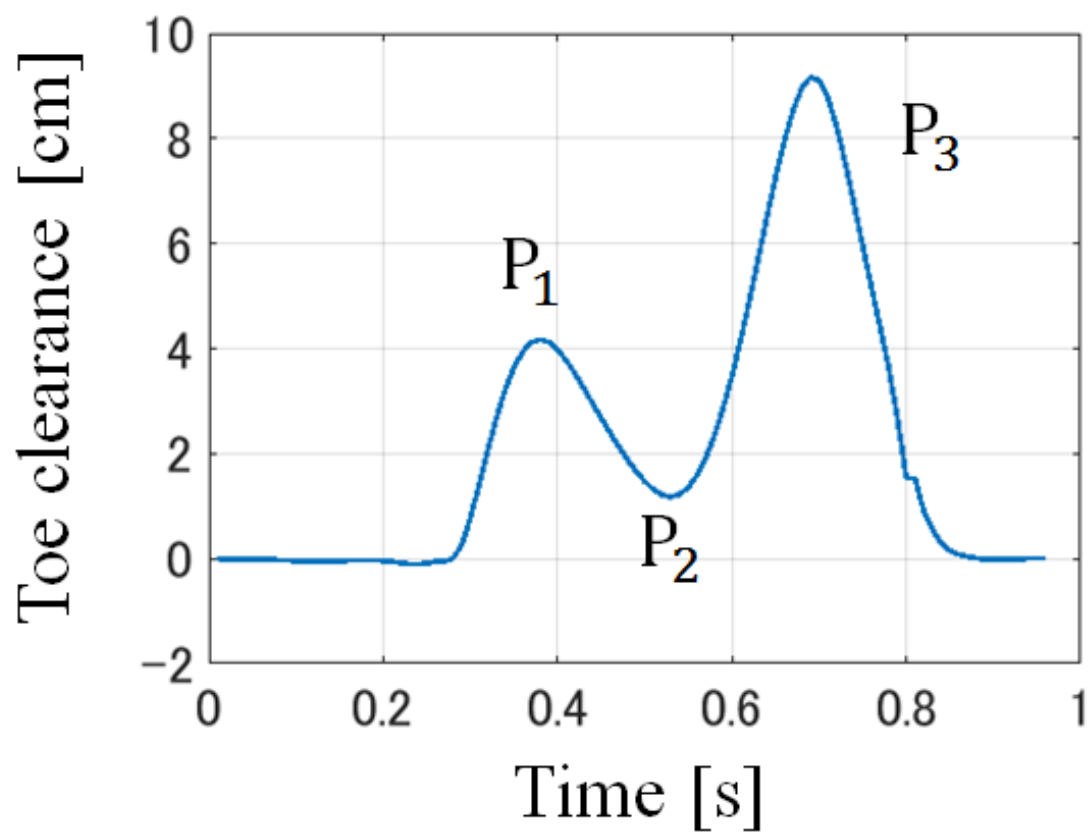


Fig. 5.12: Toe clearance recorded during swing phase.



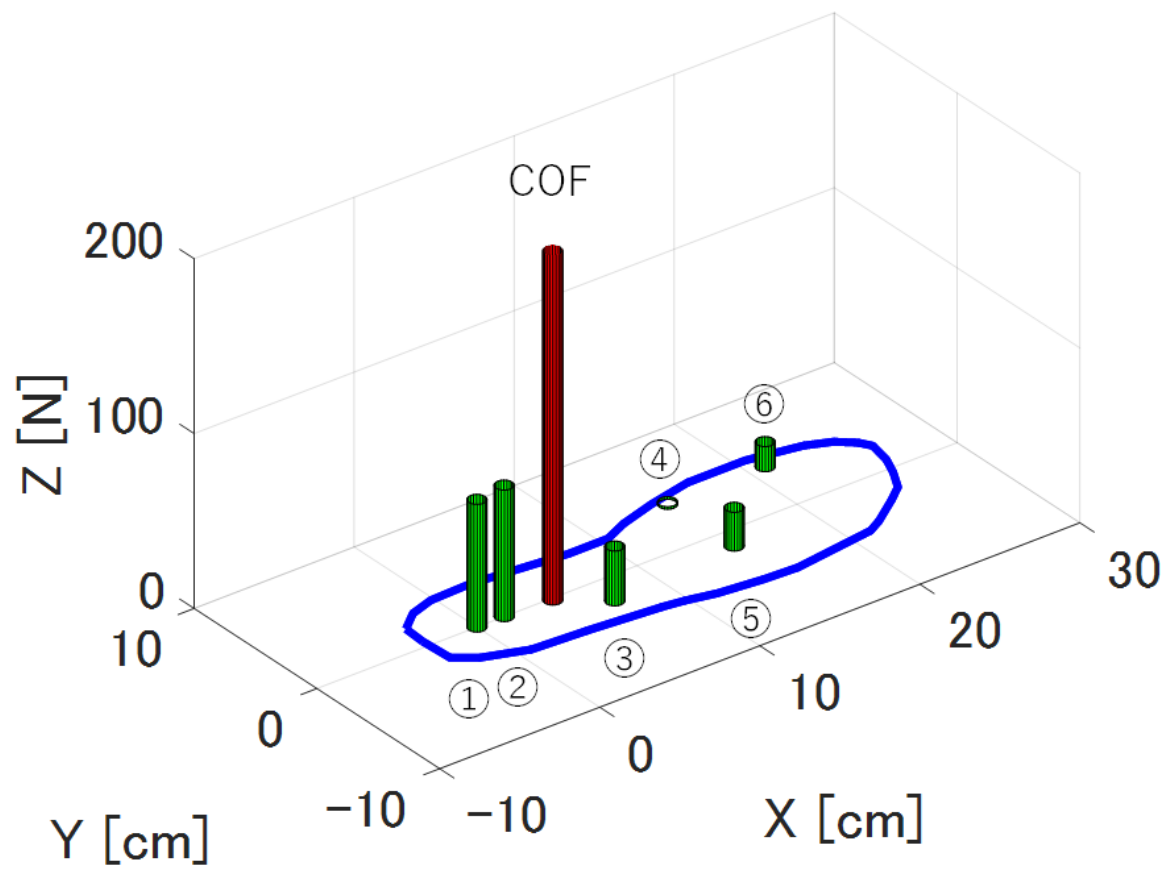


Fig. 5.13: Measured forces at 6 points on the foot (green) and COF (red) calculated from measured values and position of the 6 points.

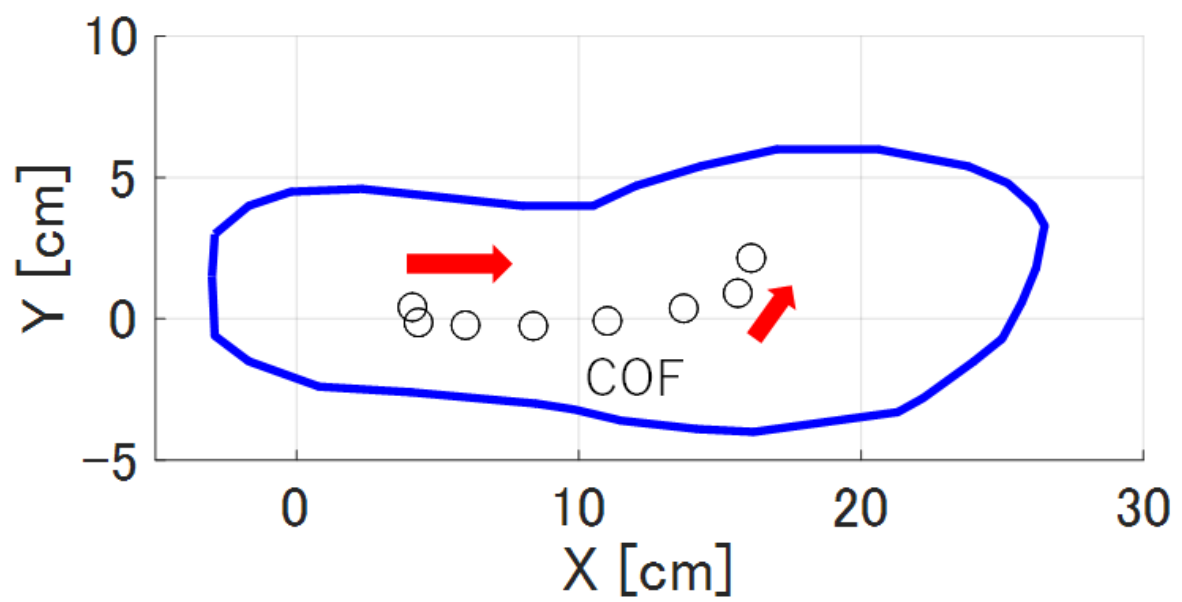


Fig. 5.14: Trajectory of COF from aerial view.

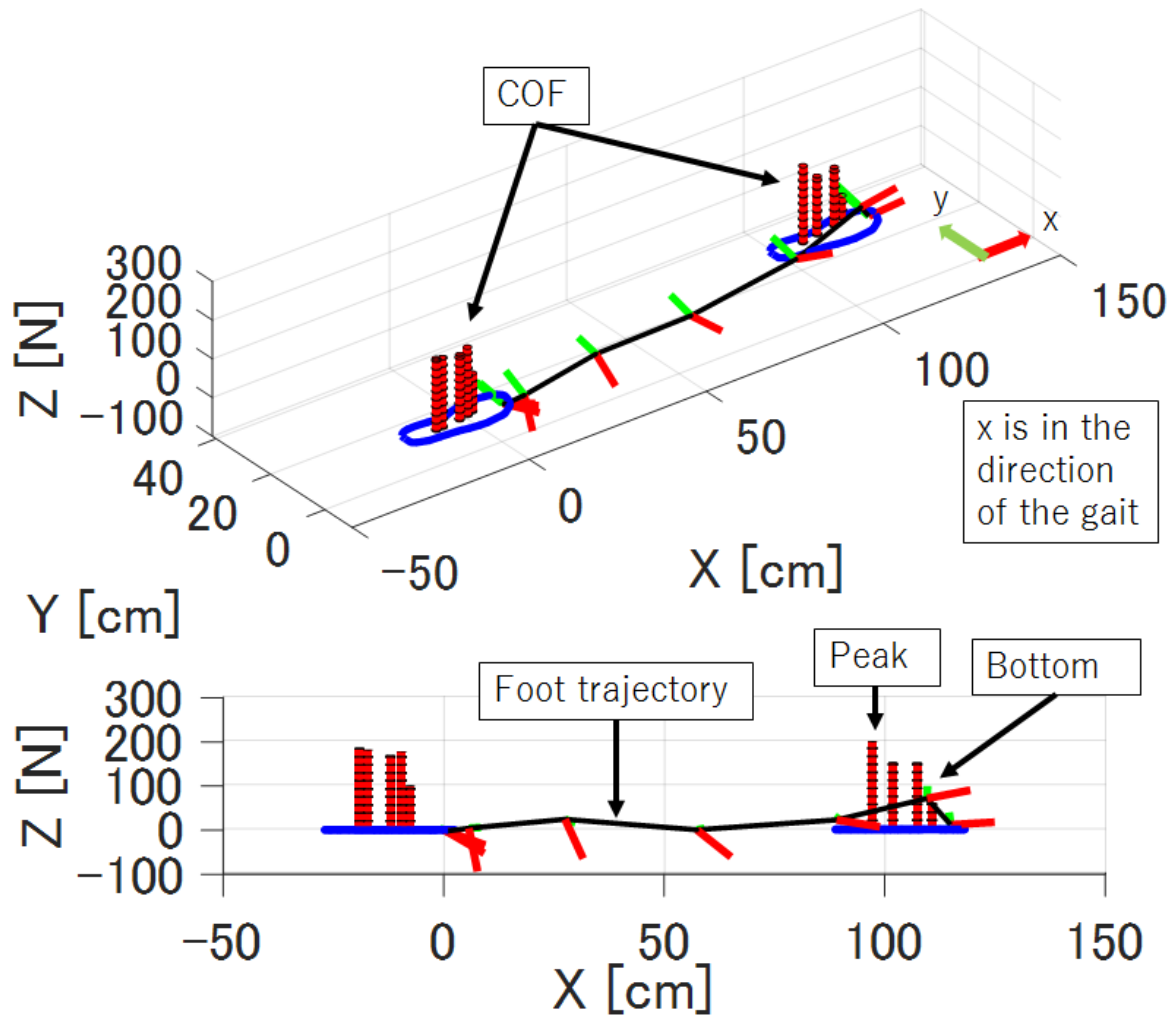


Fig. 5.15: Gait trajectory estimation of a stride with trajectory of COF.

## 5.5 Discussion

In this study, in-shoe device for plantar pressure and gait parameter monitoring during natural walking is developed. The device was designed to be user-friendly and to record natural gait easily and safely. No technical failures of the device during gait test is found and it may also potentially be used in more challenging situation such as measuring higher foot force during fast gait.

Experimental results show that the utilization of sensors in footwear provide useful information on people's activities and gait behaviors. These data are important in computing and realizing innumerable applications, for instance, in medical, sports, and entertainment. In addition to the benefit of continuous daily plantar pressure monitoring that the system offers, it may also potentially reduce the amount of time the clinician has to spend analysing the data. It is common practice for the clinician to divide the foot into a number of regions that they deem to be most important in their analysis of the pressure data with other pressure measurement systems<sup>[70]</sup>.

Other wireless in-shoe foot plantar pressure system which has almost the same concept of the system proposed in this research is proposed by Saito et al.<sup>[71]</sup> who employ unique force sensors to measure plantar pressure during daily human activity. Their device consists of a shoe insole with seven pressure-sensitive conductive rubber sensors placed at heel, lateral midfoot, great toe, head of the first metatarsal, centre midfoot and centre forefoot. The system did not use a processing unit attached to the shoe, making the electronic circuitry on the shoe side smaller than others similar system because the processing unit is at the receiving end of the wireless transmission unit. This benefit makes the power consumption lower, making the system capable of monitoring up to 20 hours with changing power source. However, the sensor system only consists of pressure sensor and not able to measure 3D motion of the foot.

## 5.6 Conclusion

Tiptoe-mounted sensor system for measuring the trajectory of COF during stance phase in addition to gait parameters during swing phase is proposed. Gait measurement system which measures gait performance of both stance phase and swing phase characteristics can be used to collect comprehensive information on the way of walking.

# Chapter 6

## Continuous blood pressure estimation during exercise using pulse photoplethysmographic signal

### 6.1 Introduction

The decline in the use of mercury sphygmomanometers has led to the development of various alternatives to blood pressure measurement. Non-invasive measurement of blood pressure (BP) using cuff-based (CB) methods provides adequate data for many applications in medicine. The mainstream method is using the oscillometric devices because they can be used to take automated measurements just by pressing a button. This method requires a cuff to compress the artery at heart level for BP measurement. During measurement, subject is required to stay still to eliminate as much noise as possible from any motion and some subjects get nervous during measurement resulting in higher measurement value. CB method also has disadvantages such as continuous measurement of BP is impossible because a pause at least 1 to 2 minutes between twice BP measurements are necessary to avoid error in the measurement. Therefore, only intermittent assessment of BP is possible. Furthermore, the inflation of the cuff may disturb the patient and resulting in error of the measurement.

An alternative approach for a continuous and non-invasive BP measurement is based on changes in pulse wave velocity (PWV) and pulse transit time (PTT)<sup>[72]</sup>. PWV is the speed of a pressure pulse propagating along the arterial wall and can be calculated from PTT. PTT is the time it takes the pulse pressure waveform to propagate through a length of the arterial tree. The pulse pressure waveform results from the ejection of blood from

the left ventricle and moves with a velocity much greater than the forward movement of the blood itself. PWV depends on the arterial pressure and the intrinsic elastic properties of the arterial wall. The velocity of the propagating arterial pulse wave has been proposed as a possibly continuous alternative measure of systolic BP<sup>[73]</sup>. PWV is classically related to BP through the Moens-Korteweg equations<sup>[74]</sup>. While many encouraging results have been achieved with this way of working, it has also been evident that the approach has its limitations. For clinical use, this theoretical model did not prove to be accurate enough to deal with the variance and complex physiologies of patients<sup>[75]</sup> and it has been found to be an inaccurate marker for both diastolic and mean arterial pressure<sup>[76]</sup>.

Many technical innovations have been developed for cuffless-based (CLB) BP monitoring such as smart phone applications and wearable device. However, no system has been developed to enable BP estimation and continuous monitoring that has comparable accuracy to the CB by a single sensor during exercise. The aim of the present study is to develop a system for recording BP without cuff for measurement during exercise or hard work. The author proposes a novel system for CLB estimation of systolic BP that requires only one sensor for capturing pulse photoplethysmographic signal (PPG). The WIMU is used as a data logger to measure BP and as a monitoring system of physical activity during daily life.

## 6.2 Principle

In previous studies<sup>[77,78]</sup>, PPG was used together with electrocardiogram (ECG) to estimate BP. Using ECG in daily life for healthy people is unrealistic and very few studies measure reference BP in the middle of exercise because it is difficult to measure BP while moving and oscillometric sphygmomanometer is sensitive to vibration such as the foot stepping on the ground during gait. The author attempted to measure BP during ergometer exercise because rotation motion of lower body gives minimal effect to reference BP measurement taken at the upper body. Pulse sensor is equipped with a green LED and photodetector to monitor changes in peripheral blood volume. In this study, PPG is taken from the earlobe (Fig. 6.1). From PPG signal (Fig. 6.2), heart rate ( $H_r$ ) and pulse width ( $P_w$ ) are obtained. Pulse is the beat of heart when pumping blood. Pulse time  $P_t$ , which is the time from a peak in a cycle to the peak of the following cycle is directly

related to changes in BP during exercise.  $H_r$  is the reciprocal of  $P_t$ .  $H_r$  is defined as follows.

$$H_r = \frac{60}{P_t} [1/\text{min}] \quad (6.1)$$

$P_W$  is the elapsed time between the rising and falling edges of a single pulse.  $P_W$  gives information of condition of blood vessel which is related on how blood flows. When the  $H_r$  rises,  $P_W$  becomes small because the pulse cycle becomes shorter. In this case, if BP rises, BP is estimated at high accuracy because of its high correlation with  $H_r$ . However if there is no change in BP, BP would be miscalculated higher. To estimate systolic BP using  $P_W$  without relying only on  $H_r$ ,  $P_W$  is normalized by dividing with  $P_t$ . Since

$$P_{NW} = P_W \pm H_R = 60 \pm \frac{P_W}{P_t} \quad (6.2)$$

The author proposes the use of multiplication of  $P_W$  and  $H_r$  because it is equivalent to normalizing  $P_W$  where  $P_{NW}$  is normalized pulse width.

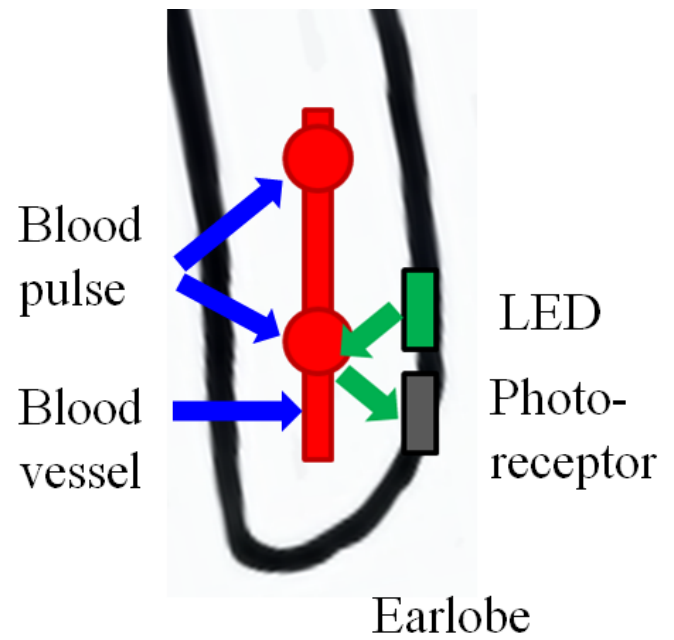
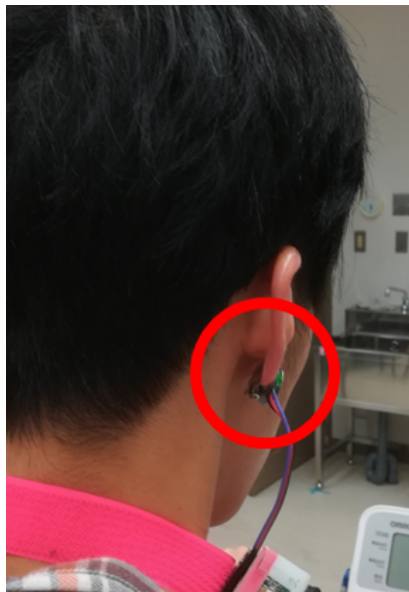


Fig. 6.1: Pulse sensor emits light and changes in light reflected from the earlobe are monitored by the photodetector.



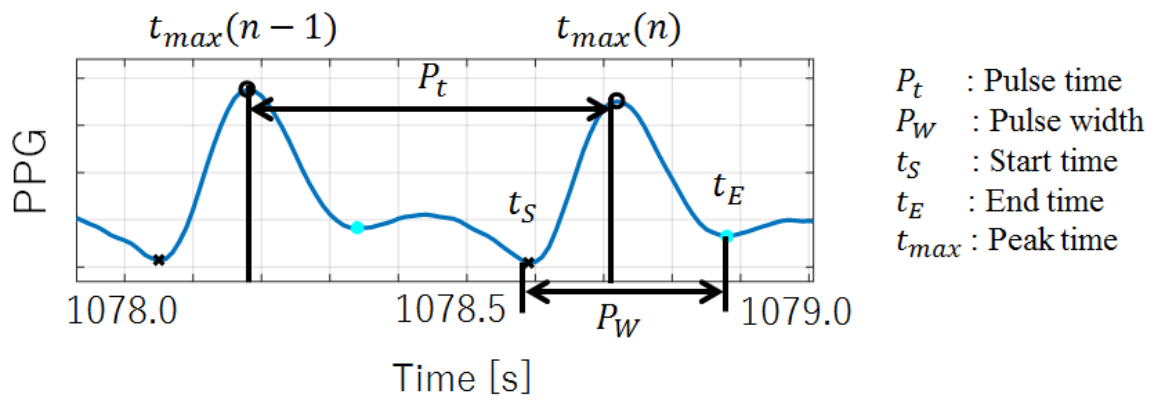


Fig. 6.2: PPG signal gives information of  $P_t$  and  $P_W$ .

## 6.3 Method

### 6.3.1 Subjects

A total of 9 healthy subjects (8 men, 1 woman; age range : 22-51 years) participated in this study. All subjects provided informed consent before the experiment is conducted.

### 6.3.2 Equipments

In this study, the CLB method uses pulse sensor (Fig. 6.3) to capture PPG signal. The sensor is equipped with a green LED (AM2520ZGC09, Kingbright, peak wavelength : 515 [nm]) and photodetector (APDS-9008, Avago) on the same side of the sensor board to monitor changes in peripheral blood volume. The light penetrates the earlobe and then reflects back and arrives at the photodetector. The photodetector detects blood flow changes, which correspond to the natural pulsation of the blood flow.

As a reference, continuous non-invasive arterial pressure monitoring using a finger cuff is conducted simultaneously using Finapres (Finapres 2300, Ohmeda)(Fig. 6.4) for comparison with the proposed method. This device produces a calibrated arterial pressure wave based on the arterial volume-clamp method described by Penaz<sup>[79]</sup>. A cuff is placed round a finger and inflated to the pressure just less than that which causes the artery to collapse (zero transmural pressure). When the pressure in the artery increases, the blood volume changes. This is sensed by infrared photoelectric receivers in the cuff, which immediately operates a servo pump, adjusting the cuff to maintain zero transmural pressure. Thus cuff pressure reflects intra-arterial pressure at all times. The instrument displays an arterial wave form and digital readings of  $H_r$ , systolic mean and diastolic arterial pressures.

Figure 6.5 shows the block diagram of experimental setup. Two WIMUs equipped with wireless module are connected to pulse sensor and Finapres each and measuring time is synchronized with remote controller.

Calibration of CLB method was performed once before the experiment by measuring the BP of the upper arm using oscillometric sphygmomanometer (HEM-7120, OMRON)(Fig. 6.6). This method provides reading of cuff-based systolic BP ( $S_{BP,C}$ ), diastolic BP ( $D_{BP,C}$ ), and  $H_{r,C}$ .

Exercise tool used in the experiment is an ergometer (KONAMI SportsLife, Aerobike 75XL3 USB model)(Fig. 6.7) because the rotating motion during cycling gives little mo-

tion noise to the reading of both Finapres and pulse sensor, unlike the walking motion which gives rhythmic noise each time the foot steps on the ground. Figure 6.8 shows the schematic of the experiment. After one time calibration is performed by CB sphygmomanometer, the subject cycles on ergometer while pulse sensor measures PPG from earlobe and Finapres measures BP from middle finger.

### 6.3.3 Exercise protocols

BP validation was performed under 3 different conditions: static (resting BP), dynamic (BP rising), and return (BP recovery). BP rise was provoked by having the subjects to cycle on an ergometer at 100 [W]. Subjects were asked to maintain cycling rate at 50 [rpm] regardless of the physical strength condition of the subject. Subjects are instructed to ride the ergometer while pulse sensor is clipped to the right earlobe and finger cuff is wrapped around the right middle finger (Fig. 6.9). The appropriate size of finger cuff was selected and applied to fit each subject. Subjects were positioned on the ergometer and transducer was positioned on the handle bar. The height of saddle was adjusted so that the transducer is at heart level. For the purpose of calibration, BP is measured using CB sphygmomanometer on the upper arm and values of  $S_{BP,C}$ ,  $D_{BP,C}$ , and  $H_{r,C}$  are recorded. Subjects are asked to stay still on the ergometer for 2-3 minutes for the Finapres reading to get stable before pedaling. Then subjects are asked to cycle for 3 minutes and then stop and stay still for 3 minutes. Readings from Finapres and pulse sensor are recorded using WIMU as an analog reader and data is saved into microSD card for analysis purpose.

### 6.3.4 Determination of pulse width

Figure 6.10 shows an example of PPG wave at rest of a healthy man. There are two heart sounds (10.25 [s] and 10.50 [s] marked with green triangles) that occur in sequence with each heartbeat. These are the first heart sound and second heart sound produced by the closing of the atrioventricular valves and semilunar valves, respectively. These sounds can be observed in the PPG, which consists of 2 peaks in a cycle. The higher peak is labeled as  $t_{max}$ , and the two bottoms before and after  $t_{max}$  are labeled as start time  $t_S$  and end time  $t_E$ .  $P_W$  is defined as the time between onset and end of PPG and is represented as the time between  $t_S$  and  $t_E$ . Pulse time  $P_t$  is defined as the time between two consecutive  $t_{max}$ . Heart rate is obtained as follows.

$$H_r = \frac{60}{P_t} [1/\text{min}] \quad (6.3)$$

During hard exercise,  $H_r$  rises and  $P_W$  is expected to become shorter. Moreover,  $t_E$  becomes unobservable and often the next  $t_S$  is mistaken as  $t_E$ . Eventually  $P_W$  becomes longer during exercise. To overcome this problem, the PPG signal is differentiated two times and the peak time obtained after  $t_{\max}$  in the wave of double differentiation of PPG is assumed to be the  $t_E$  value.

### 6.3.5 Statistics

BP consists of systolic pressure (maximum during one heartbeat) and diastolic pressure (minimum in between two heartbeats) and is measured in millimeters of mercury (mmHg), above the surrounding atmospheric pressure. In this study, systolic BP estimated using the CLB method is defined as estimated systolic blood pressure  $S_{BP,E}$ .

$S_{BP,E}$  is estimated using two components of PPG, which are  $H_r$  and  $P_W$ . The product of  $H_r$  and  $P_W$  is calculated to normalized the estimation value unit and is defined as  $P_{NW}$ .  $P_{NW}$  is assumed to have high relationship with BP. Linear function for  $P_{NW}$  against BP reading from Finapres is calculated. Then for each subject, offset of the linear function is calibrated with BP reading taken with CB from the upper arm. It is found out that normal  $H_r$  has high relationship with gradient of the linear function. Gradient of linear function is calculated using equation model explained in the next section.

### 6.3.6 Model for the PPG-BP relation

An empiric mathematical function was created to fit the data of PPG and BP obtained from 9 subjects. The function consists of a linear term, which is then corrected with a constant and gradient. This correction depends to the calibration before exercise. Figure 6.11 shows sample of  $P_{NW}$  against  $S_{BP,R}$  for a subject. The gradient of best line  $m_r$  for this subject is 4.00. Assuming  $H_{r,C}$  and  $S_{BP,C}$  are  $H_r$  and  $S_{BP}$  obtained from the CB method, and gradient of best fit line  $m_r$  of  $P_{NW}$  against reference  $S_{BP,R}$  as listed in Table 6.1, multiple regression analysis is conducted as follows

$$m_r = a + b_1 H_{r,C} + b_2 S_{BP,C} + e \quad (6.4)$$

where  $H_{r,C}$  and  $S_{BP,C}$  are independent variables,  $m_r$  is objective variable,  $a$ ,  $b_1$ , and  $b_2$  are coefficient variables, and  $e$  is an error or residual. The prediction equation of gradient  $m$  of  $P_{NW}$  against  $S_{BP,R}$  is

$$m = a + b_1 H_{r,C} + b_2 S_{BP,C} \quad (6.5)$$

For the two variables case,  $b_1$ ,  $b_2$  and  $a$  is calculated using the following equations.

$$b_1 = \frac{(\Sigma S_{BP,C}^2)(\Sigma H_{r,C}m) - (\Sigma H_{r,C}S_{BP,C})(\Sigma S_{BP,C}m)}{(\Sigma H_{r,C}^2)(\Sigma S_{BP,C}^2) - (\Sigma H_{r,C}S_{BP,C})^2} \quad (6.6)$$

$$b_2 = \frac{(\Sigma H_{r,C}^2)(\Sigma S_{BP,C}m) - (\Sigma H_{r,C}S_{BP,C})(\Sigma H_{r,C}m)}{(\Sigma H_{r,C}^2)(\Sigma S_{BP,C}^2) - (\Sigma H_{r,C}S_{BP,C})^2} \quad (6.7)$$

$$a = \bar{m} - b_1 \bar{H_{r,C}} - b_2 \bar{S_{BP,C}} \quad (6.8)$$

Solving these equations,  $a = 2.52$ ,  $b_1 = 0.05$ , and  $b_2 = 0.04$  are obtained. Therefore  $S_{BP,E}$  is estimated using the following equation:

$$m = 2.52 + 0.05H_{r,C} + 0.04S_{BP,C} \quad (6.9)$$

$$S_{BP,E} = P_{NW}m + c \quad (6.10)$$

where  $c$  is  $S_{BP}$  offset obtained from calibration.

Table 6.1: Normal  $H_{r,C}$  and  $S_{BP,C}$  taken before the experiment, and gradient  $m_r$  of best fit line of  $P_{NW}$  against reference  $S_{BP,R}$  of each subject.

Subject	Sex	Age	$H_{r,C}$	$S_{BP,C}$	$m_r$
1	Man	24	72	126	4.00
2	Man	24	63	111	3.35
3	Man	23	58	141	4.79
4	Man	22	73	100	3.07
5	Man	24	79	121	5.13
6	Woman	23	59	122	7.55
7	Man	51	58	123	2.86
8	Man	24	90	101	1.62
9	Man	22	112	130	2.19



Fig. 6.3: Pulse sensor (SEN-11574, SparkFun Electronics) used to obtain PPG signal.



Fig. 6.4: Left figure shows the Finapres machine used for continuous monitoring of BP. Right figure shows transducer fixed to the wrist and finger cuff wrapped to the middle finger.



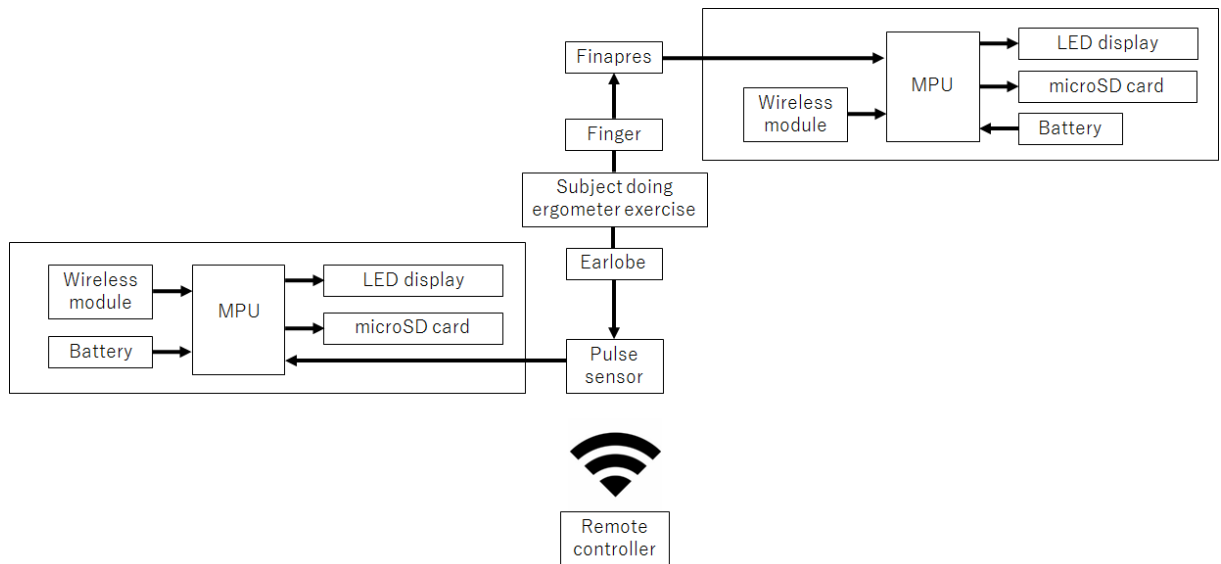


Fig. 6.5: Block diagram of the measurement system.



Fig. 6.6: Electronic oscillometric sphygmomanometer (Omron, HEM-7120) used for calibration of the CLB method.



Fig. 6.7: Ergometer (KONAMI SportsLife, Aerobike 75XL3 USB model) used in the experiment.

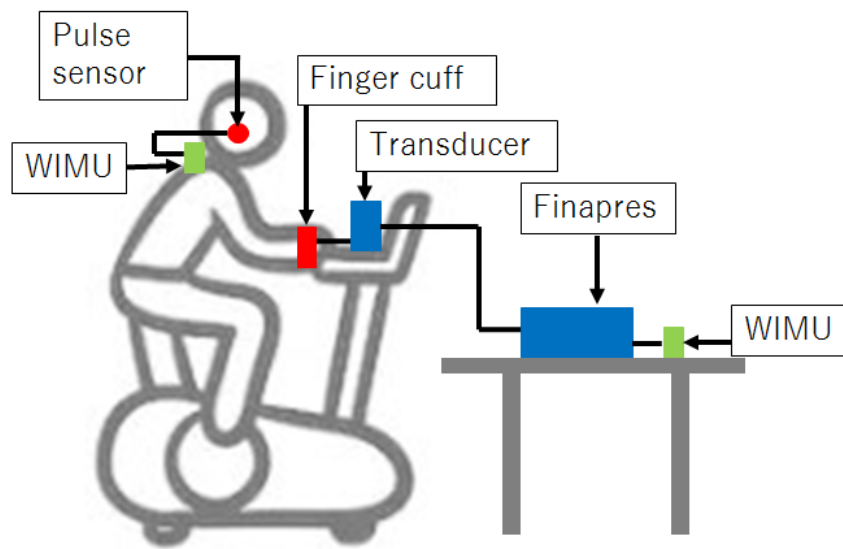


Fig. 6.8: Schematic of the experiment. After one time calibration is taken with CB sphygmomanometer, the subject cycles on ergometer while pulse sensor measures PPG from earlobe and Finapres measures BP from middle finger.



Fig. 6.9: A subject undergoing the test with BP measured at right middle finger and pulse sensor clipped at right earlobe.

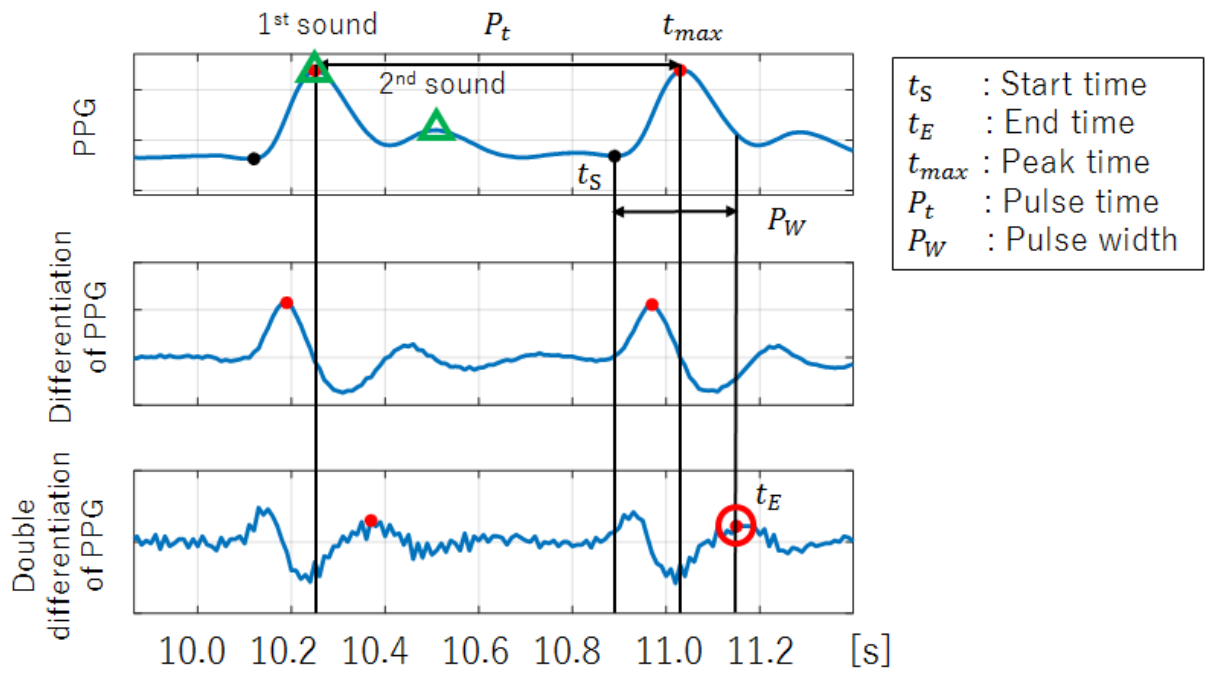


Fig. 6.10: PPG signal gives information of  $P_t$  and  $P_W$ . PPG is differentiated 2 times to obtain  $t_E$  value.

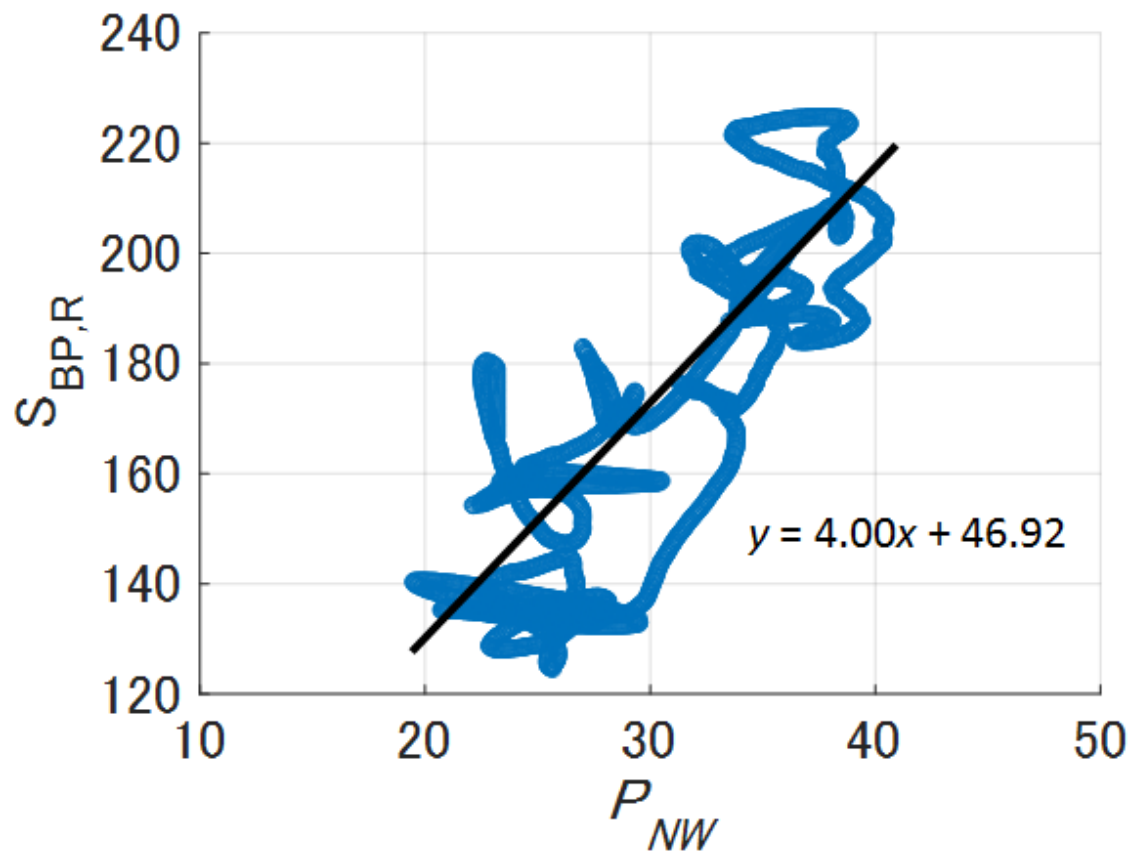


Fig. 6.11: Figure shows relationship between  $P_{NW}$  against  $S_{BP,R}$  for a subject. Gradient of best line  $m_r$  is 4.00.

## 6.4 Results

Reference  $S_{BP,R}$  measured by Finapres is compared with 3 parameters; (1)  $H_r$ , (2)  $P_W$ , and (3)  $P_{NW}$  and correlation with estimated (4)  $S_{BP,E}$  is investigated. Table 6.2 shows the results of comparison.  $H_r$  shows high correlation with  $S_{BP,R}$  with  $r = 0.82 / 0.11$ . However,  $P_W$  shows almost no relation with  $S_{BP,R}$  with  $r = 0.07 / 0.50$ . By normalized parameter for estimating  $S_{BP,E}$  from PPG,  $P_{NW}$  shows almost the same correlation with  $S_{BP,R}$  compared to  $H_r$  with  $r = 0.81 / 0.10$ . The created function in section 6.3.6 was used to calculate  $S_{BP}$  values after individual correction in 9 subjects. Mean for individual results show highest correlation with reference  $S_{BP,R}$  with  $r = 0.83 / 0.08$ . Figure 6.12 shows the plot of  $S_{BP}$  measured by Finapres  $S_{BP,R}$  and  $S_{BP,E}$  and regression of the plot. Overall, the correlation coefficient is 0.86 which is relatively high. Table 6.3 shows the  $S_{BP,E}$  estimation error for each individual. RMSE is 20.47/18.88 [mmHg] and error of the  $S_{BP,E}$  estimation system is 9.42 [%].



Table 6.2: Correlation coefficient between reference  $S_{BP,R}$  with  $H_r$  (1),  $P_W$  (2),  $P_{NW}$  (3), and estimated  $S_{BP,E}$  (4) are shown.

Subject	Sex	Age	(1)	(2)	(3)	(4)
1	Man	24	0.88	-0.47	0.80	0.77
2	Man	24	0.88	0.17	0.93	0.96
3	Man	23	0.86	-0.80	0.66	0.72
4	Man	22	0.68	0.51	0.78	0.85
5	Man	24	0.90	-0.30	0.92	0.88
6	Woman	23	0.95	-0.25	0.93	0.93
7	Man	51	0.84	-0.44	0.79	0.83
8	Man	24	0.71	0.61	0.81	0.81
9	Man	22	0.65	0.37	0.70	0.73
Mean		26.33 / 9.29	0.82 / 0.11	-0.07 / 0.50	0.81 / 0.10	0.83 / 0.08

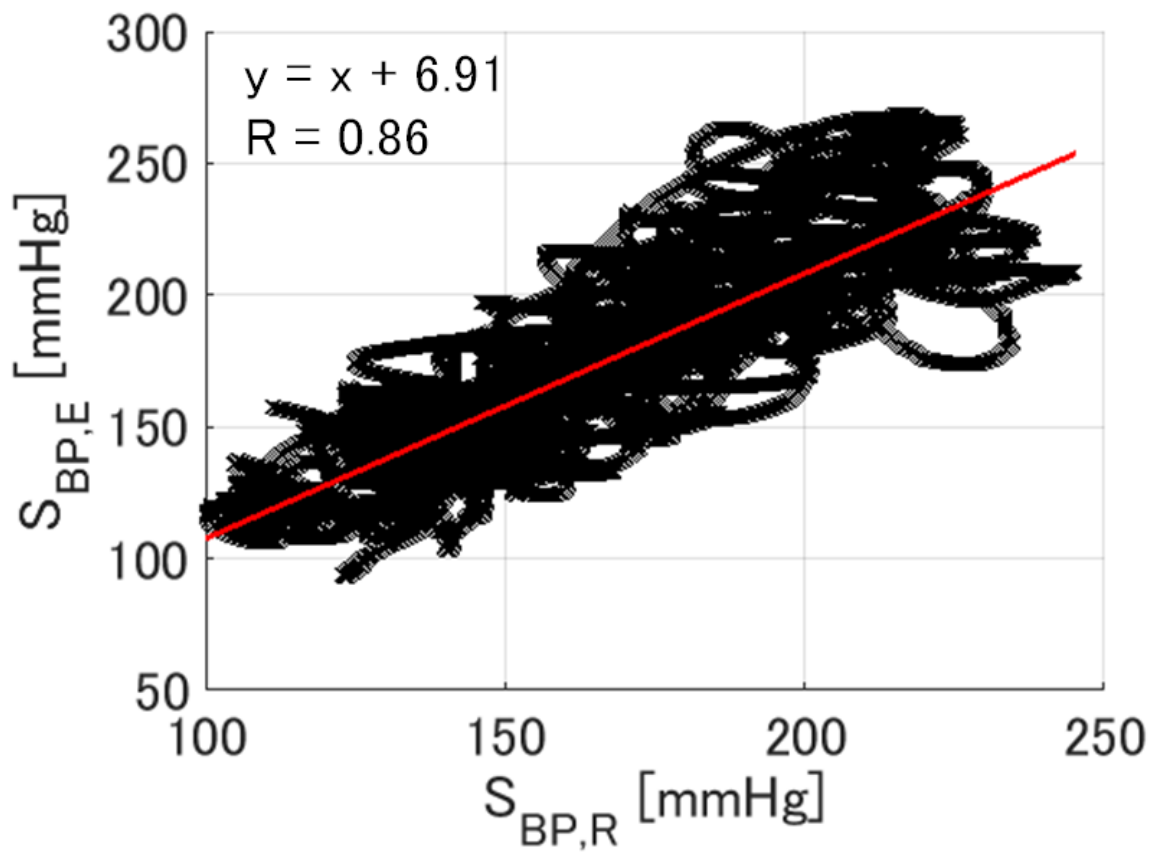


Fig. 6.12: Plot of  $S_{BP}$  measured by Finapres ( $S_{BP,R}$ ) and estimated  $S_{BP}$  ( $S_{BP,E}$ ) for all 9 subjects.

Table 6.3: RMSE for the  $S_{BP}$  estimation system for each subject.

Subject	RMSE [mmHg]
1	17.01 / 16.67
2	18.17 / 9.43
3	24.63 / 19.10
4	15.40 / 12.95
5	18.36 / 18.27
6	34.05 / 25.02
7	22.68 / 22.60
8	12.16 / 10.45
9	13.82 / 12.86
Mean	20.47 / 18.88

## 6.5 Discussion

The present study shows that the  $S_{BP}$  calculated from the PPG using a one time calibration correlates fairly with the  $S_{BP}$  measured by the cuff method. The relation between  $P_{NW}$  and  $S_{BP}$  followed a linear function. However, there is no precedent researches which use the product of  $H_r$  and  $P_W$  as parameter to estimate  $S_{BP}$ . The reason  $P_{NW}$  is used for estimating BP is to reflect the physical property of the blood vessel. In this study, experiment was conducted in warm room with temperature around 27°C. However, during cold temperature, blood vessel becomes hard and contract. This causes the blood flow to speed up. When entering cold place from warm place, the BP may rise significantly because of large temperature change. However, human body tends to adapt to the environment and the BP returns to normal. So, the changes in BP cannot be estimated by just monitoring the  $H_r$  only. Depending on the environment, the use of  $P_{NW}$  to estimate BP might becomes useful in the future research.

The most popular way of estimating arterial BP based on PTT or PWV acquisition is real time detection of the time-delay between the R-peak of QRS wave of ECG and the arrival or peak of an arterial pulse wave at the periphery. With real time detected PTT/PWV, continuous BP can be estimated using a specifically established theoretical model, which can generally express the relationship between BP and PTT/PWV.

Other researches describe non-linear relations between BP and brachial-ankle PWV in human body<sup>[80]</sup>. Others obtained a non-linear relationship between PWV and BP by grouping subjects by age and gender, considering the vessel dimensions, blood density, and arterial wall elasticity<sup>[81,82]</sup>. Even though the relation function is different, the correlation coefficient is maintained at the same level which is over 0.8 points.

The innovation of the presented method is the linear algorithm and the one time calibration. Calibration reduces the influence of the structural properties of arteries by shifting the  $P_{NW} - S_{BP}$  relationship nearing the ideal  $y = x$  relation (Figure 6.13). Normally, individual age and disease-dependent differences in the arterial stiffness do not allow calculating absolute BP values. This challenge can only be avoided by creating individual calibration points. Nevertheless, the application of the  $P_{NW} - S_{BP}$  function to the data of the 9 subjects serving for the creation of the  $S_{BP}$  estimation function resulted in fairly high individual correlation coefficients.

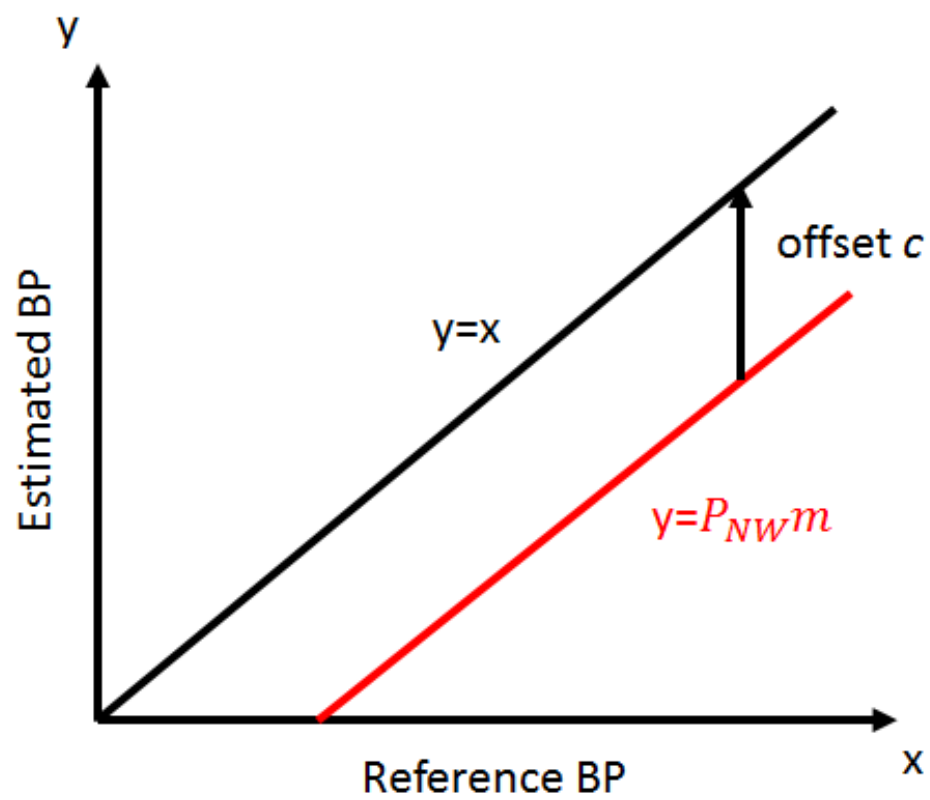


Fig. 6.13: Calibration reduces the influence of the structural properties of arteries when estimating BP.

## 6.6 Conclusions

The results show that the created  $P_{NW} - S_{BP}$  function including the one time calibration produces significant correlation between  $S_{BP}$  derived from PPG and the  $S_{BP}$  measured with continuous BP measurement device. Although the estimation accuracy differs in individuals, the results have started a new chapter for further studies with the aim to minimize variation in individuals.

# Chapter 7

## Conclusion

In this thesis, research on wearable measurement system for physical performance and biomedical information has been conducted. Other inertial sensors, force sensor, and pulse sensor are used for assessment of exercise level by measuring activities such as walking and cycling.

In chapter 2, improvement on the older version of WIMU is proposed for motion measuring. In addition to high sensitivity sensor used in the previous WIMU, low sensitivity sensor is introduced in the new sensor to enable precise measurement of fast motion. The sensor is made compact and light for the purpose of surface mounting. Compared to the previous WIMU system, integration section of measured acceleration and angular velocity during gait analysis is improved so that parameters during fastest gait can be estimated at high accuracy.

In chapter 3, WIMU system to derive gait parameters indicating cognitive impairment is developed for use during large-scale health checkups. Current health checkups conduct a 10 m fastest gait examination to assess signs of cognitive impairment and physical performance. Earlier methods require examiners to follow a subject and measure the gait time using a stopwatch. The method proposed herein reduces burdens on examiners. Several gait parameters in addition to the gait time of many subjects can be measured simultaneously and quantitatively from three-dimensional foot movements estimated using inertial sensors. Gait parameters derived from the inertial sensor are gait time, stride length, gait cycle, gait velocity, toe angle, toe height, and the percentage of swing phase. The gait condition, such as walking or running, is distinguished from the moment of toe off and heel contact of both feet. In all, 1406 subjects with ages of 19-93 years old were given instructions to walk at their highest velocity on a straight 16-m-long walking course.

MMSE is conducted on subjects. The score is used as a reference valuation of the cognitive impairment level. Experimental results show that the proposed measurement system provides equal performance to that obtained using a stopwatch and improves correlation between the MMSE score and the fastest 10 m gait time of subjects who did not run. Furthermore, it is confirmed that the proposed measurement system using inertial sensors can quantitatively provide spatiotemporal gait parameters to evaluate the physical performance in a short time during the largescale health checkups.

In chapter 4, in addition to conventional method of gait analysis using WIMU, pressure sensor on sole is introduced for gait measurement system which measures gait performance of both stance phase and swing phase. Six pressure sensors are mounted under the inner sole of shoe and information of gait is taken from inertial sensor mounted on the tiptoe combined with pressure sensors. Trajectory of COP is calculated. It is confirmed that COP moves from heel and curves out to foot thumb during stance phase. Results show that the utilization of sensors in footwear provide opportune information on people's activities and gait behaviors and is important in innumerable applications.

In chapter 5, measurement system for recording BP without cuff for measurement during exercise or hard work is developed. CLB estimation that requires only 1 sensor for capturing PPG signal is introduced. New parameter  $P_{NW}$  derived from the product of  $H_r$  and  $P_W$  is introduced for estimation of mean BP. Experiment is conducted on 9 healthy subjects and functions for BP estimation are obtained.  $P_{NW}$  shows high correlation with BP with  $r = 0.81 / 0.10$  and average RMSE for the  $S_{BP}$  estimation system is  $20.47 / 18.88$ . Results show that the created  $P_{NW}$ -BP function including the one time calibration produces significant correlation between BP derived from PPG and BP measured with CB continuous BP measurement device.



# References

- [1] Y. Jia, “Dietetic and exercise therapy against diabetes mellitus,” in Second International Conference on Intelligent Networks and Intelligent Systems, pp. 693–696, 2009
- [2] J. Yin, Q. Yang, and J. Pan, “Sensor-based abnormal human-activity detection,” IEEE Trans. Knowl. Data Eng., vol. 20, no. 8, pp. 1082–1090, 2008.
- [3] P. Turaga, R. Chellappa, V. Subrahmanian, and O. Udrea, “Machine recognition of human activities: A survey,” IEEE Trans. Circuits Syst. Video Technol., vol. 18, no. 11, pp. 1473–1488, 2008.
- [4] J. Candamo, M. Shreve, D. Goldgof, D. Sapper, and R. Kasturi, “Understanding transit scenes: A survey on human behavior-recognition algorithms,” IEEE Trans. Intell. Transp. Syst., vol. 11, no. 1, pp. 206–224, 2010.
- [5] C. N. Joseph, S. Kokulakumaran, K. Srijevanth, A. Thusyanth, C. Gunasekara, and C. Gamage, “A framework for whole-body gesture recognition from video feeds,” in International Conference on Industrial and Information Systems (ICIIS), pp. 430–435, 2010.
- [6] M. Ahad, J. Tan, H. Kim, and S. Ishikawa, “Human activity recognition: Various paradigms,” in International Conference on Control, Automation and Systems, pp. 1896–1901, 2008.
- [7] Fahrenberg J, Foerster F, Smeja M, Muller W: ”Assessment of Posture and Motion by Multichannel Piezoresistive Accelerometer Recordings”, Psychophysiology, Vol.34, pp.607-612, 1997

- [8] Naja B, Aminian K, Paraschiv-Ionescu A, Loew F, Bula CJ, Robert P: "Ambulatory System for Human Motion Analysis Using a Kinematic Sensor-Monitoring of Daily Physical Activity in the Elderly", IEEE Trans. Biomed. Eng., Vol.50, No.6, pp.711-723, 2003
- [9] Miyazaki S: "Long-Term Unrestrained Measurement of Stride Length and Walking Velocity Utilizing a Piezoelectric Gyroscope", IEEE Trans. Biomed. Eng., Vol.44, No.8, pp.753-759, 1997
- [10] JA Lee, SH Cho, YJ Lee, HK Yang, JW Lee, "Portable activity monitoring system for temporal parameters of gait cycles", J Med Syst (2010) 34:959–966
- [11] Shu, L., Hua, T., Wang, Y., Qiao Li, Q., Feng, D.D., Tao, X.: In-shoe plantar pressure measurement and analysis system based on fabric pressure sensing array. IEEE Trans. Inf. Technol. Biomed. 14(3), 767–775 (2010)
- [12] Adriana Arza, Jesús Lázaro, Eduardo Gil, Pablo Laguna, Jordi Aguiló, Raquel Bailon, Pulse Transit Time and Pulse Width as Potential Measure for Estimating Beat-to-Beat Systolic and Diastolic Blood Pressure, Computing in Cardiology 2013; 40:887-890
- [13] Awad AA, Haddadin AS, Tantawy H, Badr TM, Stout RG, Silverman DG, Shelley KH. The relationship between the photoplethysmographic waveform and systemic vascular resistance. J Clin Monit Comput 2007; 21: 365-372.
- [14] 坂上滉哉, 佐藤駿祐, 本井幸介, 高橋一平, 澤田かほり, 中路重之, 佐川貢一, つま先センサを用いた 10m 歩行時間推定の精度について計測自動制御学会東北支部 50 周年記念学術講演会, 59-62 (USB メモリ), 2014
- [15] Kuga, H. and Sagawa, K., Estimation of walking distance of 10 meter fastest walk using tiptoe-mounted inertial sensor, Proceedings of International Conference on Mechatronics and Information Technology (ICMIT2015), (2015), pp.201–205.
- [16] Allali, G., Assal, F., Kressig, R. W., Dubost, V., Herrmann, F. R. and Beauchet, O., Impact of impaired executive function on gait stability, Dement Geriatr Cogn Disord, Vol.26 (2008), pp.364–369.

- [17] Tanaka, H. and Sagawa, K., Judgement of the stance phase using tiptoe-mounted sensor, The Society of Instrument and Control Engineers Tohoku Chapter 258th Research Meeting, 258-8 (2010) (in Japanese).
- [18] Kramer, A. F., Colcombe, S. J., McAuley, E., Scalf, P. E. and Erickson, K. I., Fitness, aging and neurocognitive function. *Neurobiology of Aging*, Vol.26, Issue 1, Supplement, (2005), pp.124–127.
- [19] Ijmker, T. and Lamoth, C. J., Gait and cognition: The relationship between gait stability and variability with executive function in persons with and without dementia, *Gait & Posture*, Vol.35 (2012), pp.126–130.
- [20] Lamoth, C. J., Deudekom, F. J., Van Campen, J. P., Appels, B., De Vries, O. J. and Pijnappels, M., Gait stability and variability measures show effects of impaired cognition and dual tasking in frail people, *J Neuroeng Rehabil*, Vol.8 (2011), p.2.
- [21] Manckoundia, P., Pfitzenmeyer, P., d’Athis, P., Dubost, V. and Mourey, F., Impact of cognitive task on the posture of elderly subjects with Alzheimer’s disease compared to healthy elderly subjects, *Mov Disord*, Vol.21 (2006), pp.236–241.
- [22] Sheridan, P. L., Solomont, J., Kowall, N. and Hausdorff, J. M., Influence of executive function on locomotor function: divided attention increases gait variability in Alzheimer’s disease, *J Am Geriatr Soc*, Vol.51 (2003), pp.1633–1637.
- [23] Abbott, R. D., White, L. R., Ross, G. W., Masaki, K. H., Curb, J. D. and Petrovitch, H., Walking and dementia in physically capable elderly men, *JAMA*, Vol.292, No. 12 (2004), pp.1447–1453.
- [24] Beauchet, O., Allali, G., Berrut, G., Hommet, C., Dubost, V. and Assal, F., Gait analysis in demented subjects: interests and perspectives, *Neuropsychiatr Dis Treat*, Vol.4 (2008), pp.155–160.
- [25] Hausdorff et al., 2005. Walking is more like catching than tapping: gait in the elderly as a complex cognitive task. *Exp. Brain Res.* 164(4), 541-548
- [26] Marquis et al., 2002. Independent predictors of cognitive decline in healthy elderly persons. *Arch Neurol.* 59(4), 601-606

- [27] Rosie Morris et al., 2016. Gait and cognition: Mapping the global and discrete relationships in ageing and neurodegenerative disease. *Neuroscience and Biobehavioral Reviews*, Vol.64, 326-345
- [28] Persad, C. C., Jones, J. L., Ashton-Miller, J. A., Alexander, N. B., and Giordani, B., Executive function and gait in older adults with cognitive impairment, *J Gerontol A Biol Sci Med Sci*, Vol.63 (2008), pp.1350–1355.
- [29] Yogev-Seligmann, G., Hausdorff, J. M. and Giladi, N., The role of executive function and attention in gait, *Mov Disord*, Vol.23 (2008), pp.329–342.
- [30] Barnes, D. E., Yaffe, K., Satariano, W. A. and Tager, I. B., A longitudinal study of cardiorespiratory fitness and cognitive function in healthy older adults, *J Am Geriatr Soc*, Vol.51 (2003), pp.459–465.
- [31] Hausdorff, J. M., Schweiger, A., Herman, T., Yogev-Seligmann, G. and Giladi, N., Dual-task decrements in gait: contributing factors among healthy older adults, *J Gerontol A Biol Sci Med Sci*, Vol.63 (2008), pp.1335–1343.
- [32] Lamothe, C. J., Ainsworth, E., Polonski, W. and Houdijk, H., Variability and stability analysis of walking of transfemoral amputees, *Med Eng Phys*, Vol.32 (2010), pp.1009–1014.
- [33] Lockhart, T. E. and Liu, J., Differentiating fall-prone and healthy adults using local dynamic stability, *Ergonomics*, Vol.51 (2008), pp.1860–1872.
- [34] Yaffe, K., Barnes, D., Nevitt, M., Lui, L. Y. and Covinsky, K., A prospective study of physical activity and cognitive decline in elderly women, *Arch Inter Med*, Vol.161 (2001), pp.1703–1708.
- [35] Verghese, J., Ayers, E., Barzilai, N., Bennett, D. A., Buchman, A. S., Holtzer, R., Katz, M. J., Lipton, R. B. and Wang, C., Motoric cognitive risk syndrome: multi-country prevalence and dementia risk, *Neurology*, Vol.83 No.8 (2014), pp.718–726.
- [36] Esser, P., Dawes, H., Collett J., Feltham, M. G. and Howells, K., Assessment of spatiotemporal gait parameters using inertial measurement units in neurological populations, *Gait & Posture*, Vol.34 (2011), pp.558–560.

- [37] Ohtaki, Y., Inooka, H., Sagawa, K., Suzuki, A., Xiumin, Z., Okutsu, M. and Nagatomi, R., Recognition of daily ambulatory movements utilizing accelerometer and barometer, Proceedings of the Second IASTED International Conference BIOMECHANICS (2004), pp.18-21.
- [38] Chen, K. Y., and Bassett, D. R., The technology of accelerometry-based activity monitors: current and future, *Medicine and science in sports and exercise*, Vol.37, No.11 (2005), S490, DOI: 10.1249/01.mss.0000185571.49104.82
- [39] Khan, M., Ahamed, S. I., Rahman, M. and Smith, R. O., A feature extraction method for realtime human activity recognition on cell phones, Proceedings of 3rd International Symposium on Quality of Life Technology (2011).
- [40] Ibata, Y., Kitamura, S., Motoi, K. and Sagawa K., Measurement of three-dimensional posture and trajectory of lower body during standing long jumping utilizing body-mounted sensors, 2013 35th Annual International Conference of the IEEE (2013), pp.4891-4894.
- [41] Bao, L. and Intille, S. S., Activity recognition from user-annotated acceleration data, *Pervasive computing* (2004), pp.1–17.
- [42] Maurer, U., Smailagic, A., Siewiorek, D. P. and Deisher, M., Activity recognition and monitoring using multiple sensors on different body positions, *International Workshop on Wearable and Implantable Body Sensor Networks*, (2006). DOI: 10.1109/BSN.2006.6
- [43] Ermes, M., Pärkkä, J., Mäntyjärvi, J. and Korhonen, I., Detection of daily activities and sports with wearable sensors in controlled and uncontrolled conditions. *IEEE Transactions on Information Technology in Biomedicine*, Vol.12, No.1 (2008), pp.20–26.
- [44] Arif, M., Bilal, M., Kattan, A. and Ahamed, S. I., Better physical activity classification using smartphone acceleration sensor, *J Med Syst*, Vol.38:95 (2014), DOI: 10.1007/s10916-014-0095-0

- [45] Lee, J. A., Cho, S. H., Lee, Y. J., Yang, H. Y. and Lee, J. W., Portable Activity Monitoring System for Temporal Parameters of Gait Cycles, *Journal of Medical Systems*, Vol.34, No.5 (2010), pp.959–966.
- [46] Yu, M., Piao, Y. J., Eun, H. I., Kim, D. W., Ryu, M. H. and Kim, N. G., Development of Abnormal Gait Detection and Vibratory Stimulation System on Lower Limbs to Improve Gait Stability, *Journal of Medical Systems*, Vol.34, No.5 (2019), pp.787–797.
- [47] Mariani, B., Hoskovec, C., Rochat, S., Bûla, C., Penders, J. and Aminian, K., 3D gait assessment in young and elderly subjects using foot-worn inertial sensors, *Journal of Biomechanics*, Vol.43, Issue 15, 16 (2010), pp.2999–3006.
- [48] Ojeda, L. and Borenstein, J., Non-GPS navigation for security personnel and first responders, *J Navig*, Vol.60 No. 3 (2007), pp.391–407.
- [49] Sagawa, K. and Ohkubo, K., 2D trajectory estimation during free walking using a tiptoe-mounted inertial sensor, *J. Biomech*, Vol.48 No. 10 (2015), pp.2054–2059.
- [50] Yang, S. and Li, Q., Inertial sensor-based methods in walking speed estimation: a systematic review, *Sensors (Basel)*, Vol.12 No.5 (2012), pp.6102–6116.
- [51] Azman, A. M., Kuga, H., Sagawa, K. and Nagai, C., Fastest gait parameters estimation precision comparison using high-sensitivity and low-sensitivity inertial sensor, *IFMBE Proceedings* (2017), Vol.67, pp.79–84.
- [52] Azman, A. M., Nagai, C., Sagawa, K., Hirakawa, Y. and Sawada, K., Predicting possibility of mild cognitive impairment from gait parameter measured using inertial sensor, *Conference on Information, Intelligence, and Precision Equipment*, 1B03 (2019).
- [53] Pangman, V. C., Sloan, J. and Guse, L., An Examination of Psychometric Properties of the Mini-Mental Status Examination and the Standardized Mini-Mental Status Examination: Implications for Clinical Practice, *Applied Nursing Research*, Vol.13, No.4 (2000), pp.209–213.

- [54] Tombaugh, T. N. and McIntyre, N. J., The mini-mental Status Examination: A comprehensive Review, *Journal of the American Geriatrics Society*, Vol.40, No.9 (1992), pp.922–935, DOI: 10.1111/j.1532-5415.1992.tb01992.x
- [55] Harrell, L. E., Marson, D., Chatterjee, A. and Parrish, J. A., The Severe Mini-Mental Status Examination: A New Neuropsychologic Instrument for the Bedside Assessment of Severely Impaired with Alzheimer’s Disease, *Alzheimer Disease and Associated Disorders*, Vol.14 No.3 (2000) 168–175.
- [56] Sagawa, K., Kuga, H., Azman, A. M., Nagai, C., Nakaji, S. and Kurauchi, S., Improvement of measurement precision of wearable gait evaluation system used in large scale health checkup, *Conference on Information, Intelligence, and Precision Equipment*, 1B16 (2018) (in Japanese).
- [57] Rosenbaum D, Becker HP. Plantar pressure distribution measurements. Technical background and clinical applications. *Foot Ankle Surg* 1997;3(1):1–14.
- [58] Stokes IAF, Faris IB, Hutton WC. The neuropathic ulcer and loads on the foot in diabetic patients. *Acta Orthop Scand* 1975;46(5):839–47.
- [59] Veves A, Murray HJ, Young MJ, Boulton AJM. The risk of foot ulceration in diabetic patients with high foot pressure: a prospective study. *Diabetologia* 1992;35(7):660–3.
- [60] Li, J., Xu, B.: Novel highly sensitive and wearable pressure sensors from conductive three- dimensional fabric structures. *Smart Mater. Struct.* 24(12), 125022 (2015)
- [61] Hanson, D., Thompson, P., Langemo, D., Hunter, S., Anderson, J.: Pressure mapping: A new path to pressure ulcer prevention. *Wound Care Advis.* 1(1), 15–19 (2012)
- [62] Tarchanidis, K.N., Lygouras, J.N.: Data glove with a force sensor. *IEEE Trans. Instrum. Meas.* 52(3), 984–989 (2003)
- [63] Rovira, C., Coyle, S., Corcoran, B., Diamond, D., Stroiescu, F., Daly, K.: Integration of textile-based sensors and Shimmer for breathing rate and volume measurement. In: *International Conference Pervasive Computer Technology Healthcare*, vol. m, pp. 238– 241 (2011)

- [64] Huang, C.T., Shen, C.L., Tang, C.F., Chang, S.H.: A wearable yarn-based piezo-resistive sensor. *Sens. Actuators A Phys.* 141(2), 396–403 (2008)
- [65] Abdul Razak, A.H., Zayegh, A., Begg, R.K., Wahab, Y.: Foot plantar pressure measurement system: A review. *Sensors (Switzerland)* 12(7), 9884–9912 (2012)
- [66] Paredes-Madrid, L., Torruella, P., Solache, P., Galiana, I., & de Santos, P. G. (2010, May). Accurate modeling of low-cost piezoresistive force sensors for haptic interfaces. In *Robotics and Automation (ICRA), 2010 IEEE International Conference on* (pp. 1828-1833). IEEE
- [67] MacWilliams, B.A.; Armstrong, P.F. Clinical Applications of Plantar Pressure Measurement in Pediatric Orthopedics. In *Proceeding of Pediatric Gait, 2000. A New Millennium in Clinical Care and Motion Analysis Technology*, Chicago, IL, USA, 22 July 2000; pp. 143–150.
- [68] Gefen, A. Pressure-sensing devices for assessment of soft tissue loading under bony prominences: Technological concepts and clinical utilization. *Wounds* 2007, 19, 350–362.
- [69] R.W. Soames. Foot pressure patterns during gait. *Journal of Biomedical Engineering* Volume 7, Issue 2, April 1985, Pages 120-126.
- [70] Aoife H, Philip B.W, Roozbeh N, Nachiappan C. Repeatability of WalkinSense® in shoe pressure measurement system: A preliminary study. *The Foot* 22 (2012) 35-39
- [71] Saito M., Nakajima K., Takano C., Ohta Y., Sugimoto C., Ezoe R., Sasaki K., Hosaka H., Ifukube T., Ino S., Yamashita K. An in-shoe device to measure plantar pressure during daily human activity. *Med. Eng. Phys.* 2011;33:638–645.
- [72] Mukkamala, R., et al., 2015. Toward ubiquitous blood pressure monitoring via pulse transit time: theory and practice. *IEEE Transactions on Biomedical Engineering*, 62(8), pp.1879–1901.
- [73] Radha, M., Zhang. G., Gelissen, J., Groot, K., Haakma, R. and Aarts, R. M., Arterial path selection to measure pulse wave velocity as a surrogate marker of blood pressure, *Biomed. Phys. Eng. Express* 3 (2017), 015022, DOI: 10.1088/2057-1976/aa5b40



- [74] Proença, J., Muehlsteff, J., Aubert, X. and Carvalho, P., Is pulse transit time a good indicator of blood pressure changes during short physical exercise in a young population?, 32nd Annual International Conference of the IEEE EMBS Buenos Aires, Argentina, August 31 - September 4, 2010
- [75] Smith, R. P., Argod, J., Pépin J.-L. and Lévy, P., Pulse transit time: an appraisal of potential clinical applications, *Thorax* (1999), 54 452–7
- [76] Payne, R. A., Symeonides, C. N., Webb, D. J. and Maxwell, S. R. J., Pulse transit time measured from the ECG: an unreliable marker of beat-to-beat blood pressure, *J. Appl. Physiol.* (2006), 100 136–41
- [77] Gesche H, Grosskurth D, Kuchler G, Patzak A, Continuous blood pressure measurement by using the pulse transit time: comparison to a cuff-based method, *Eur J Appl Physiol.* 2012 Jan;112(1):309-15. DOI: 10.1007/s00421-011-1983-3.
- [78] Mico Yee-Man Wong, Carmen Chung-Yan Poon, Yuan-Ting Zhang, An Evaluation of the Cuffless Blood Pressure Estimation Based on Pulse Transit Time Technique: a Half Year Study on Normotensive Subjects, *Cardiovasc Eng.* DOI 10.1007/s10558-009-9070-7
- [79] Penaz, J., Automatic noninvasive blood pressure monitor, US Patent 4869261 (1989)
- [80] Yamashina, A., Tomiyama, H., Arai, T., Koji, Y., Yambe, M., Motobe, H., Glunizia, Z., Yamamoto, Y. and Hori, S., Nomogram of the relation of brachial–ankle pulse wave velocity with blood pressure, *Hypertens Res* (2003), 26:801-806
- [81] Chen, Y., Wen, C., Tao, G., Bi, M. and Li, G., Continuous and noninvasive blood pressure measurement: a novel modeling methodology of the relationship between blood pressure and pulse wave velocity, *Ann Biomed Eng* (2009), 37:2222–2233
- [82] Zheng, D. and Murray, A., Non-invasive quantification of peripheral arterial volume distensibility and its non-linear relationship with arterial pressure. *J Biomech* (2009), 42:1032–1037

# Acknowledgments

This research was conducted in Graduate School of Science and Technology, Department of Mechanical Science and Engineering, Safety Science and Technology, Hirosaki University for three years from April 2017 to March 2020.

During conducting this research, I would like to express my sincere gratitude to Professor Koichi Sagawa of Department of Mechanical Science and Engineering, Hirosaki University who gave me guidance and encouragement from time to time.

I would also like to express my sincere gratitude to Professor Kazuhiko Sasagawa and Professor Kazuhiko Oka of Department of Science and Technology, Hirosaki University who gave me appraisal and guidance during conducting the researches.

My sincere thanks also goes to Professor Manabu Totsuka of the Faculty of Education, Hirosaki University and Associate Professor Takayuki Hoshino of Department of Science and Technology, Hirosaki University for their encouragement, insightful comments, and opportunities conducting the studies.

A part of this study was supported by JSPS KAKENHI Grant Number 25350663. I wish to express my gratitude to Dr. Shigeyuki Nakaji for his acceptance of the sensor system at the City of Hirosaki's Iwaki Health Promotion Project.

Throughout this research, I would like to express my sincere gratitude to everyone at Faculty of Science and Technology / Graduate School of Science and Technology, Hirosaki University who cooperated in conducting and participating in the experiments.

I would like to express my deep gratitude to all of the laboratory members who help me and support in these researches.